PB88-169586

REPORT NO.
UCB/EERC-87/05
MAY 1987

EARTHQUAKE ENGINEERING RESEARCH CENTER

THREE-DIMENSIONAL INELASTIC ANALYSIS OF REINFORCED CONCRETE FRAME-WALL STRUCTURES

by

SARA MOAZZAMI
VITELMO V. BERTERO

Report to the National Science Foundation

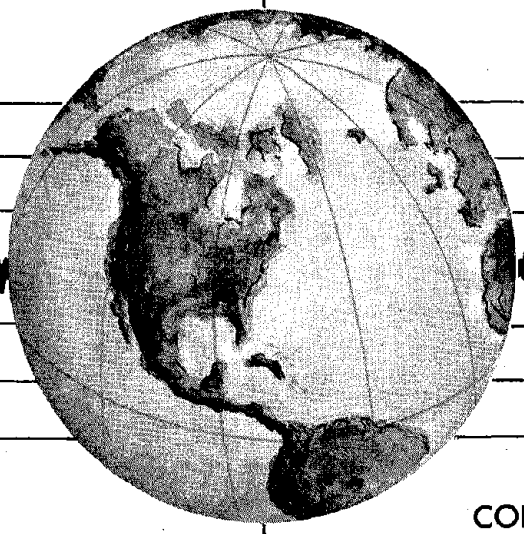

COLLEGE OF ENGINEERING

UNIVERSITY OF CALIFORNIA · Berkeley, California

For sale by the National Technical Information Service, U.S. Department of Commerce, Springfield, Virginia 22161.

See back of report for up to date listing of EERC reports.

DISCLAIMER

50272-101

REPORT DOCUMENTATION PAGE	1. REPORT NO. NSF/ENG-87032	2.	3. Recipient's Accession No. PB88 169586/AS

4. Title and Subtitle
Three-Dimensional Inelastic Analysis of Reinforced Concrete Frame-Wall Structures

5. Report Date
May 1987

6.

7. Author(s)
Sara Moazzami and Vitelmo V. Bertero

8. Performing Organization Rept. No.
UCB/EERC-87/05

9. Performing Organization Name and Address
Earthquake Engineering Research Center
University of California
1301 South 46th Street
Richmond, Ca. 94804

10. Project/Task/Work Unit No.

11. Contract(C) or Grant(G) No.
(C)
(G) CEE 80-09478

12. Sponsoring Organization Name and Address
National Science Foundation
1800 G. Street, N.W.
Washington, D.C. 20550

13. Type of Report & Period Covered

14.

15. Supplementary Notes

16. Abstract (Limit: 200 words)

An analytical method based on mathematical programming techniques has been developed to evaluate the three-dimensional response of structures in order to study the nonlinear behavior of reinforced concrete frame-wall structures at damageability and ultimate limit states. The method also incorporates a finite element model of the shear wall that is capable of simulating some of the physical characteristics of the wall. The model is based on the distributed material properties of reinforcing bars and concrete, and is capable of predicting the crack pattern and the failure mode of the wall.

The application of this analytical method is illustrated by a series of nonlinear static analyses of a 1/5-scale model of a 7-story reinforced concrete frame-wall structure. This model has been tested dynamically at the University of California, Berkeley, and a full-scale prototype was tested pseudo-dynamically at Tsukuba, Japan.

The nonlinear static analyses are found to be in good agreement with the envelope of experimental dynamic response of the structure, but the predicted crack pattern and mode of failure of the wall are not similar to that of the 1/5-scale model. Instead they are representative of the crack pattern and the type of failure observed in the full-scale model (which was tested pseudo-dynamically).

17. Document Analysis a. Descriptors

earthquake response
pseudo-dynamic testing
nonlinear static analysis
finite element shear wall model
frame-wall structure
reinforced concrete

b. Identifiers/Open-Ended Terms

c. COSATI Field/Group

18. Availability Statement:	19. Security Class (This Report)	21. No. of Pages
Release unlimited	unclassified	163
	20. Security Class (This Page) unclassified	22. Price PC 19.95 / MF A06

U.S.-JAPAN COOPERATIVE EARTHQUAKE RESEARCH PROGRAM

THREE-DIMENSIONAL INELASTIC ANALYSIS OF REINFORCED CONCRETE FRAME-WALL STRUCTURES

by

Sara Moazzami

and

Vitelmo V. Bertero

A Report to Sponsor:

National Science Foundation

Report No. UCB/EERC-87/05

Earthquake Engineering Research Center

College of Engineering

University of California

Berkeley, California

May 1987

ABSTRACT

In order to study the nonlinear behavior of reinforced concrete frame-wall structures at damageability and ultimate limit states, an analytical method based on mathematical programming techniques has been developed. Since the actual response of a frame-wall structure in the inelastic range is generally dominated by the rocking of the shear wall and a three-dimensional mechanism of motion, the analytical method developed here is designed to evaluate the three-dimensional response of structures.

The analytical method presented here also incorporates a finite element model of the shear wall that is capable of simulating some of the physical characteristics of the wall. This model is based on the distributed material properties of reinforcing bars and concrete, and is capable of predicting the crack pattern and the failure mode of the wall.

In order to illustrate the application of this analytical method, a series of nonlinear static analyses are conducted on a 1/5-scale model of a 7-story reinforced concrete frame-wall structure. This model has been tested dynamically at the University of California, Berkeley, and a full-scale prototype of this structure was tested pseudo-dynamically at Tsukuba, Japan.

The results of the nonlinear static analyses of this structure are found to be in good agreement with the envelope of experimental dynamic response of the structure. But the predicted crack pattern and mode of failure of the wall are not similar to that of the 1/5-scale model. Instead they are representative of the crack pattern and the type of failure observed in the full-scale model (which was tested pseudo-dynamically).

ACKNOWLEDGEMENTS

The research reported here was supported, in part, by the National Science Foundation Grant Number CEE 80-09478. This work has been completed by Sara Moazzami as a partial requirement for the degree of Doctor of Philosophy in Engineering under the supervision of Professor V.V. Bertero. This report reproduces the dissertation submitted in December 1986 to the Graduate Division of the University of California, Berkeley.

Professors E.L. Wilson and S.S. Oren reviewed this report and offered many valuable suggestions during the course of this research.

Acknowledgement is also given to Professor M.Z. Cohn of the University of Waterloo for supplying information regarding mathematical programming in engineering plasticity.

Finally, acknowledgement is given to Reza Moazzami for providing assistance in typesetting the thesis and to Dr. Beverley Bolt for editing the manuscript.

TABLE OF CONTENTS

Chapter 1 - INTRODUCTION 1

1.1 Introductory Remarks 1

1.2 Background 2

1.3 Objectives and Scope 2

1.4 Organization and Layout of the Report 3

1.5 Notation 4

Chapter 2 - ANALYTICAL METHOD 5

2.1 Method of Analysis 5

2.2 Types of Elements 10

Chapter 3 - FUNDAMENTALS OF ELASTOPLASTIC ANALYSIS 13

3.1 Constitutive Laws for Holonomic Behavior 13

3.1.1 Constitutive Laws for a Single Stress Component 13

3.1.2 Constitutive Laws for Two Stress Components 16

3.2 Constitutive Laws for Nonholonomic Behavior 20

3.3 Holonomic Analysis 21

3.4 Nonholonomic Analysis 28

Chapter 4 - STRUCTURAL ELEMENTS 30

4.1 Frame Elements 30

4.1.1 Truss Elements 31

4.1.2 Beam Elements 31

4.1.3 Beam-Column Elements 33

4.2 Finite Elements 34

4.2.1 Stress-Strain Relationship for Isotropic Plane Stress Elements 35

4.2.2 Stress-Strain Relationship for Reinforcing Bars 37

4.2.3 Force-Deformation Relationship for Plane Stress Elements 39

4.3 Element Connections 40

Chapter 5 - COMPUTER ANALYSIS 44

5.1 Mathematical Programming Methods 44

5.2 Analytical Procedure 46

5.3 Computer Program 49

5.3.1 Linear Complementarity Problem 52

5.3.2 Updating the Inverse of the Hessian Matrix A_{aa} 54

Chapter 6 - APPLICATION OF THE ELASTOPLASTIC ANALYSIS PROGRAM TO A REINFORCED CONCRETE FRAME-WALL STRUCTURE

6.1 Description of the Test Structure 56

6.2 An Overview of the Experimental Testing Program and the Experimental Response of the Model 56

6.3 Development of the Model for the Nonlinear Static Analysis 58

6.3.1 Modeling of the Shear Wall 59

6.3.2 Modeling of the Longitudinal and the Transverse Girder 64

6.3.3 Modeling of the Columns 66

6.3.4 Modeling of the End Walls 67

6.4 Analytical Response to Monotonically Increasing Lateral Loads 67

6.4.1 Global Analytical Response of the Model 68

6.4.2 Comparison of the Experimental and the Analytical Responses of the Structure 69

6.4.3 Local Response of the Shear Wall 70

6.5 Crack Pattern and Type of Failure Observed in the Shear Wall 73

6.6 Conclusions 76

Chapter 7 - SUMMARY AND CONCLUSIONS 77

7.1 Summary 77

7.2 Conclusions 79

7.3 Recommendations for Future Research 80

APPENDIX A 82

APPENDIX B 83

REFERENCES 85

TABLES 89

FIGURES 91

1 INTRODUCTION

1.1 Introductory Remarks

In 1977, the U.S.-Japan cooperative research program was organized primarily to investigate and improve the seismically resistant design practices of some typical building structures. Among the structures considered in this program were a reinforced concrete frame-wall structure, concentrically and eccentrically braced steel frames, and some masonry and timber structures.

During the first phase of this project the seismic response of the reinforced concrete frame-wall structure was studied in depth. The primary objective was to recognize the actual structural behavior and to develop analytical models that predict the observed behavior of the frame-wall structural system.

The investigation of the behavior of the reinforced concrete frame-wall structure was based on the results of tests performed on a full-scale model and several reduced-scale models of a 7-story reinforced concrete frame-wall structure. In particular, a 1/5-scale model of this structure was designed and tested at the University of California, Berkeley. The interpretation of the behavior of this model to different earthquake motions has been documented in references 1, 2, and 3. The basic conclusion from these studies was that the response of the model in the inelastic range was dominated by the rocking of the main shear wall which induced a three dimensional mechanism of motion. As a result, in the analytical studies following the testing of the model, an attempt was made to use special modeling techniques to incorporate the three dimensional behavior of the structure into a simplified two dimensional mathematical model. However, because of the limitations and shortcomings of this simple model in predicting the response of the frame-wall structure, in this report, new analytical techniques have been adopted in this report to efficiently conduct a three-dimensional analysis of reinforced concrete

frame-wall structures.

1.2 Background

Recent development in the field of engineering plasticity (by mathematical programming) has led to the development of very efficient techniques for solving limit analysis [4] and elastoplastic analysis of structures [5]. Since these techniques can be applied to the analysis of any type of structure, an attempt will be made here to utilize these mathematical programming techniques to solve the three-dimensional inelastic analysis of reinforced concrete frame-wall structures.

1.3 Objectives and Scope

The primary objective of the studies reported herein was to develop analytical techniques suitable for nonlinear static analysis of reinforced concrete frame-wall structures.

Since the behavior of the test structure observed during the experimental testing program indicates that the response of the model in the inelastic range is dominated by the rocking of the main shear wall and a three dimensional mechanism of motion, the analytical techniques developed here are designed to evaluate the three dimensional response of the structure.

Besides inducing a three-dimensional mechanism of motion, the shear wall exhibits other aspects of nonlinear behavior such as nonlinear shear deformation and nonlinear variation in flexural and shear stiffnesses, which can not be modeled directly by a beam-column element. Therefore, an important objective of these studies has been to develop an analytical model that is capable of simulating some of the physical characteristics of the shear wall.

The ultimate goal of these studies is to provide an efficient and reliable analytical technique such that the three dimensional analysis of the structure is

economically feasible. The analytical methods selected for the analysis are based on mathematical programming techniques, primarily because theses methods are considerably faster than most classical nonlinear analysis methods.

1.4 Organization and Layout of the Report

This report is divided into seven chapters. In the second chapter, the analytical method for the inelastic analysis of structures is briefly described with reference to a beam element, and the mechanical models of some typical elements are presented. In order to fully explain the analytical formulation and show its relation to mathematical programming, in the third chapter of this report, the elastoplastic constitutive laws are introduced along with the compatibility and equilibrium relations. In the final formulation, the nonlinear response of the structure is presented in a mathematical form known as the linear complementarity problem. Chapter four contains the description of the elastoplastic behavior of a selected group of frame elements and finite elements. The treatment of the finite size of the joints and the connection of frame elements to finite elements are presented there as well. In chapter five, the solution to the linear complementarity problem of chapter three is presented with reference to an algorithm that clearly outlines the steps involved in an elastoplastic analysis problem. In chapter six, an analytical model of a 7-story reinforced concrete frame-wall structure is introduced, and the results of a series of nonlinear static analyses performed on this model are compared with the envelope of the experimental response. The evaluation of the success of this model in predicting the response of the structure is delayed until chapter seven, where the results of the studies and the conclusions drawn from those studies are summarized.

1.5 Notation

Matrix notation is adopted throughout this report to present the analytical formulations. Bold face letters denote matrices and column-vectors, normal letters represent scalar quantities, and a superposed "t" means "transpose of".

2. ANALYTICAL METHOD

In this chapter, an analytical method for the inelastic analysis of structures is presented. This method works on an event-to-event basis where an increment of load is added until the next plastic hinge forms. Unlike most nonlinear analysis methods, the stiffness matrix of the structure is not updated at the end of each step. Instead, a pattern of self-equilibrating stress distribution, which represents the redistribution of stresses imposed by the plastic hinge, is computed. This method has the capability to detect a collapse mechanism and to determine the displacement and the strength of the structure at incipient collapse.

For the analytical model of the structure, both frame and finite elements are used. The frame elements considered here include truss elements, beam elements, and both uniaxial and biaxial beam-column elements. The discussion of finite elements, however, will be confined to plane stress elements that are suitable for the analysis of reinforced concrete shear walls.

Frame elements are elastic throughout their length. Inelastic deformations are assumed to be concentrated at the ends of members (see Fig. 2.1). For finite elements, the state of stress and strain is computed at integration points and inelastic deformation can be induced at any one of these points (i.e., partial yielding of elements is allowed).

The following sections describe briefly the fundamentals of the nonlinear analysis and the main features of the elements used in the analysis. The analytical formulation of the nonlinear analysis and the elastoplastic behavior of the elements is presented in the next two chapters.

2.1 Method of Analysis

It is convenient to illustrate the method of analysis with reference to the structure shown in Fig. 2.2. An analytical model of this structure consists of two

beam elements and four critical sections. The beam elements are assumed to be linear elastic-perfectly plastic with an elastic flexural stiffness of EI, and a plastic moment capacity of M_p. Given that the structure is subjected to a uniform load of sW (where s is the applied load factor), an elastoplastic analysis of this structure will be conducted to determine the response of the structure up to the collapse limit state.

The first step involved in formulating the elastoplastic analysis of this problem is to carry out a linear elastic analysis of the structure. The moments, $\mathbf{M}^t = \left[M_1, \ldots, M_4 \right]$, at the critical sections must then be compared with the plastic moment capacity of each section. The smallest ratio of plastic moment capacity to elastic moment, $\min s_i = \dfrac{M_{p_i}}{M_i}$ (where $i = 1, \ldots, 4$ refers to the critical sections), determines the elastic limit load factor of the structure.

For the structure in Fig. 2.2, the elastic limit ($s_{elastic\ limit} = \dfrac{12\ M_p}{WL^2}$) is reached when the critical sections 1 and 4 attain their plastic moment capacity (see Fig. 2.3). We shall adopt the terminology *plastic hinge* to identify plastic rotation (or deformation) at a critical section.

After the formation of these two plastic hinges (at critical sections 1 and 4), the stiffness matrix of the entire structure changes. Therefore, to continue the elastoplastic analysis, we must either update the stiffness matrix of the structure or consider the original structure to resist the plastic rotation in exactly the same way that it resists the external loads.

In order to illustrate the second procedure, it is necessary to compute a pattern of self-equilibrating internal stresses that resists a unit plastic rotation at critical sections 1 and 4 (see Fig. 2.4(c)) . This pattern of moment distribution is obtained by applying a unit rotation at critical sections 1 and 4 and restraining

displacement at all other critical sections (as shown in Fig. 2.4(a)). Maintaining zero displacement at critical sections 2 and 3 introduces a set of external forces at these nodes. In order to eliminate these forces, we apply the external forces to the original structure (i.e., the one with no plastic hinges and no restraint at any critical section, Fig. 2.4(b)), and subtract the resulting internal stresses from the one shown in Fig. 2.4(a) . Now, the internal moment distribution of Fig. 2.4(c) only resists the unit rotations introduced at the plastic hinges (i.e., it is self-equilibrating).

The overall behavior of the structure can be formulated as follows: Prior to the formation of plastic hinges, the structure resists the applied external forces. Therefore, the moment distribution is a multiple of the elastic moment distribution:

$$\mathbf{M} = \mathbf{M}_{elastic}\, s \tag{2.1}$$

where s = load factor, $s \leq s_{elastic\ limit}$

Subsequent to the formation of plastic hinges, the original structure supports new increments of applied external forces plus increments of plastic deformation that accumulate at the plastic hinges. Therefore, the change in moment distribution can be expressed as

$$\Delta\mathbf{M} = \mathbf{M}_{elastic}\, \Delta s + \mathbf{M}_{self-equilibrating}\, \Delta\theta \tag{2.2}$$

where Δs = change in the applied load factor

$\Delta\theta$ = change in the plastic deformation.

Now, the analysis can be continued by determining the location of the next plastic hinge. This can be accomplished by solving Equation (2.2) for the minimum value of Δs that will drive one of the remaining critical sections to its plastic moment capacity.

Prior to solving Equation (2.2), we must evaluate the left hand side of the equation (the change in moment distribution, $\Delta\mathbf{M}$). Consider the moment

distribution at the elastic limit $\mathbf{M}^{t}_{elastic\ limit} = \begin{bmatrix} -M_p & 0.5M_p & 0.5M_p & -M_p \end{bmatrix}$ (see Fig. 2.3). If we locate the state of stress at every cross section on the force-deformation curves of Fig. 2.5, we can measure the extra resistance that each section can tolerate before its plastic moment capacity is reached. Since the vector $\Delta\mathbf{M}^{t} = \begin{bmatrix} 0 & 0.5M_p & 0.5M_p & 0 \end{bmatrix}$ represents the maximum allowable change in cross-sectional moment, we can use it on the left hand side of Equation (2.2):

$$\begin{bmatrix} 0 \\ 0.5M_p \\ 0.5M_p \\ 0 \end{bmatrix} \geq \begin{bmatrix} -\frac{1}{12}WL^2 \\ \frac{1}{24}WL^2 \\ \frac{1}{24}WL^2 \\ -\frac{1}{12}WL^2 \end{bmatrix} \Delta s + \begin{bmatrix} 2\frac{EI}{L} \\ 2\frac{EI}{L} \\ 2\frac{EI}{L} \\ 2\frac{EI}{L} \end{bmatrix} \Delta\theta \qquad (2.3)$$

Equation (2.3) can be reduced to the following set of independent relations:

$$\begin{bmatrix} 0 \\ 0.5M_p \end{bmatrix} \geq \begin{bmatrix} -\frac{1}{12}WL^2 \\ \frac{1}{24}WL^2 \end{bmatrix} \Delta s + \begin{bmatrix} 2\frac{EI}{L} \\ 2\frac{EI}{L} \end{bmatrix} \Delta\theta \qquad (2.4)$$

The inequality in Equation (2.4) actually applies to the critical sections that have not reached their plastic moment capacity. Since the first relation represents the balance of forces at the active plastic hinges 1 and 4, it must be satisfied as the equality [†]:

$$0 = -\frac{1}{12}WL^2\,\Delta s + 2\frac{EI}{L}\,\Delta\theta \qquad (2.5)$$

[†] This relation is satisfied with an inequality only when the critical sections 1 and 4 are unloading. For a detailed discussion of this topic, refer to Chapters 3 and 5.

We can solve Equation (2.5) for $\Delta\theta$:

$$\Delta\theta = \frac{1}{24}\frac{WL^3}{EI}\Delta s \tag{2.6}$$

and eliminate $\Delta\theta$ from the remaining relation in (2.4):

$$0.5M_p \geq \frac{1}{24}WL^2\,\Delta s + \frac{1}{12}WL^2\,\Delta s \tag{2.7}$$

An increase of $\Delta s = 4\dfrac{M_p}{WL^2}$ in the applied load factor will induce plastic hinges at critical sections 2 and 3. It is clear from Fig. 2.6 and the following internal moment distribution that a collapse mechanism has formed in the structure:

$$\mathbf{M} = \mathbf{M}_{elastic\ limit} + \Delta\mathbf{M} = \begin{bmatrix} -M_p \\ 0.5M_p \\ 0.5M_p \\ -M_p \end{bmatrix} + \begin{bmatrix} 0 \\ 0.5M_p \\ 0.5M_p \\ 0 \end{bmatrix} = \begin{bmatrix} -M_p \\ M_p \\ M_p \\ -M_p \end{bmatrix} \tag{2.8}$$

But rather than screening the moment distribution to detect the collapse mechanism, we can continue the analysis by solving for the self-equilibrating internal stresses that resist rotation at the new plastic hinges (critical sections 2 and 3) [see Fig. 2.7(c)]:

$$\mathbf{M}^{t}_{self-equilibrating} = \begin{bmatrix} \dfrac{EI}{L} & \dfrac{EI}{L} & \dfrac{EI}{L} & \dfrac{EI}{L} \end{bmatrix} \tag{2.9}$$

Equation (2.2) can now be updated as follows:

$$\Delta\mathbf{M} = \mathbf{M}_{elastic}\,\Delta s + \mathbf{M}_{s_1}\,\Delta\theta_1 + \mathbf{M}_{s_2}\,\Delta\theta_2 \tag{2.10}$$

where $\mathbf{M}_{s_1}$ and $\mathbf{M}_{s_2}$ represent the self-equilibrating stresses that resist plastic rotations at sections 1 and 4 and sections 2 and 3, respectively. Substituting the actual values for the internal stress vectors in Equation (2.10), we obtain:

$$\Delta \mathbf{M} = \begin{bmatrix} -\frac{1}{12}WL^2 \\ \frac{1}{24}WL^2 \\ \frac{1}{24}WL^2 \\ -\frac{1}{12}WL^2 \end{bmatrix} \Delta s + \begin{bmatrix} 2\frac{EI}{L} \\ 2\frac{EI}{L} \\ 2\frac{EI}{L} \\ 2\frac{EI}{L} \end{bmatrix} \Delta\theta_1 + \begin{bmatrix} \frac{EI}{L} \\ \frac{EI}{L} \\ \frac{EI}{L} \\ \frac{EI}{L} \end{bmatrix} \Delta\theta_2 \qquad (2.11)$$

It is obvious that Equation (2.11) does not have a unique solution because the self-equilibrating moments are not independent. At this stage, the structure may undergo some plastic deformation ($\Delta\theta_1 = 1$, $\Delta\theta_2 = -2$) even though there may be no increase in the applied load (i.e. $\Delta s = 0$). This is the criterion that actually determines the collapse mechanism.

In this example, it is clearly illustrated how the elastoplastic analysis can be carried out without updating the stiffness matrix of the structure. The primary advantage of this method compared to classical methods is that rather than updating and inverting the stiffness matrix (a process which basically requires N^2M numerical operations, where N and M denote the number of degrees of freedom and the band width of the structure stiffness matrix, respectively), a pattern of self-equilibrating stresses that resist the plastic deformation is computed (this process requires NM numerical operations). A complete analytical formulation of this method will be presented in chapter 3. In the next section, the mechanical model of some typical elements will be briefly described.

2.2 Types of Elements

The analytical model of the structure consists of two kinds of elements: frame elements and finite elements.

Frame elements are typically used to model prismatic one-dimensional

members. A structure made of prismatic members is usually discretized into a number of elements connected by nodes. A node must be provided at the intersection of two or more members or at the critical section of the span. A mechanical model of a frame element is shown in Fig. 2.1 . It consists of an elastic member with plastic deformation concentrated at its two far ends. Plastic hinges at the ends of members can provide for any type of plastic deformation: e.g., axial, flexural, torsional, or any combination of these.

Finite elements are generally used to model continuum problems. Here, the discussion of finite elements is confined to plane stress elements that are suitable for the analysis of reinforced concrete plate elements. The major concern in modeling these elements is in the treatment of cracking. Two basically different approaches are used to model the development of cracks [6]. Cracks can be treated either as discrete individual cracks between concrete elements or as distributed cracks within the element.

In the discrete method, a crack is formed by detaching elements at their boundaries as shown in Fig. 2.8 . This method offers the advantages that the displacement at a crack can be calculated and effects such as aggregate interlock and dowel action can be accounted for by providing link elements between the concrete elements and the reinforcing bars. However, this model is quite complicated and one of its major drawbacks is that additional degrees of freedom must be introduced each time a crack forms.

In the distributed crack model, the element is generally divided into a number of layers as shown in Fig. 2.9 . Each layer is in a state of plane stress and may have different material properties corresponding to the material it represents. The reinforcement is generally modeled as anisotropic layers in which the material properties are assumed to be smeared or distributed over the whole element. The concrete is modeled as an isotropic material under biaxial stresses. In this method,

cracking is treated as a phenomenon similar to plastic deformation and the full bond between the reinforcement and the concrete is enforced through compatibility at the nodes.

Because of the complications involved in using discrete crack modeling, the distributed crack model is adopted to represent the reinforced concrete element. In this model, cracking progresses from one integration point to the next similar to the yielding of an element. This method has the advantage of permitting the use of the same structural nodal-point topology throughout the entire nonlinear solution. But it does not provide a measure of crack width to be used in simulating the effect of aggregate interlock and dowel action.

3. FUNDAMENTALS OF ELASTOPLASTIC ANALYSIS

In this chapter, the nonlinear analysis of the structure is formulated with reference to two different material behavior: reversible nonlinear behavior (holonomic behavior), and irreversible nonlinear behavior (nonholonomic behavior). In particular, holonomic behavior implies that the analysis is independent of the loading history, whereas nonholonomic behavior implies that the analysis is dependent on the loading history.

The analytical formulations of these problems are derived assuming the associated flow rule, the piecewise-linearized yield condition, and the small-displacement theory. In the final formulation, both problems are cast as a Linear Complementarity problem or an equivalent Quadratic Programming problem. Full details of the material presented here may be found in references 7, 8, 9, and 10.

3.1 Constitutive Laws for Holonomic Behavior

We will introduce the inelastic constitutive law with reference to a beam cross section where the behavior is characterized by a single force component (moment) and a single deformation component (curvature). Later in the chapter, we will describe the general constitutive laws for a multi-component force-deformation relationship.

3.1.1 Constitutive Laws for a Single Stress Component

It will be convenient first to consider the elastic-perfectly plastic moment-curvature relationship of Fig. 3.1 . The plastic moment capacity of section i will be denoted by R_i^+ and R_i^- and the elastic stiffness by k_i . The feasible stress region is described by the inequality:

$$-R_i^- \le M_i \le R_i^+ \tag{3.1}$$

Another way of expressing the same relation is to introduce two yield functions,

$$\phi_i^+ \leq 0 \quad \text{and} \quad \phi_i^- \leq 0 \tag{3.2}$$

defined as follows:

$$\phi_i^+ = M_i - R_i^+ \leq 0 \tag{3.3a}$$

$$\phi_i^- = -M_i - R_i^- \leq 0 \tag{3.3b}$$

where $\phi_i^+ = 0$ (or $\phi_i^- = 0$) indicates that the positive (or the negative) yield mode has been activated. To measure the intensity of the activation of the yield surfaces, two plastic multipliers are introduced:

$$\lambda_i^+ \geq 0 \quad , \quad \lambda_i^- \geq 0 \tag{3.4}$$

The plastic elongation (θ_i^p) can now be expressed in terms of the plastic multipliers λ_i:

$$\theta_i^p = \lambda_i^+ - \lambda_i^- \tag{3.5}$$

It is obvious that a plastic multiplier has a positive value ($\lambda_i > 0$) only if the particular yield mode is activated ($\phi_i^+ = 0$), and it must be zero ($\lambda_i^+ = 0$) when the element is in the elastic range ($\phi_i^+ < 0$). This relationship between the plastic multiplier (λ) and the plastic function (ϕ) expresses the holonomic (reversible) hypothesis and can be condensed as follows:

$$\phi_i^+ \lambda_i^+ = 0 \quad , \quad \phi_i^- \lambda_i^- = 0 \tag{3.6}$$

We can also describe the elastic range of the moment-curvature relationship by the following relation:

$$M_i = k_i \theta_i^e \quad or \quad \theta_i^e = k_i^{-1} M_i \tag{3.7}$$

where k_i and θ_i^e represent the elastic stiffness and the elastic curvature.

In order to express relations (3.2) to (3.7) in a condensed form, the following four vectors are introduced:

$$\phi_i = \begin{bmatrix} \phi^+ \\ \phi^- \end{bmatrix} \quad , \quad \lambda_i = \begin{bmatrix} \lambda^+ \\ \lambda^- \end{bmatrix} \quad , \quad \mathbf{R}_i = \begin{bmatrix} R^+ \\ R^- \end{bmatrix} \quad , \quad \mathbf{n}_i^t = \begin{bmatrix} 1 \\ -1 \end{bmatrix} \tag{3.8}$$

The first three vectors correspond to the yield function, the plastic multiplier, and the plastic resistance vector. The last vector represents the outward unit normal to the yield planes.

Finally, equations (3.2) to (3.7) may be expressed as follows:

$$\phi_i = \mathbf{n}_i^t M_i - \mathbf{R}_i \qquad \phi_i \le 0 \qquad \lambda_i \ge 0 \tag{3.9a,b,c}$$

$$\phi_i^t \lambda_i = 0 \qquad \theta_i^p = \mathbf{n}_i \lambda_i \qquad \theta_i^e = k_i^{-1} M_i \tag{3.9d,e,f}$$

$$\theta_i = \theta_i^e + \theta_i^p \tag{3.9g}$$

Now, let us consider the behavior of section i when the moment-curvature relationship has been approximated by elastic-linear work-hardening behavior as shown in Fig. 3.2 . If we introduce a hardening parameter, H, for each yield mode such that $H_1^+\lambda_1^+$ measures the extra resistance sustained as a result of activation of yield mode 1, the yield functions will read:

$$\begin{aligned} \phi_1^+ &= M - R_1^+ - H_1^+\lambda_1^+ \le 0 \\ \phi_2^+ &= M - R_2^+ - H_2^+\lambda_2^+ \le 0 \\ \phi_1^- &= -M - R_1^- - H_1^-\lambda_1^- \le 0 \end{aligned} \tag{3.10}$$

The hardening parameters, H_1^+, H_2^+, and H_1^- can be determined from the strain hardening stiffnesses, k_1^+, k_2^+, and k_1^- and the elastic stiffness k_o:

$$\frac{1}{H_1^+} = \frac{1}{k_1^+} - \frac{1}{k_o}$$

$$\frac{1}{H_2^+} = \frac{1}{k_2^+} - \frac{1}{k_1^+}$$
$$\frac{1}{H_1^-} = \frac{1}{k_1^-} - \frac{1}{k_o} \tag{3.11}$$

The derivation of equations (3.11) is given in Appendix A. All the other equations (3.9b,c,d,e,f,g) for the perfectly plastic case still hold. However, the vectors defined in equation (3.8) must reflect the three yield modes:

$$\phi_i = \begin{bmatrix} \phi_1^+ \\ \phi_2^+ \\ \phi_1^- \end{bmatrix} \quad , \quad \lambda_i = \begin{bmatrix} \lambda_1^+ \\ \lambda_2^+ \\ \lambda_1^- \end{bmatrix} \quad , \quad \mathbf{R}_i = \begin{bmatrix} R_1^+ \\ R_2^+ \\ R_1^- \end{bmatrix} \quad , \quad \mathbf{n}_i^t = \begin{bmatrix} 1 \\ 1 \\ -1 \end{bmatrix} \tag{3.12}$$

With the aid of the hardening matrix, $\mathbf{H}_i$,

$$\mathbf{H}_i = \begin{bmatrix} H_1^+ & 0 & 0 \\ 0 & H_2^+ & 0 \\ 0 & 0 & H_1^- \end{bmatrix} \tag{3.13}$$

the constitutive relations for the linear hardening case can be expressed as follows:

$$\phi_i = \mathbf{n}_i^t M_i - \mathbf{H}_i \lambda_i - \mathbf{R}_i \quad , \quad \phi_i \leq 0 \quad , \quad \lambda_i \geq 0$$
$$\phi_i^t \lambda_i = 0 \quad , \quad \theta_i^p = \mathbf{n}_i \lambda_i \quad , \quad \theta_i^e = k_i^{-1} M_i \tag{3.14}$$
$$\theta_i = \theta_i^e + \theta_i^p$$

3.1.2 Constitutive Laws for Two Stress Components

Let us now consider the beam-column cross section i where the moment-axial load ($M-P$) relationship has been defined by the polygon of Fig. 3.3 . The orthogonal distances from the origin to the yield surfaces (sides of the polygon) measure the plastic capacity of the yield modes:

$$\mathbf{R}_i^t = \left[R_1 \, , R_2 \, , R_3 \, , R_4 \, , R_5 \, , R_6 \right] \tag{3.15}$$

The outward unit normal to each surface is defined in terms of the two components oriented along the moment and axial load axis:

$$\mathbf{n}_i = \begin{bmatrix} n_1^M & n_2^M & n_3^M & n_4^M & n_5^M & n_6^M \\ n_1^P & n_2^P & n_3^P & n_4^P & n_5^P & n_6^P \end{bmatrix} \tag{3.16}$$

Let $\mathbf{S}_i^t = \left[M_i \, , P_i \right]$ denote the stress resultant vector where M_i and P_i are the bending moment and the axial force active at cross section i; then, we can express the yield function ϕ for the perfectly plastic case as follows:

$$\phi_i = \mathbf{n}_i^t \, \mathbf{S}_i - \mathbf{R}_i \leq 0 \tag{3.17}$$

The total strain vector, $\mathbf{s}_i^t = \left[\theta_i \, , \delta_i \right]$, representing the total curvature θ_i and axial extension δ_i corresponding to M_i and P_i can be expressed as the sum of the elastic and plastic strain:

$$\mathbf{s}_i = \mathbf{e}_i + \mathbf{p}_i \tag{3.18}$$

where the elastic strain is derived from the stress vector, $\mathbf{S}_i$:

$$\mathbf{e}_i = \mathbf{k}_i^{-1} \mathbf{S}_i \tag{3.19}$$

and the plastic strain is determined from the normality rule:

$$\mathbf{p}_i = \mathbf{n}_i \lambda_i \tag{3.20}$$

The components of vector $\lambda_i^t = \left[\lambda_1 \, , \lambda_2 \, , \lambda_3 \, , \lambda_4 \, , \lambda_5 \, , \lambda_6 \right]$ measure the intensity of activation of each yield mode. Since the stress point can only lie either on a particular yield mode or at the intersection of two yield modes, there can be at most two nonzero components of the plastic multiplier (for example, if $\lambda_1 > 0$ and

$\lambda_6 > 0$, then $\lambda_2 = \lambda_3 = \lambda_4 = \lambda_5 = 0$).

Finally, we include the holonomy hypothesis, that for each yield surface, at least one of the two variables λ^j or ϕ^j must be zero; either the yield mode j is not activated ($\phi^j < 0$ and $\lambda^j = 0$) or there exists plastic strain due to its activation ($\lambda^j > 0$ and $\phi^j = 0$)

$$\phi^j \lambda^j = 0 \qquad (3.21)$$

for all yield surfaces j = 1,2,3,4,5,6.

We can also introduce the vector $\phi_i = \left[\phi_1 \ , \ \phi_2 \ , \ \phi_3 \ , \ \phi_4 \ , \ \phi_5 \ , \ \phi_6 \right]$ and write equation (3.21) in a more compact form:

$$\phi_i^t \ \lambda_i = 0 \qquad (3.22)$$

Putting equations (3.17) through (3.21) together, we have the constitutive laws for the perfectly plastic case:

$$\begin{gathered} \phi_i = \mathbf{n}_i^t \, \mathbf{S}_i - \mathbf{R}_i \quad , \quad \phi_i \le 0 \quad , \quad \lambda_i \ge 0 \\ \phi_i^t \ \lambda_i = 0 \quad , \quad \mathbf{p}_i = \mathbf{n}_i \lambda_i \quad , \quad \mathbf{e}_i = \mathbf{k}_i^{-1} \mathbf{S}_i \\ \mathbf{s}_i = \mathbf{e}_i + \mathbf{p}_i \end{gathered} \qquad (3.23)$$

Comparing equations (3.9) to (3.23), it is obvious that the constitutive laws for the single stress component and the two stress components are identical except for dimensions of the vectors and matrices which must be consistent with the number of yield planes and the number of stress resultant components. Therefore, there is no need to reformulate the constitutive laws for the multi-stress component; equation (3.23) derived for the two-stress component applies to the multi-stress component as well.

It only remains to include the linear work-hardening behavior in the constitutive laws of equation (3.23). Linear hardening implies that the yield

surfaces translate (*not* rotate) through the space domain.

Two different linear hardening models [9] are shown in Fig. 3.4 . In one case, the activation of yield surface j will only increase the magnitude of the plastic capacity, R_j, by $H_j\lambda_j$ and the remaining yield modes are not affected. Here, the hardening matrix, $\mathbf{H}_i$, is diagonal:

$$\mathbf{H}_i = \begin{bmatrix} H_1 & 0 & 0 & 0 & 0 & 0 \\ 0 & H_2 & 0 & 0 & 0 & 0 \\ 0 & 0 & H_3 & 0 & 0 & 0 \\ 0 & 0 & 0 & H_4 & 0 & 0 \\ 0 & 0 & 0 & 0 & H_5 & 0 \\ 0 & 0 & 0 & 0 & 0 & H_6 \end{bmatrix} \tag{3.24}$$

In the second case, the activation of yield surface j will change the plastic capacity of all other yield modes as well. This can be represented by including off-diagonal terms in the hardening matrix. In general, a positive hardening coefficient indicates an outward translation of the yield mode and a negative hardening coefficient indicates an inward translation of the yield mode.

It should only be emphasized that for all cases of linear hardening, the plastic potential function can be expressed as follows:

$$\phi_i = \mathbf{n}_i^t\, \mathbf{S}_i - \mathbf{H}_i\lambda_i - \mathbf{R}_i \le 0 \tag{3.25}$$

Therefore, the constitutive laws for the elastic-linear hardening behavior for cross section i may be described by:

$$\begin{gathered} \phi_i = \mathbf{n}_i^t\, \mathbf{S}_i - \mathbf{H}_i\lambda_i - \mathbf{R}_i \quad , \quad \phi_i \le 0 \quad , \quad \lambda_i \ge 0 \\ \phi_i^t\, \lambda_i = 0 \quad , \quad \mathbf{p}_i = \mathbf{n}_i\lambda_i \\ \mathbf{e}_i = \mathbf{k}_i^{-1}\mathbf{S}_i \quad , \quad \mathbf{s}_i = \mathbf{e}_i + \mathbf{p}_i \end{gathered} \tag{3.26}$$

3.2 Constitutive Laws for Nonholonomic Behavior

In this section, the constitutive laws for the material behavior that demonstrate irreversible plastic deformations are formulated. The laws governing the nonholonomic behavior will be derived with reference to the elastic-linear hardening behavior of the beam cross section i (Fig. 3.5).

When the stress point p is on a particular yield mode j ($\phi_j = 0$), a small increase in applied loads will either increase the activation intensity by $\Delta\lambda_j \geq 0$ such that the stress point remains on the yield mode j, i.e. $\Delta\phi_j = 0$, or the yield surface j is unloaded in which case $\Delta\phi_j < 0$ and $\Delta\lambda_j = 0$. In other words, the nonholonomy hypothesis requires that:

$$\Delta\phi_j \, \Delta\lambda_j = 0 \tag{3.27}$$

$$\text{and} \quad \phi_j \, \Delta\lambda_j = 0 \tag{3.28}$$

The second relationship is required to show that the stress point must be on the particular yield mode ($\phi_j = 0$) in order to increase the activation intensity ($\Delta\lambda_j > 0$). The first relation simply states that once a yield surface has been activated, it is possible either to increase the activation intensity ($\Delta\lambda_j > 0$, in which case $\Delta\phi_j = 0$) or to unload the yield mode ($\Delta\phi_j < 0$, in which case $\Delta\lambda_j = 0$).

If we consider the holonomic relation for the plastic function ϕ

$$\phi_i = \mathbf{n}_i^t \, \mathbf{S}_i - \mathbf{H}_i\lambda_i - \mathbf{R}_i \leq 0 \tag{3.29}$$

the corresponding difference relationship becomes

$$\Delta\phi_i = \mathbf{n}_i^t \, \Delta\mathbf{S}_i - \mathbf{H}_i\Delta\lambda_i \leq 0 \tag{3.30}$$

The vector of plastic resistances $\mathbf{R}_i$ does not appear in this relation because it is constant. Similarly, the difference counterpart of the remaining relations (3.26) can

be written as follows:

$$\Delta \mathbf{p}_i = \mathbf{n}_i \Delta\lambda_i \tag{3.31}$$

$$\Delta \mathbf{e}_i = \mathbf{k}_i^{-1} \Delta \mathbf{S}_i \tag{3.32}$$

$$\Delta \mathbf{s}_i = \Delta \mathbf{p}_i + \Delta \mathbf{e}_i \tag{3.33}$$

Now, the constitutive laws for the nonholonomic behavior can be expressed as follows:

$$\begin{gathered} \Delta\phi_i = \mathbf{n}_i^t \, \Delta \mathbf{S}_i - \mathbf{H}_i \Delta\lambda_i \quad , \quad \phi_i + \Delta\phi_i \le 0 \quad , \quad \Delta\lambda_i \ge 0 \\ \Delta\phi_i^t \, \Delta\lambda_i = 0 \quad , \quad \phi_i^t \, \Delta\lambda_i = 0 \\ \Delta \mathbf{p}_i = \mathbf{n}_i \Delta\lambda_i \quad , \quad \Delta \mathbf{e}_i = \mathbf{k}_i^{-1} \Delta \mathbf{S}_i \quad , \quad \Delta \mathbf{s}_i = \Delta \mathbf{e}_i + \Delta \mathbf{p}_i \end{gathered} \tag{3.34}$$

It is important to emphasize that the nonholonomic constitutive laws are only essential for the active yield modes. For the remaining (inactive) yield modes, the holonomy hypothesis applies (when a yield surface is inactive, the stress point lies in the elastic range of that yield mode and the elastic behavior is generally assumed to be reversible.).

So far, the constitutive laws that govern the elastoplastic behavior of a cross section have been discussed. In the following section, the constitutive laws along with the equilibrium and compatibility relations that govern the behavior of a frame element are formulated, and these relations are also extended over all elements to describe the behavior of the entire structure.

3.3 Holonomic Analysis

The plastic behavior of a frame element *e* is assumed to be confined to its end sections *i* and *k* (Fig. 3.6(a)). For a general frame element, the state of stress at the ends of the member is defined in terms of the twelve components of the stress resultant shown in Fig. 3.6(b) . However, if the element is in equilibrium, only six of the twelve components will be independent. These independent stress

components which ensure equilibrium along the length of the member are called the natural stress resultant. The natural plastic deformation of Fig. 3.6(c) is similarly derived from the plastic deformation of Fig. 3.6(b) by excluding the rigid body motion of the element.

In the previous sections, the constitutive laws were expressed as a function of the active stress resultant (and active deformation) at a cross section. If we relate the active stress resultant (and deformation) at element end sections to the natural stress resultant (and deformation), we can express the constitutive laws of the element in terms of its natural stress resultant (and deformation). This is essential because the compatibility and equilibrium conditions are generally expressed in terms of natural quantities.

Consider the planar beam-column element of Fig. 3.6(d). The active stress resultant $\mathbf{S}^t = \left[\mathbf{S}_i^t \, , \, \mathbf{S}_k^t \right]$ are related to the natural stress resultant $\mathbf{Q}^t = \left[Q_1 \, , \, Q_3 \, , \, Q_5 \right]$ by the following relation:

$$\mathbf{S} = \begin{bmatrix} \mathbf{S}_i \\ \mathbf{S}_k \end{bmatrix} = \left[\begin{array}{c} S_1 \\ S_2 \\ \hline S_3 \\ S_4 \end{array}\right] = \begin{bmatrix} 1 & 0 & 0 \\ 0 & 1 & 0 \\ 1 & 0 & 0 \\ 0 & 0 & 1 \end{bmatrix} \begin{bmatrix} Q_1 \\ Q_3 \\ Q_5 \end{bmatrix} \tag{3.35}$$

For the biaxial beam-column element of Fig. 3.6(e), a similar relation can be written as follows:

$$\mathbf{S} = \left[\begin{array}{c} S_1 \\ S_2 \\ S_3 \\ \hline S_4 \\ S_5 \\ S_6 \end{array}\right] = \begin{bmatrix} 1 & 0 & 0 & 0 & 0 & 0 \\ 0 & 0 & 1 & 0 & 0 & 0 \\ 0 & 0 & 0 & 1 & 0 & 0 \\ 1 & 0 & 0 & 0 & 0 & 0 \\ 0 & 0 & 0 & 0 & 1 & 0 \\ 0 & 0 & 0 & 0 & 0 & 1 \end{bmatrix} \begin{bmatrix} Q_1 \\ Q_2 \\ Q_3 \\ Q_4 \\ Q_5 \\ Q_6 \end{bmatrix} \tag{3.36}$$

Any combination of active stress resultant, e.g. axial load + shear as in Fig. 3.6(f), can be related to the corresponding natural stress component:

$$\mathbf{S} = \begin{bmatrix} S_1 \\ S_2 \\ \hline S_3 \\ S_4 \end{bmatrix} = \begin{bmatrix} 1 & 0 & 0 \\ 0 & \frac{1}{L} & -\frac{1}{L} \\ 1 & 0 & 0 \\ 0 & \frac{1}{L} & -\frac{1}{L} \end{bmatrix} \begin{bmatrix} Q_1 \\ Q_3 \\ Q_5 \end{bmatrix} \tag{3.37}$$

We can generalize the above relations by introducing the static transformation matrix, **B**:

$$\mathbf{S} = \mathbf{B}\,\mathbf{Q} \tag{3.38}$$

Similarly, the corresponding kinematic relation between the active deformations, **s**, and the natural deformation, **q**, can be expressed as follows:

$$\mathbf{q} = \mathbf{B}^t\mathbf{s} \tag{3.39}$$

Now, if we have the yield condition for frame element e in terms of the active stress resultant $\mathbf{S}^t = \left[\, \mathbf{S}_i^t \,,\, \mathbf{S}_k^t \,\right]$ at the end sections i and k:

$$\phi^e = \begin{bmatrix} \phi_i \\ \hline \phi_k \end{bmatrix} = \begin{bmatrix} \mathbf{n}_i^t & 0 \\ 0 & \mathbf{n}_k^t \end{bmatrix} \begin{bmatrix} \mathbf{S}_i \\ \hline \mathbf{S}_k \end{bmatrix} - \begin{bmatrix} \mathbf{H}_i & 0 \\ 0 & \mathbf{H}_k \end{bmatrix} \begin{bmatrix} \lambda_i \\ \hline \lambda_k \end{bmatrix} - \begin{bmatrix} \mathbf{R}_i \\ \hline \mathbf{R}_k \end{bmatrix}$$

$$\phi^e = \mathbf{n}^{et}\mathbf{S}^e - \mathbf{H}^e\lambda^e - \mathbf{R}^e \le 0 \tag{3.40}$$

We can replace the active stress resultant by expression (3.38) and obtain the yield condition in terms of the natural stress resultant:

$$\phi^e = \mathbf{n}^{et}\mathbf{B}^e\mathbf{Q}^e - \mathbf{H}^e\lambda^e - \mathbf{R}^e \le 0 \tag{3.41}$$

The plastic flow rule for frame element e can also be expressed in terms of the active plastic deformation $\mathbf{p}_s^t = \left[\, \mathbf{p}_{s_i}{}^t \,,\, \mathbf{p}_{s_k}{}^t \,\right]$ at the end sections i and k:

$$\mathbf{p}_s = \begin{bmatrix} \mathbf{p}_{s_i} \\ \hline \mathbf{p}_{s_k} \end{bmatrix} = \begin{bmatrix} \mathbf{n}_i & 0 \\ 0 & \mathbf{n}_k \end{bmatrix} \begin{bmatrix} \lambda_i \\ \hline \lambda_k \end{bmatrix} = \mathbf{n}^e\lambda^e \tag{3.42}$$

Using relation (3.39), we can obtain the plastic flow rule in terms of the natural plastic deformation $\mathbf{p}_q$:

$$\mathbf{p}_q^e = \mathbf{B}^{e\,t}\mathbf{p}_s^e = \mathbf{B}^{e\,t}\mathbf{n}^e\lambda^e \tag{3.43}$$

Equations (3.41) and (3.43) can be written in a compact form if we set $\mathbf{B}^{e\,t}\mathbf{n}^e = \mathbf{N}^e$:

$$\phi^e = \mathbf{N}^{e\,t}\mathbf{Q}^e - \mathbf{H}^e\lambda^e - \mathbf{R}^e \le 0 \tag{3.44}$$

$$\mathbf{p}_q^e = \mathbf{N}^e\lambda^e \tag{3.45}$$

Finally, the constitutive laws for an elastic-linear hardening behavior of frame element e can be expressed as:

$$\begin{gathered}\phi^e = \mathbf{N}^{e\,t}\mathbf{Q}^e - \mathbf{H}^e\lambda^e - \mathbf{R}^e \quad , \quad \phi^e \le 0 \quad , \quad \lambda^e \ge 0 \\ \phi^{e\,t}\lambda^e = 0 \quad , \quad \mathbf{p}^e = \mathbf{N}^e\lambda^e \\ \mathbf{e}^e = \mathbf{k}^{e-1}\,\mathbf{Q}^e \quad , \quad \mathbf{q}^e = \mathbf{e}^e + \mathbf{p}^e\end{gathered} \tag{3.46}$$

For a structure composed of m elements, the constitutive laws for the (unassembled) structure can be obtained by extending equations (3.46) over all elements:

$$\phi = \mathbf{N}^t\mathbf{Q} - \mathbf{H}\,\lambda - \mathbf{R} \quad , \quad \phi \le 0 \quad , \quad \lambda \ge 0 \tag{3.47a,b,c}$$

$$\phi^t\lambda = 0 \quad , \quad \mathbf{p} = \mathbf{N}\,\lambda \tag{3.47d,e}$$

$$\mathbf{e} = \mathbf{k}^{-1}\,\mathbf{Q} \quad , \quad \mathbf{q} = \mathbf{e} + \mathbf{p} \tag{3.47f,g}$$

where the vectors $\mathbf{Q}$, $\mathbf{q}$, $\mathbf{e}$, $\mathbf{p}$, ϕ, λ, and $\mathbf{R}$ contain the corresponding vectors for the m individual frame elements in a particular order, and $\mathbf{N}$, $\mathbf{H}$, and $\mathbf{k}$ are the block-diagonal matrices of the element matrices $\mathbf{N}^e$, $\mathbf{H}^e$, and $\mathbf{k}^e$.

The global displacement vector, $\mathbf{u}$, and the corresponding external load vector, $\mathbf{F}$, identified at the nodal degrees of freedom for the assembled structure are now introduced. The natural deformation vector, $\mathbf{q}^e$, for frame element e is geometrically related to the global displacement vector, $\mathbf{u}$, through the compatibility

matrix, C^e:

$$\mathbf{q}^e = \mathbf{C}^e\mathbf{u} \tag{3.48}$$

Equation (3.48) can be extended over all elements of the structure to obtain the compatibility condition for the assembled structure:

$$\mathbf{q} = \mathbf{C}\ \mathbf{u} \tag{3.49}$$

where the matrix C is the block-column matrix of the compatibility matrix, C^e, for the m individual elements.

Similarly, the equilibrium conditions for the assembled structure can also be stated as follows:

$$\mathbf{C}^t\mathbf{Q} = \mathbf{F} \tag{3.50}$$

Equations (3.47), (3.49), and (3.50) fully govern the elastoplastic holonomic behavior of the structure. If we ignore equations (3.47a) through (3.47e), the remaining equations express the linear elastic behavior of the structure when it is subjected to an external force F and an initial strain p.

$$\mathbf{e} = \mathbf{k}^{-1}\ \mathbf{Q} \tag{3.47f}$$

$$\mathbf{q} = \mathbf{e} + \mathbf{p} \tag{3.47g}$$

$$\mathbf{q} = \mathbf{C}\ \mathbf{u} \tag{3.49}$$

$$\mathbf{C}^t\mathbf{Q} = \mathbf{F} \tag{3.50}$$

Replacing the vector Q in the equilibrium relations (3.50) with equation (3.47f) and using equation (3.47g) to eliminate elastic deformation, we obtain:

$$\mathbf{C}^t\mathbf{k}\ \mathbf{e} = \mathbf{F} \tag{3.51}$$

$$\mathbf{C}^t\mathbf{k}\ (\ \mathbf{q} - \mathbf{p}\ ) = \mathbf{F} \tag{3.52}$$

The compatibility relation (3.49) can also be used to eliminate the element deformation vector, q:

$$\mathbf{C}^t\mathbf{k}\,\mathbf{C}\,\mathbf{u} - \mathbf{C}^t\mathbf{k}\,\mathbf{p} = \mathbf{F} \tag{3.53}$$

Now, we can solve equation (3.53) for the global displacement, **u**, in terms of the plastic deformation, **p**, and the external load, **F**:

$$\mathbf{u} = \mathbf{K}^{-1}\,(\,\mathbf{F}+\mathbf{C}^t\mathbf{k}\,\mathbf{p}\,) \tag{3.54}$$

where $\mathbf{K} = \mathbf{C}^t\mathbf{k}\,\mathbf{C}$ is the assembled structure stiffness matrix. The element deformation, **q**, and the element stresses, **Q**, can also be determined as follows:

$$\mathbf{q} = \mathbf{C}\,\mathbf{u} = \mathbf{C}\,\mathbf{K}^{-1}\,\mathbf{F} + \mathbf{C}\,\mathbf{K}^{-1}\,\mathbf{C}^t\mathbf{k}\,\mathbf{p} \tag{3.55}$$

$$\mathbf{e} = \mathbf{q} - \mathbf{p} = \mathbf{C}\,\mathbf{K}^{-1}\,\mathbf{F} + \mathbf{C}\,\mathbf{K}^{-1}\,\mathbf{C}^t\mathbf{k}\,\mathbf{p} - \mathbf{p} \tag{3.56}$$

$$\mathbf{Q} = \mathbf{k}\,\mathbf{e} = \mathbf{k}\,\mathbf{C}\,\mathbf{K}^{-1}\,\mathbf{F} + \mathbf{k}\,\mathbf{C}\,\mathbf{K}^{-1}\,\mathbf{C}^t\mathbf{k}\,\mathbf{p} - \mathbf{k}\,\mathbf{p} \tag{3.57}$$

It is obvious that the element stresses are composed of two components: one that resists the external forces,

$$\mathbf{Q}^{el} = \mathbf{k}\,\mathbf{C}\,\mathbf{K}^{-1}\,\mathbf{F} \tag{3.58}$$

and a second component that resists the plastic deformation:

$$\mathbf{Q}^{s} = \mathbf{k}\,\mathbf{C}\,\mathbf{K}^{-1}\,\mathbf{C}^t\mathbf{k}\,\mathbf{p} - \mathbf{k}\,\mathbf{p} = \mathbf{Z}\,\mathbf{p} \tag{3.59}$$

where $\mathbf{Z} = \mathbf{k}\,\mathbf{C}\,\mathbf{K}^{-1}\,\mathbf{C}^t\mathbf{k} - \mathbf{k}$ is the matrix of plastic influence coefficients. Note that the second component is self-equilibrating; this can be easily verified by writing the equilibrium relation (3.50) for each component of the stress vector separately:

$$\mathbf{C}^t\mathbf{Q}^{el} = \mathbf{C}^t\mathbf{k}\,\mathbf{C}\,\mathbf{K}^{-1}\,\mathbf{F} = \mathbf{F} \tag{3.60}$$

$$\mathbf{C}^t\mathbf{Q}^{s} = \mathbf{C}^t\mathbf{k}\,\mathbf{C}\,\mathbf{K}^{-1}\,\mathbf{C}^t\mathbf{k}\,\mathbf{p} - \mathbf{C}^t\mathbf{k}\,\mathbf{p} = 0 \tag{3.61}$$

The global displacement vector, **u**, and the element deformation vector, **q**, can be decomposed into components as well:

$$\mathbf{u} = \mathbf{K}^{-1}\,\mathbf{F} + \mathbf{K}^{-1}\,\mathbf{C}^t\mathbf{k}\,\mathbf{p} = \mathbf{u}^{el} + \mathbf{u}^{p} \tag{3.62}$$

$$\mathbf{q} = \underline{\mathbf{C}\,\mathbf{K}^{-1}\,\mathbf{F}} + \underline{\mathbf{C}\,\mathbf{K}^{-1}\,\mathbf{C}^t\mathbf{k}\,\mathbf{p} - \mathbf{p}} + \underline{\mathbf{p}} = \mathbf{q}^{el} + \mathbf{q}^{ep} + \mathbf{q}^{p} \tag{3.63}$$

Let us now introduce the yield condition (3.47a) and the plastic flow rule (3.47e) along with the following equation for the element stresses:

$$\mathbf{Q} = \mathbf{Q}^{el} + \mathbf{Q}^{s} = \mathbf{Q}^{el} + \mathbf{Z}\mathbf{p} \tag{3.64}$$

$$\phi = \mathbf{N}^t\mathbf{Q} - \mathbf{H}\,\lambda - \mathbf{R} \tag{3.47a}$$

$$\mathbf{p} = \mathbf{N}\,\lambda \tag{3.47e}$$

If we replace $\mathbf{p}$ in equation (3.64) with equation (3.47e) and substitute equation (3.64) for the stress vector, $\mathbf{Q}$, in (3.47a), we obtain:

$$\phi = \mathbf{N}^t(\,\mathbf{Q}^{el} + \mathbf{Z}\,\mathbf{N}\,\lambda\,) - \mathbf{H}\,\lambda - \mathbf{R} = \mathbf{N}^t\mathbf{Q}^{el} + \mathbf{N}^t\mathbf{Z}\,\mathbf{N}\,\lambda - \mathbf{H}\,\lambda - \mathbf{R} \le 0 \tag{3.65}$$

The yield condition (3.65) together with equations (3.47b) through (3.47d) fully govern the nonlinear holonomic response of the structure:

$$\begin{cases} \phi = (\,\mathbf{N}^t\mathbf{Q}^{el} - \mathbf{R}\,) - \mathbf{A}\,\lambda & (3.65) \\ \phi \le 0 \quad , \quad \lambda \ge 0 & (3.47b,c) \\ \phi^t\,\lambda = 0 & (3.47d) \end{cases}$$

where $\mathbf{A} = \mathbf{H} - \mathbf{N}^t\mathbf{Z}\,\mathbf{N}$

This relation set in the unknown vectors ϕ and λ is known in operations research as the Linear Complementarity Problem (L.C.P.).

The matrix $\mathbf{A}$ is symmetric positive-semidefinite if $\mathbf{H}$ is also symmetric positive-semidefinite. This is true because $\mathbf{Z}$ is negative-semidefinite (refer to Appendix B).

When matrix A is symmetric positive-semidefinite, the above L.C.P. can be transformed through the Kuhn-Tucker Theorem to the following dual Quadratic Programming (Q.P.) problems [10]:

$$\begin{cases} \max \quad \lambda^t\,(\,\mathbf{N}^t\mathbf{Q}^{el} - \mathbf{R}\,) - \tfrac{1}{2}\,\lambda^t\mathbf{A}\,\lambda & (3.66) \\ \text{subject to} \quad \lambda \ge 0 \end{cases}$$

$$\begin{cases} \min \quad \tfrac{1}{2}\,\lambda^t\mathbf{A}\,\lambda & (3.67) \\ \text{subject to} \quad \mathbf{A}\,\lambda - (\,\mathbf{N}^t\mathbf{Q}^{el} - \mathbf{R}\,) \ge 0 \end{cases}$$

This property of matrix A ensures that a solution exists for the above L.C.P. problem.

When matrix H is of a general form, a solution may be obtained from the following (possibly non-convex) Quadratic Programming problem [9]:

$$\begin{cases} \min \quad \lambda^t \mathbf{A}\, \lambda - (\mathbf{N}^t \mathbf{Q}^{el} - \mathbf{R})\, \lambda \\ \text{subject to} \quad \mathbf{A}\, \lambda - (\mathbf{N}^t \mathbf{Q}^{el} - \mathbf{R}) \geq 0 \quad \text{and} \quad \lambda \geq 0 \end{cases} \tag{3.68}$$

In this case, a solution exists only if the Q.P. problem has an optimal value of zero.

3.4 Nonholonomic Analysis

The nonholonomic analysis is treated in the same manner as the holonomic analysis. The constitutive laws for the unassembled structure are obtained by extending the nonholonomic laws over all elements that have active yield modes:

$$\begin{gathered} \Delta\phi = \mathbf{N}^t \Delta\mathbf{Q} - \mathbf{H}\, \Delta\lambda \quad , \quad \phi + \Delta\phi \leq 0 \quad , \quad \Delta\lambda \geq 0 \\ \Delta\phi^t \Delta\lambda = 0 \quad , \quad \phi^t \Delta\lambda = 0 \\ \Delta\mathbf{p} = \mathbf{N}\, \Delta\lambda \quad , \quad \Delta\mathbf{e} = \mathbf{k}^{-1} \Delta\mathbf{Q} \quad , \quad \Delta\mathbf{q} = \Delta\mathbf{e} + \Delta\mathbf{p} \end{gathered} \tag{3.69}$$

The compatibility and equilibrium relations for the assembled structure become:

$$\Delta\mathbf{q} = \mathbf{C}\, \Delta\mathbf{u} \tag{3.70}$$

$$\mathbf{C}^t \Delta\mathbf{Q} = \Delta\mathbf{F} \tag{3.71}$$

Now, the corresponding L.C.P. can be obtained by presenting the above relation in terms of the variables $\Delta\phi$ and $\Delta\lambda$:

$$\begin{cases} \Delta\phi = \mathbf{N}^t \Delta\mathbf{Q}^{el} - \mathbf{A}\, \Delta\lambda \\ \phi + \Delta\phi \leq 0 \quad , \quad \Delta\lambda \geq 0 \\ \Delta\phi^t \Delta\lambda = 0 \quad , \quad \phi^t \Delta\lambda = 0 \end{cases} \tag{3.72}$$

Assuming that the matrix $\mathbf{A} = \mathbf{H} - \mathbf{N}^t \mathbf{Z}\, \mathbf{N}$ is symmetric positive-semidefinite, then

the dual Quadratic Programming formulation becomes:

$$\begin{cases} \max \quad \Delta\lambda^t \mathbf{N}^t \Delta\mathbf{Q}^{el} - \tfrac{1}{2}\, \Delta\lambda^t \mathbf{A}\, \Delta\lambda \\ \text{subject to} \quad \Delta\lambda \geq 0 \end{cases} \tag{3.73}$$

$$\begin{cases} \min \quad \tfrac{1}{2}\, \Delta\lambda^t \mathbf{A}\, \Delta\lambda \\ \text{subject to} \quad \mathbf{A}\, \Delta\lambda - \mathbf{N}^t \Delta\mathbf{Q}^{el} \geq 0 \end{cases} \tag{3.74}$$

This concludes the analytical description of the elastoplastic analysis. In chapter 4, the elastoplastic behavior of both frame and finite elements will be discussed; and in chapter 5, the above equations are solved using linear and quadratic programming techniques.

4. STRUCTURAL ELEMENTS

The analytical model of a structure is always described with the aid of a number of elements. In this chapter, the elastoplastic behavior of both the frame elements and the finite elements are discussed.

The frame elements can be of any type. All that is needed to model the elements is the elastic properties and yield conditions that govern the behavior of end sections. Some typical frame elements are considered in this chapter. These include: truss elements, beam elements, and both uniaxial and biaxial beam column elements.

For finite elements, a set of constitutive laws similar to that of frame elements is established. Finite elements can be used to model a variety of structural components. In this chapter, we consider planar elements in general plane stress state in order to model reinforced concrete shear walls.

Two different types of element connection are discussed here as well. The first type is used to model joints between frame elements and the second type is used to join frame elements to finite elements.

4.1 Frame Elements

Frame elements are grouped according to the type of stress component active at a cross section. Here, we will discuss two typical single stress component elements: the truss element (axial force, P), and the beam element (bending moment, M); a two stress component element: the beam-column element (bending moment + axial force); and a three stress component element: the biaxial beam-column element (bending moments about the element y and z axes + axial force). This list can be expanded to include other single and multi-stress component elements in the future.

4.1.1 Truss Elements

Truss elements are only capable of transmitting axial forces. Therefore, the elastic force-deformation relationship is expressed as

$$Q = \frac{EA}{L} q \tag{4.1}$$

where q is the axial extension; Q is the corresponding axial force; E is the elastic (Young's) modulus; A is the element cross-sectional area; and L is the element length.

The yield criterion for the truss element is expressed in terms of a multilinear force-deformation relationship as shown in Fig. 4.1. Since there is no limit on the number of linear hardening branches, different tension and compression axial stiffnesses can be easily modeled (see Fig. 4.1). Similarly, the tension and compression yield surfaces can be of different magnitude, and any hardening rule which results in a symmetric positive semi-definite hardening matrix can be considered.

4.1.2 Beam Elements

Beam elements are only capable of resisting flexural (and shear) deformation. Considering the member end moments to be Q_i and Q_k and the corresponding flexural deformation to be q_i and q_k, the elastic force-deformation relation becomes

$$\begin{bmatrix} Q_i \\ Q_k \end{bmatrix} = \frac{2EI}{L(1+2\beta)} \begin{bmatrix} 2(2+\beta) & (-1+\beta) \\ (-1+\beta) & 2(2+\beta) \end{bmatrix} \begin{bmatrix} q_i \\ q_k \end{bmatrix} \tag{4.2}$$

where I is the moment of inertia and $\beta = \frac{6EI}{L^2 A' G}$ is a parameter that measures the flexural shear deformation. Note that shear deformation is included only when the shear area (A') and the shear modulus (G) are specified; otherwise, the element is

assumed to be infinitely stiff with respect to shear deformations.

The yield conditions for the beam element are expressed in terms of the plastic behavior of its end sections i and k (refer to section 3.3). The plastic resistance vector and the hardening properties specified for each section are totally independent of one another.

$$\phi^e = \begin{bmatrix} \phi_i \\ \hline \phi_k \end{bmatrix} = \begin{bmatrix} \mathbf{n}_i^t & 0 \\ 0 & \mathbf{n}_k^t \end{bmatrix} \begin{bmatrix} \mathbf{S}_i \\ \hline \mathbf{S}_k \end{bmatrix} - \begin{bmatrix} \mathbf{H}_i & 0 \\ 0 & \mathbf{H}_k \end{bmatrix} \begin{bmatrix} \lambda_i \\ \hline \lambda_k \end{bmatrix} - \begin{bmatrix} \mathbf{R}_i \\ \hline \mathbf{R}_k \end{bmatrix}$$

$$\phi^e = \mathbf{n}^{et}\mathbf{S}^e - \mathbf{H}^e\lambda^e - \mathbf{R}^e \leq 0 \tag{3.40}$$

It is interesting to note that due to the general form of the hardening parameters, it is easy to model some of the response characteristics of beam elements. For example, the pinching phenomenon (see Fig. 4.2) observed at the end section of a reinforced concrete beam element during a cyclic loading program, can be easily modeled by considering the following yield surfaces and hardening parameters:

$$\mathbf{R}_i = \begin{bmatrix} M_0^+ \\ M_1^+ \\ M_2^+ \\ M_0^- \\ M_1^- \\ M_2^- \end{bmatrix} \qquad \mathbf{H}_i = \begin{bmatrix} H_0 & 0 & 0 & -H_0 & 0 & 0 \\ 0 & H_1 & 0 & 0 & 0 & 0 \\ 0 & 0 & H_2 & 0 & 0 & 0 \\ -H_0 & 0 & 0 & H_0 & 0 & 0 \\ 0 & 0 & 0 & 0 & H_3 & 0 \\ 0 & 0 & 0 & 0 & 0 & H_4 \end{bmatrix} \tag{4.3}$$

The two yield surfaces M_0^+ and M_0^- (in Fig. 4.2) are provided to model the pinching phenomenon. When the first positive yield surface (characterized by the yield limit M_0^+) is activated ($\lambda_0^+ \geq 0$), the negative yield limit (M_0^-) decreases by $H_0\,\lambda_0^+$, and similarly when the first negative yield surface (M_0^-) is activated ($\lambda_0^- \geq 0$), the

positive yield limit (M_0^+) decreases by $H_0\,\lambda_0^-$.

The remaining yield surfaces (characterized by the yield limit M_1^+, M_2^+, and M_1^- , M_2^-) are provided to model the workhardening behavior of the element during positive and negative loading stages. It is interesting to note that the hardening parameters H_1 and H_3 turn out to be negative quantities, simply because the stiffness of the second positive and negative yield surfaces (k_2^+ and k_2^-) are larger in magnitude than the stiffness of the first yield surfaces (k_1^+ and k_1^-) hence $H_1 = \left[\frac{1}{k_2^+} - \frac{1}{k_1^+} \right]^{-1} \leq 0$ and $H_3 = \left[\frac{1}{k_2^-} - \frac{1}{k_1^-} \right]^{-1} \leq 0$. This might create some problem because then the positive definiteness of matrix $\mathbf{A} = \mathbf{H} - \mathbf{N}^t\,\mathbf{Z}\,\mathbf{N}$ might be jeopardized. In order to circumvent this problem, for the second set of yield surfaces, the activation intensity (λ_2^+, λ_2^-) will be measured in the opposite sense (see Fig. 4.2). This mathematical trick can be provided only for the single stress component elements on the non-interactive yield surfaces.

4.1.3 Beam-Column Elements

The uniaxial and biaxial beam-column elements resist axial, flexural, and shear deformation. In the elastic range, the force-deformation relationships (between the force vector **Q** and the deformation vector **q** are respectively

$$\begin{bmatrix} Q_1 \\ Q_3 \\ Q_5 \end{bmatrix} = \begin{bmatrix} \frac{EA}{L} & 0 & 0 \\ 0 & \frac{4EI(2+\beta)}{L(1+2\beta)} & \frac{2EI(-1+\beta)}{L(1+2\beta)} \\ 0 & \frac{2EI(-1+\beta)}{L(1+2\beta)} & \frac{4EI(2+\beta)}{L(1+2\beta)} \end{bmatrix} \begin{bmatrix} q_1 \\ q_3 \\ q_5 \end{bmatrix} \qquad (4.4)$$

$$\begin{bmatrix} Q_1 \\ Q_3 \\ Q_4 \\ Q_5 \\ Q_6 \end{bmatrix} = \begin{bmatrix} \frac{EA}{L} & 0 & 0 & 0 & 0 \\ 0 & \frac{4EI_z}{L}\gamma_z & 0 & \frac{2EI_z}{L}\xi_z & 0 \\ 0 & 0 & \frac{4EI_y}{L}\gamma_y & 0 & \frac{2EI_y}{L}\xi_y \\ 0 & \frac{2EI_z}{L}\xi_z & 0 & \frac{4EI_z}{L}\gamma_z & 0 \\ 0 & 0 & \frac{2EI_y}{L}\xi_y & 0 & \frac{4EI_y}{L}\gamma_y \end{bmatrix} \begin{bmatrix} q_1 \\ q_3 \\ q_4 \\ q_5 \\ q_6 \end{bmatrix} \qquad (4.5)$$

$$\text{where } \gamma_z = \frac{2+\beta_z}{1+2\beta_z} \;,\; \xi_z = \frac{-1+\beta_z}{1+2\beta_z}$$

$$\text{similarly } \gamma_y = \frac{2+\beta_y}{1+2\beta_y} \;,\; \xi_y = \frac{-1+\beta_y}{1+2\beta_y}$$

In the plastic range, the axial and flexural (or shear) deformations interact according to the normality rule (i.e., the normal components to the yield surface determine the ratio of axial to flexural plastic deformation).

In order to illustrate the elastoplastic behavior of the reinforced concrete column elements, some typical moment-axial force interaction diagrams are illustrated in Fig. 4.3. Generally the reinforced concrete column elements have limited ductility, but if they are designed properly (with small axial and shear forces and with proper confinement) the behavior of the member can be modeled by an elastic-workhardening moment-axial load relationship. In order to model the yield planes it is only necessary to discretize the interaction diagrams into a finite number of piecewise linearized yield planes. This is illustrated in Fig. 4.3 for both the uniaxial and biaxial interaction diagrams.

4.2 Finite Elements

In this section, the force-deformation relationships for the plane stress

elements are discussed. These elements are generally used for the analysis of two-dimensional continuum problems. Since we are primarily interested in developing models for the analysis of reinforced concrete shear walls, the elements developed here are intended for idealization of reinforced concrete components: the concrete and the reinforcing bars.

The reinforcing steels are considered to be anisotropic material, capable of resisting uniaxial stresses along the length of the bar. The uncracked concrete is modeled as isotropic homogeneous material, and cracking is conceived as a phenomenon like plastic deformation. Therefore, the elastoplastic constitutive laws can be used to model both the concrete and the reinforcing bars.

4.2.1 Stress-Strain Relationship for Isotropic Plane Stress Elements

Plane stress elements are only capable of transmitting in-plane stresses. These elements are characterized by the following stress and strain resultant vectors:

$$\mathbf{Q}^t = \begin{bmatrix} \sigma_{xx} & \sigma_{yy} & \tau_{xy} \end{bmatrix} \tag{4.8}$$

$$\mathbf{q}^t = \begin{bmatrix} \varepsilon_{xx} & \varepsilon_{yy} & \gamma_{xy} \end{bmatrix}$$

The elastic stress-strain relationship is generally expressed in terms of a 3 × 3 stiffness matrix **D**:

$$\mathbf{Q} = \mathbf{D}\,\mathbf{q} \tag{4.9}$$

For an isotropic homogeneous material obeying Hooke's law, the stiffness matrix takes the following form

$$\mathbf{D} = \frac{E}{1-\nu^2} \begin{bmatrix} 1 & \nu & 0 \\ \nu & 1 & 0 \\ 0 & 0 & \dfrac{1-\nu}{2} \end{bmatrix} \tag{4.10}$$

where ν is Poisson's ratio and E is the elastic modulus.

In here, plane stress elements are used to model concrete section. Since concrete is assumed to behave like an elastoplastic material, a set of yield criteria is defined for this material. In reference 11, Chen and Chen have developed a model for the initial and failure yield surfaces of concrete sections. This model (shown in Fig. 4.4) was established on the basis of biaxial experimental data on concrete specimens. Basically two different yield surfaces were proposed for the concrete: in the compression-compression region

$$f_0(\sigma_{ij}) = J_2 + \frac{1}{3}A_0 I_1 - \tau_0^2 = 0 \tag{4.11}$$

and in the tension-tension or tension-compression region:

$$f_0(\sigma_{ij}) = J_2 - \frac{1}{6}I_1^2 + \frac{1}{3}A_0 I_1 - \tau_0^2 = 0 \tag{4.12}$$

In equation (4.11) and (4.12), I_1 and J_2 refer to the first invariant of the stress tensor and to the second invariant of the deviatoric stress tensor, respectively:

$$I_1 = \sigma_{xx} + \sigma_{yy} + \sigma_{zz} \tag{4.13}$$

$$J_2 = \frac{1}{6}\left[(\sigma_{xx} - \sigma_{yy})^2 + (\sigma_{yy} - \sigma_{zz})^2 + (\sigma_{zz} - \sigma_{xx})^2\right] + \tau_{xy}^2 + \tau_{yz}^2 + \tau_{zx}^2$$

The parameters A_0 and τ_0 are material constants and have different values in the compression-compression and tension-tension (or tension-compression) region. Thus, for the compression-compression region

$$\frac{A_0}{f_c'} = \frac{\bar{f}_{bc}^2 - \bar{f}_c^2}{2\bar{f}_{bc} - \bar{f}_c} \tag{4.14}$$

$$\left[\frac{\tau_0}{f_c'}\right]^2 = \frac{\bar{f}_c\bar{f}_{bc}(2\bar{f}_c - \bar{f}_{bc})}{3(2\bar{f}_{bc} - \bar{f}_c)} \tag{4.15}$$

and for tension-compression or tension-tension region

$$\frac{A_0}{f_c'} = \frac{\bar{f}_c - \bar{f}_t}{2} \tag{4.16}$$

$$\left[\frac{\tau_0}{f_c'}\right]^2 = \frac{\bar{f}_c\,\bar{f}_t}{6} \tag{4.17}$$

where f_c, f_{bc}, f_t refer to the uniaxial and biaxial compressive strength and uniaxial tensile strength of concrete at the corresponding yield surfaces (see Fig. 4.4), and the bar denotes that the parameters have been normalized with respect to the uniaxial compressive strength of the concrete (f_c').

These yield surfaces are illustrated in the plane of principal stresses (σ_1, σ_2) in Fig 4.4, and in general stress space (σ_{xx}, σ_{yy}, τ_{xy}) in Fig. 4.5. The yield surfaces adopted for the concrete sections are based on a piecewise linearized approximation to this model.

4.2.2 Stress-Strain Relationship for Reinforcing Bars

In this section, the elastoplastic behavior of the reinforcing bars embedded in the concrete is defined. The reinforcing bars are generally subjected to uniaxial loading along the length of the bar. Therefore, the elastic stress-strain relationship in the $x'-y'$ coordinate system (where x' is oriented along the length of the bar) is:

$$\sigma_x' = E\ \varepsilon_x' \tag{4.18}$$

To model the reinforcing bars as plane stress elements, it is necessary to transform the stress-strain relation of Eqn. (4.18) into the element ($x-y$) coordinate system (see Fig. 4.6). This is accomplished by writing Cauchy's formula for the strain component ε_x'

$$\varepsilon_x' = \begin{bmatrix} \cos\theta & \sin\theta \end{bmatrix} \begin{bmatrix} \varepsilon_{xx} & \varepsilon_{xy} \\ \varepsilon_{yx} & \varepsilon_{yy} \end{bmatrix} \begin{bmatrix} \cos\theta \\ \sin\theta \end{bmatrix}$$

$$\varepsilon_x' = \begin{bmatrix} \cos^2\theta & \sin^2\theta & \cos\theta\,\sin\theta \end{bmatrix} \begin{bmatrix} \varepsilon_{xx} \\ \varepsilon_{yy} \\ 2\varepsilon_{xy} \end{bmatrix} \tag{4.19}$$

and transforming the stress component σ_x' to the $x-y$ coordinate system:

$$\begin{bmatrix} \sigma_{xx} & \sigma_{xy} \\ \sigma_{yx} & \sigma_{yy} \end{bmatrix} = \begin{bmatrix} \cos\theta \\ \sin\theta \end{bmatrix} \sigma_x' \begin{bmatrix} \cos\theta & \sin\theta \end{bmatrix}$$

$$\begin{bmatrix} \sigma_{xx} \\ \sigma_{yy} \\ \sigma_{xy} \end{bmatrix} = \begin{bmatrix} \cos^2\theta \\ \sin^2\theta \\ \sin\theta\,\cos\theta \end{bmatrix} \sigma_x' \tag{4.20}$$

Now the stress-strain relationship of Eqn. (4.18) becomes:

$$\begin{bmatrix} \sigma_{xx} \\ \sigma_{yy} \\ \sigma_{xy} \end{bmatrix} = \begin{bmatrix} \cos^2\theta \\ \sin^2\theta \\ \sin\theta\,\cos\theta \end{bmatrix} E \begin{bmatrix} \cos^2\theta & \sin^2\theta & \sin\theta\,\cos\theta \end{bmatrix} \begin{bmatrix} \varepsilon_{xx} \\ \varepsilon_{yy} \\ 2\varepsilon_{xy} \end{bmatrix}$$

$$\begin{bmatrix} \sigma_{xx} \\ \sigma_{yy} \\ \sigma_{xy} \end{bmatrix} = E \begin{bmatrix} \cos^4\theta & \cos^2\theta\,\sin^2\theta & \cos^3\theta\,\sin\theta \\ \cos^2\theta\,\sin^2\theta & \sin^4\theta & \cos\theta\,\sin^3\theta \\ \cos^3\theta\,\sin\theta & \cos\theta\,\sin^3\theta & \cos^2\theta\,\sin^2\theta \end{bmatrix} \begin{bmatrix} \varepsilon_{xx} \\ \varepsilon_{yy} \\ 2\varepsilon_{xy} \end{bmatrix} \tag{4.21}$$

$$\mathbf{Q} = \mathbf{D}\,\mathbf{q} \tag{4.9}$$

The yield conditions for the reinforcing bars are generally expressed in terms of the uniaxial stress-strain relationship (Fig. 4.7). Therefore, to establish the yield condition in terms of the active stress resultant vector $\mathbf{Q} = \begin{bmatrix} \sigma_{xx} & \sigma_{yy} & \sigma_{xy} \end{bmatrix}$, we must write Cauchy's formula for the stress component σ_x':

$$\sigma_x' = \begin{bmatrix} \cos^2\theta & \sin^2\theta & 2\,\sin\theta\,\cos\theta \end{bmatrix} \begin{bmatrix} \sigma_{xx} \\ \sigma_{yy} \\ \sigma_{xy} \end{bmatrix} = \mathbf{N}^t\mathbf{Q} \tag{4.22}$$

Now the yield condition $\pm\sigma_x' \le \sigma_y$ or $\pm\sigma_x' \le \sigma_y + H\,\lambda$ becomes:

$$\phi = \pm\sigma_x' - \sigma_y \le 0 \qquad \phi = \pm \mathbf{N}'\mathbf{Q} - R \le 0 \tag{4.23}$$

$$\phi = \pm\sigma_x' - \sigma_y - H\,\lambda \le 0 \qquad \phi = \pm \mathbf{N}'\mathbf{Q} - R - H\,\lambda \le 0$$

Furthermore, the plastic strain component ε_{x_p}' † can be used as a measure of intensity of activation of the yield surface if the following relationship between the plastic strain vector $\mathbf{p} = \begin{bmatrix} \varepsilon_{xx} & \varepsilon_{yy} & 2\varepsilon_{xy} \end{bmatrix}$ and the plastic strain component ε_{x_p}' is considered:

$$\begin{bmatrix} \varepsilon_{xx} \\ \varepsilon_{yy} \\ 2\varepsilon_{xy} \end{bmatrix}_p = \begin{bmatrix} \cos^2\theta \\ \sin^2\theta \\ 2\sin\theta\cos\theta \end{bmatrix} \varepsilon_{x_p}' \tag{4.24}$$

$$\mathbf{p} = \mathbf{N}\,\lambda$$

Finally, the hardening coefficients, H, are readily determined from the uniaxial stress-strain relationships of Fig. 4.7.

4.2.3 Force-Deformation Relationship for Plane Stress Elements

So far, we have established the internal stress-strain relationship for the plane stress elements. The element stiffness matrix **k**, which relates the nodal displacement vector **u** to the nodal force vector **F**, can now be obtained by writing the strain-displacement relationship (kinematic condition),

$$\varepsilon = \mathbf{B}\,\mathbf{u} \tag{4.25}$$

and applying the principle of virtual work (equilibrium condition):

$$\mathbf{F} = \int_v \mathbf{B}'\mathbf{D}\,\mathbf{B}\,dv\,\mathbf{u} \tag{4.26}$$

$$\text{or} \quad \mathbf{F} = \mathbf{k}\,\mathbf{u} \tag{4.27}$$

† To be precise, the absolute value of ε_{x_p}' is a measure of the activation intensity λ.

Here, $\mathbf{k} = \int_v \mathbf{B}^t \mathbf{D}\ \mathbf{B}\ dv$ is the element stiffness matrix.

The above formulation of the finite element stiffness matrix applies to every type or shape of element. Since we are primarily interested in solving elastoplastic problems of reinforced concrete shear walls, the rest of this section is devoted to a description of the type of element and the shape functions that would be suitable for the analysis of the shear walls.

Figure 4.8 illustrates the cubic rectangular elements used for the analysis of the shear walls. These elements provide a useful model of the shear wall because they satisfy beam theory exactly. The internal displacements for this element are approximated by the products of cubic polynomials in two coordinates

$$H_{IJ}(x,y) = G_I(x)\ G_J(y) \tag{4.28}$$

where H is the displacement pattern generated at node IJ (I and J identify the location of the node), and G is a cubic Lagrange polynomial.

The element stiffness matrix $\mathbf{k} = \int_v \mathbf{B}^t \mathbf{D}\ \mathbf{B}\ dv$ is evaluated exactly by numerical integration provided that there is a minimum of four sampling points in each coordinate. This follows from the fact that the strain-displacement compatibility matrix $\mathbf{B}$ consists of partial derivatives of H. Therefore, the order of the polynomials in the integrand $\mathbf{B}^t\mathbf{D}\ \mathbf{B}$ can be as high as six in each coordinate. According to the Gauss quadrature principle, n sampling points provide an exact answer for polynomials of order $\leq 2n - 1$.

4.3 Element Connection

Two different types of element connections are discussed in this section. The first type is used to model the finite size of the joint between frame elements and the second type is used to join frame elements to finite elements.

It must be pointed out that these element connections are not provided to

model any type of inelastic behavior; their main purpose is to maintain equilibrium and compatibility at some special connections. If it is desirable to model inelastic deformation (like slippage due to bond deterioration) at the face of the joint, a separate element (with some elastoplastic properties) must be provided adjacent to the joint. A detailed discussion of element modeling is given in chapter 6. The following discussion is confined to the equilibrium and compatibility requirement at particular connections.

Since frame members are assumed to span between the faces of the supports, we need joint elements to connect the members. The joint elements are in general parallelogram prisms (see Fig. 4.9), but they can have zero thickness along any one of their axes. To include these elements in the analysis of the structure, the following compatibility and equilibrium relations are set up.

The compatibility relation can be easily formulated if the element end displacements $\mathbf{u}_i^e$ are determined as a function of the nodal displacement at the joint center $\mathbf{u}_i$

$$\begin{bmatrix} u_{x_i}^e \\ u_{y_i}^e \\ u_{z_i}^e \\ \theta_{x_i}^e \\ \theta_{y_i}^e \\ \theta_{z_i}^e \end{bmatrix} = \begin{bmatrix} 1 & 0 & 0 & 0 & \Delta z & -\Delta y \\ 0 & 1 & 0 & -\Delta z & 0 & \Delta x \\ 0 & 0 & 1 & \Delta y & -\Delta x & 0 \\ 0 & 0 & 0 & 1 & 0 & 0 \\ 0 & 0 & 0 & 0 & 1 & 0 \\ 0 & 0 & 0 & 0 & 0 & 1 \end{bmatrix} \begin{bmatrix} u_{x_i} \\ u_{y_i} \\ u_{z_i} \\ \theta_{x_i} \\ \theta_{y_i} \\ \theta_{z_i} \end{bmatrix} \tag{4.29}$$

$$\mathbf{u}_i^e = \mathbf{C}_i \mathbf{u}_i$$

and the equilibrium condition takes the following form:

$$\begin{bmatrix} F_{x_i} \\ F_{y_i} \\ F_{z_i} \\ M_{x_i} \\ M_{y_i} \\ M_{z_i} \end{bmatrix} = \begin{bmatrix} 1 & 0 & 0 & 0 & 0 & 0 \\ 0 & 1 & 0 & 0 & 0 & 0 \\ 0 & 0 & 1 & 0 & 0 & 0 \\ 0 & -\Delta z & \Delta y & 1 & 0 & 0 \\ \Delta z & 0 & -\Delta x & 0 & 1 & 0 \\ -\Delta y & \Delta x & 0 & 0 & 0 & 1 \end{bmatrix} \begin{bmatrix} F^e_{x_i} \\ F^e_{y_i} \\ F^e_{z_i} \\ M^e_{x_i} \\ M^e_{y_i} \\ M^e_{z_i} \end{bmatrix} \tag{4.30}$$

$$\mathbf{F}_i = \mathbf{C}_i^t \, \mathbf{F}_i^e$$

If these relations are expressed for nodes i and j of every frame element, then the finite size of the joints are included in the analysis of the structure.

In section 4.2, the plane stress elements for the modeling of reinforced concrete shear walls have been considered. In order to incorporate the shear walls as part of the frame-wall structural system, a joint element between the beam element and the plane stress element has to be designed.

Figure 4.10 shows that the displacement degrees of freedom at the end of a beam element consist of two displacements and a rotation, whereas the displacement degrees of freedom for a plane stress element consist of only two displacements. In order to transfer the moment and rotation of the beam element to the finite element, a rigid link that spans two consecutive nodes of the plane stress element is introduced. Now the compatibility relation between the finite element degrees of freedom and the beam element degrees of freedom becomes

$$\begin{bmatrix} u_1 \\ u_2 \\ v_1 \\ v_2 \end{bmatrix} = \begin{bmatrix} 1 & 0 & -\alpha d \\ 1 & 0 & (1-\alpha)d \\ 0 & 1 & 0 \\ 0 & 1 & 0 \end{bmatrix} \begin{bmatrix} x_1 \\ y_1 \\ \theta_1 \end{bmatrix} \tag{4.31}$$

and the equilibrium condition takes the following form:

$$\begin{bmatrix} F_{x_1} \\ F_{y_1} \\ M_z \end{bmatrix} = \begin{bmatrix} 1 & 1 & 0 & 0 \\ 0 & 0 & 1 & 1 \\ -\alpha d & (1-\alpha)d & 0 & 0 \end{bmatrix} \begin{bmatrix} F_{u_1} \\ F_{u_2} \\ F_{v_1} \\ F_{v_2} \end{bmatrix} \qquad 0 \le \alpha \le 1 \qquad (4.32)$$

Note that the parameter d measures the width of the rigid link.

5. COMPUTER ANALYSIS

In this chapter, the solution to the elastoplastic problems of chapter 3 is discussed in terms of mathematical programming techniques. Both the holonomic (reversible) and the nonholonomic (irreversible) response of the structure are addressed, but the primary emphasis is on the nonholonomic (i.e., path dependent) response. For these classes of problems, any general nonlinear loading path may be considered as long as it can be approximated by a finite number of proportional loading stages (see Fig. 5.1).

5.1 Mathematical Programming Methods

The elastoplastic analyses formulated in chapter 3 can be solved by the restricted basis linear programming method. This method was originally developed in reference 12 for solving quadratic programming problems and was proposed for solving structural mechanics problems in references 9 and 13. In a recent study [5], this method has been implemented for the computer analysis of structures. Here, the method is applied to the nonlinear analysis of structures.

In chapter 3, it was noted that when the material properties are assumed to be reversible, the response of the structure for a given load pattern $\mathbf{F}$ can be obtained from the following linear complementarity problem:

$$\begin{aligned} &\text{find} && \phi \ , \ \lambda \\ &\text{such that} && \phi = \mathbf{N}^t \, \mathbf{Q}^{el} - \mathbf{A} \, \lambda - \mathbf{R} \\ & && \phi \le 0 \ , \ \lambda \ge 0 \\ & && \phi^t \, \lambda = 0 \end{aligned} \tag{5.1}$$

where $\mathbf{Q}^{el} = \mathbf{k} \, \mathbf{c} \, \mathbf{K}^{-1} \, \mathbf{F}$ represents the elastic stresses that resist the applied load factor $\mathbf{F}$.

If rather than solving for a given load condition, $\mathbf{F}$, the relation (5.1) is reinstated to calculate the maximum load factor s_{max} at the time of collapse of the

structure (i.e. when the applied loads are s_{max} **F**), then the following equation is obtained:

$$\begin{aligned} &\max \quad s \\ \text{such that} \quad &\phi = \mathbf{N}^t \mathbf{Q}^{el} s - \mathbf{A}\lambda - \mathbf{R} \\ &\phi \le 0 \ , \ \lambda \ge 0 \\ &\phi^t \lambda = 0 \end{aligned} \tag{5.2}$$

Generally, the solution to this problem can be obtained from the linear programming problem:

$$\begin{aligned} &\max \quad s \\ \text{subject to} \quad &\phi = \mathbf{N}^t \mathbf{Q}^{el} s - \mathbf{A}\lambda - \mathbf{R} \\ &\phi \le 0 \ , \ \lambda \ge 0 \end{aligned} \tag{5.3}$$

provided that the linear complementarity rule $\phi^t \lambda = 0$ is satisfied by the restricted basis rule that the two corresponding variables ϕ and λ can not both be nonzero quantities at the same time.

Similarly, if the nonholonomic response of the structure (i.e. assuming irreversible material properties) is considered, the incremental elastoplastic problem takes the following form:

$$\begin{aligned} &\max \quad \Delta s \\ \text{subject to} \quad &\Delta\phi = \mathbf{N}^t \mathbf{Q}^{el} \Delta s - \mathbf{A}\Delta\lambda && \text{(5.4a)} \\ &\phi + \Delta\phi \le 0 \ , \ \Delta\lambda \ge 0 && \text{(5.4b,c)} \\ &\phi^t \Delta\lambda = 0 \ , \ \Delta\phi^t \Delta\lambda = 0 && \text{(5.4d,e)} \end{aligned}$$

This problem can be cast as a linear programming problem if active yield modes (with $\phi_j = 0$) are only considered during each increment of loading, and the nonlinear constraint $\Delta\phi^t \Delta\lambda = 0$ is satisfied by the restricted basis rule that "two corresponding variables $\Delta\phi$ and $\Delta\lambda$ can not be in the basis as nonzero quantities at the same time".

5.2 Analytical Procedure

The analysis procedure will be described with reference to the nonholonomic behavior of structures. Consider a structure subjected to a sequence of proportional loading stages (see Fig. 5.1). During each stage of loading equation (5.4) is solved for an increment of loading (Δs) necessary to activate the next plastic hinge.

The first step in solving equation (5.4) is to partition the relation $\Delta\phi = \mathbf{N}^t\, \mathbf{Q}^{el}\, \Delta s - \mathbf{A}\, \Delta\lambda$ into *a*ctive (a) and *i*nactive (i) yield modes:

$$\begin{bmatrix} \Delta\phi_a \\ \hline \Delta\phi i \end{bmatrix} = \begin{bmatrix} \mathbf{N}_a^t \\ \hline \mathbf{N}_i^t \end{bmatrix} \mathbf{Q}^{el}\, \Delta s - \begin{bmatrix} \mathbf{A}_{aa} & \mathbf{A}_{ai} \\ \mathbf{A}_{ia} & \mathbf{A}_{ii} \end{bmatrix} \begin{bmatrix} \Delta\lambda_a \\ \hline \mathbf{0} \end{bmatrix} \tag{5.5}$$

In equation (5.5), the components of $\Delta\lambda_i$ corresponding to the inactive yield modes have been set to zero to comply with the constraint $\phi^t\, \Delta\lambda = 0$.

Now the entire elastoplastic analysis can be divided into a restricted basis linear programming problem for the active yield modes:

$$\begin{aligned} &\text{find} && \Delta\phi_a \ , \ \Delta\lambda_a \\ &\text{subject to} && \Delta\phi_a = \mathbf{N}_a^t\, \mathbf{Q}^{el}\, \Delta s - \mathbf{A}_{aa}\, \Delta\lambda_a \\ & && \Delta\phi_a \le 0 \ , \ \Delta\lambda_a \ge 0 \\ & && + \text{restricted basis rule} \ \ \Delta\phi_a^t\, \Delta\lambda_a = 0 \end{aligned} \tag{5.6}$$

and another linear programming problem for the inactive yield modes:

$$\begin{aligned} &\text{max} && \Delta s \\ &\text{subject to} && \Delta\phi_i = \mathbf{N}_i^t\, \mathbf{Q}^{el}\, \Delta s - \mathbf{A}_{ia}\, \Delta\lambda_a \le 0 \end{aligned} \tag{5.7}$$

In equation (5.6), there is one more unknown (Δs) than the number of equations,

hence the variable Δs can be factored out of all the constraints:

$$\begin{aligned} &\text{find} && \mathbf{y} \ , \ \mathbf{x} \\ &\text{subject to} && \mathbf{y} = \mathbf{N}_a^t \, \mathbf{Q}^{el} - \mathbf{A}_{aa} \, \mathbf{x} \\ & && \mathbf{y} \le 0 \ , \ \mathbf{x} \ge 0 \\ & && + \text{ restricted basis rule } \ \mathbf{y}^t \, \mathbf{x} = 0 \end{aligned} \tag{5.8}$$

$$\text{where} \qquad \Delta\phi_a = \mathbf{y} \, \Delta s \ \text{ and } \ \Delta\lambda_a = \mathbf{x} \, \Delta s$$

Generally, the procedure consists of solving for the active quantities x and y from equation (5.8) and substituting for the plastic multiplier vector $\Delta\lambda_a = \mathbf{x} \, \Delta s$ in equation (5.7) to determine the applied load factor Δs.

The algorithm in Fig 5.2 [†] illustrates the steps involved in the solution of the L.P. problems (5.8) and (5.7). Basically, the solution to problem (5.8) takes one of the following forms:

(1) When the Hessian matrix $\mathbf{A}_{aa}$ is positive definite, it is originally assumed that all active yield surfaces remain active, i.e. y is assumed to be zero and all components of x (the plastic deformation rates) are assumed to increase with the increase in the applied load:

$$\mathbf{y} = 0 \ \text{ and } \ \mathbf{x} = \mathbf{A}_{aa}^{-1} \, \mathbf{N}_a^t \, \mathbf{Q}^{el} \ge 0 \tag{5.9}$$

If the components of x are not all positive, then some of the yield surfaces are unloading. To determine the yield surfaces that are unloading, the following linear complementarity problem is solved:

$$\begin{aligned} &\text{find} && \mathbf{x} \ , \ \mathbf{y} \\ &\text{subject to} && \mathbf{y} = \mathbf{N}_a^t \, \mathbf{Q}^{el} - \mathbf{A}_{aa} \, \mathbf{x} \\ & && \mathbf{y} \le 0 \ , \ \mathbf{x} \ge 0 \\ & && \mathbf{y}^t \, \mathbf{x} = 0 \end{aligned} \tag{5.10}$$

[†] This algorithm has been adopted from a procedure in reference 5.

The technique required to solve the linear complementarity problem is discussed in section 5.3.1.

(2) When the Hessian matrix A_{aa} is positive semi-definite, the structure may undergo some plastic deformation even though there may be no increase in the applied loads (i.e. equation (5.8) has a nontrivial solution x corresponding to $\Delta s = 0$):

$$\mathbf{A}_{aa}\,\mathbf{x} = 0 \tag{5.11}$$

In that case, x defines the motion of the collapse mechanism provided that its components are all positive. Otherwise, a pseudomechanism ($\mathbf{x} \ngeq 0$) that does not ensure energy dissipation at all critical sections is obtained.

If the last yield surface activated at the end of the previous step $(I-1)$ is denoted by k, then the matrix $\mathbf{A}_{aa}$ can be partitioned as follows:

$$\mathbf{A}_{aa} = \begin{bmatrix} \mathbf{A}_{I-1} & \mathbf{a}_k \\ \mathbf{a}_k^t & a_{kk} \end{bmatrix} \tag{5.12}$$

and x can be obtained from:

$$\begin{bmatrix} \mathbf{A}_{I-1} & \mathbf{a}_k \\ \mathbf{a}_k^t & a_{kk} \end{bmatrix} \begin{bmatrix} \mathbf{x}_{I-1} \\ x_k \end{bmatrix} = 0 \tag{5.13}$$

$$\mathbf{x}_{I-1} = -\mathbf{A}_{I-1}^{-1}\,\mathbf{a}_k\,x_k \tag{5.14}$$

$$\begin{bmatrix} \mathbf{x}_{I-1} \\ \hline x_k \end{bmatrix} = \begin{bmatrix} -\mathbf{A}_{I-1}^{-1}\,\mathbf{a}_k \\ \hline 1 \end{bmatrix} x_k \tag{5.15}$$

If the components of this vector are not all positive, then the linear complementarity problem of (5.10) will be solved to determine the yield surfaces that unload (i.e. $y < 0$). If these yield modes are removed from the set of active yield modes, the

matrix A_{aa} will be restored to a positive definite matrix.

As discussed before, equation (5.6) or (5.8) only provides the deformation rate x (i.e. $\Delta\lambda_a = x\,\Delta s$). In order to determine the increase in the applied load factor (Δs), equation (5.7) must be solved:

$$\begin{aligned} &\max && \Delta s \\ &\text{subject to} && \Delta\phi_i = N_i^t\, Q^{el}\, \Delta s - A_{ia}\, x\, \Delta s \le 0 \\ &\text{where} && \Delta\phi_i = \phi_I - \phi_{I-1} \end{aligned} \tag{5.7}$$

If it is assumed that at the end of every step (I), a new yield surface (denoted by k) is activated, then:

$$\phi_I^k = 0 \tag{5.16}$$

$$\text{and} \qquad \Delta\phi_i^k = -\,\phi_{I-1}^k \tag{5.17}$$

Therefore, equation (5.7) can be restated as follows

$$\Delta s = \min_{over\ all\ i} \left\{ \frac{-\phi_{I-1}}{N_i^t\, Q^{el} - A_{ia}\, x} \right\} \tag{5.18}$$

where i = inactive yield surfaces.

5.3 Computer Program

The general flow diagram for the complete analysis of the structure is shown in Fig. 5.3. Basically, the information required for the analysis consists of the geometry of the structure and the elastoplastic properties of the materials.

In order to begin the analysis, the program first generates the (assembled) elastic stiffness matrix of the structure (**K**) and then conducts an elastic analysis for the first pattern of applied load **F**. The resulting displacement ($\mathbf{b} = \mathbf{K}^{-1}\,\mathbf{F}$) and

elastic stresses ($\mathbf{Q}^{el} = \mathbf{k}\ \mathbf{c}\ \mathbf{K}^{-1}\ \mathbf{F} + \mathbf{Q}^{FEMA\dagger}$) are computed assuming an applied load factor of unity ($s = 1$).

In order to determine the load factor at which the first plastic hinge is formed (i.e. elastic limit load factor $s_{elastic\ limit}$), equation (5.3) is solved for the case that the plastic deformation vector λ vanishes:

$$\begin{aligned} &\max \quad s \\ &\text{subject to} \quad \boldsymbol{\phi} = \mathbf{N}^t\ \mathbf{Q}^{el}\ s - \mathbf{R} \le 0 \end{aligned} \tag{5.19}$$

Similar to the solution of equation (5.7), the solution of equation (5.19) is obtained when the first yield surface (denoted by k) is activated (i.e. $\phi^k = 0$):

$$\text{therefore,} \qquad s_{elastic\ limit} = \min_{over\ all\ yield\ surfaces} \left\{ \frac{\mathbf{R}}{\mathbf{N}^t\ \mathbf{Q}^{el}} \right\} \tag{5.20}$$

Elastic limit is considered to be the first step of loading, at the end of this step, the plastic potential vector ϕ is updated:

$$\boldsymbol{\phi} = \mathbf{N}^t\ \mathbf{Q}^{el}\ s_{elastic\ limit} - \mathbf{R} \le 0 \tag{5.21}$$

After the formation of the first plastic hinge, the program evaluates the self-equilibrating stresses that resist a unit of plastic deformation ($\mathbf{p}_a^e = \mathbf{N}^e\ \lambda_a$) at the first active yield mode ($\lambda_a = 1$):

$$\mathbf{Q}^s = \left(\mathbf{k}\ \mathbf{c}\ \mathbf{K}^{-1}\ \mathbf{c}^{e^t}\ \mathbf{k}^e - \mathbf{k}^e \right)\ \mathbf{N}^e\ \lambda_a \tag{5.22}$$

Here, e refers to the element that contains the active yield mode.

The elastoplastic analysis is now conducted using the plastic coefficient

† FEMA refers to Fixed End Member Action.

vector $\mathbf{a} = \mathbf{H}^e - \mathbf{N}^t\,\mathbf{Q}^s$ in the expression (5.4):

$$\begin{aligned} &\max \qquad \Delta s \\ \text{subject to} \quad &\Delta\phi = \mathbf{N}^t\,\mathbf{Q}^{el}\,\Delta s - \mathbf{a}\,\Delta\lambda_a \\ &\phi + \Delta\phi \le 0 \;\;,\;\; \Delta\lambda_a \ge 0 \\ &\phi_a^t\,\Delta\lambda_a = 0 \;\;,\;\; \Delta\phi_a^t\,\Delta\lambda_a = 0 \end{aligned} \tag{5.23}$$

As mentioned in section 5.2, the solution to equation (5.23) is obtained by separating the active and inactive yield modes and solving the linear programming problems (5.8) and (5.7) according to the procedure outlined in Fig. 5.2.

Once the plastic deformation rate x (and/or the unloading stress rate y) is evaluated, the step size necessary to activate the next plastic hinge is determined. Then the program updates the plastic potential function (ϕ_I), the plastic multipliers (λ_I), and the applied load factor (s_I) as follows:

$$\begin{aligned} \phi_I &= \phi_{I-1} + \Delta\phi_I \\ \lambda_I &= \lambda_{I-1} + \Delta\lambda_I \\ s_I &= s_{I-1} + \Delta s \end{aligned} \tag{5.24}$$

where $$\Delta\phi_I = \begin{bmatrix} \Delta\phi_a \\ \hline \Delta\phi_i \end{bmatrix} = \begin{bmatrix} \mathbf{y} \\ \hline \mathbf{A}_{ia}\,\mathbf{x} - \mathbf{N}_i^t\,\mathbf{Q}^{el} \end{bmatrix} \Delta s$$

$$\Delta\lambda_I = \begin{bmatrix} \Delta\lambda_a \\ \hline \Delta\lambda_i \end{bmatrix} = \begin{bmatrix} \mathbf{x} \\ \hline \mathbf{0} \end{bmatrix} \Delta s$$

If the maximum specified applied load factor ($s_{\max}$) has been reached, the program starts analyzing the structure for the next proportional loading stage. Generally, the program stops when a collapse mechanism has been reached or when the computed load factor s_I exceeds the input load factor $s_{\max}$ for the last loading stage.

The elastoplastic response of the structure may be found in terms of the total

stresses and total displacements:

$$\begin{aligned} \Delta q^p &= N\, \Delta\lambda \\ \Delta Q^s &= Z\, \Delta q^p \\ \Delta u^p &= K^{-1}\, c^t\, k\, \Delta q^p \\ Q_I &= Q_{I-1} + \Delta Q^s + Q^{el}\, \Delta s \\ u_I &= u_{I-1} + \Delta u^p + u^{el}\, \Delta s \end{aligned} \tag{5.25}$$

But it is worth noting that the only variables that are essential for solving the elastoplastic problem are the plastic multipliers and the plastic potentials.

For the most part this program involves simple matrix manipulation. There are, however, two particular features in the program that require some special techniques. These are (1) updating the inverse of the Hessian matrix A_{aa}, and (2) solving the linear complementarity problem of equation (5.10). These will be the topics of discussion in the next two sections.

5.3.1 Linear Complementarity Problem

As mentioned earlier, if the plastic deformation rate x computed from equations (5.9) or (5.15) have negative components, the linear complementarity problem of (5.10) has to be solved in order to determine the stress points that unload:

$$\begin{aligned} &\text{find} && x\ ,\ y \\ &\text{subject to} && y = N_a^t\, Q^{el} - A_{aa}\, x \\ & && y \le 0\ ,\ x \ge 0 \\ & && y^t\, x = 0 \end{aligned} \tag{5.10}$$

Unloading stress points are characterized by a decrease in the stress level below the yield limit (i.e. $y < 0$). Therefore, it is necessary to partition the vectors

x and y to separate the unloading yield modes:

$$\mathbf{x} = \begin{bmatrix} \mathbf{x}_{loading} \\ \hline 0 \end{bmatrix} \geq 0 \quad , \quad \mathbf{y} = \begin{bmatrix} 0 \\ \hline \mathbf{y}_{unloading} \end{bmatrix} \leq 0 \tag{5.26}$$

Generally, the analysis can be started by assuming that the negative components of x correspond to the unloading yield modes. Furthermore, x is assumed to consist of the positive components already computed (in equations (5.9) or (5.15)) $\bar{\mathbf{x}} = \begin{bmatrix} \bar{\mathbf{x}}_{positive} \\ \hline 0 \end{bmatrix}$ plus a vector $\bar{\mathbf{p}} = \begin{bmatrix} \bar{\mathbf{p}} \\ \hline 0 \end{bmatrix}$ that might be required to satisfy the relation (5.10):

$$\mathbf{x} = \bar{\mathbf{x}} + \bar{\mathbf{p}}$$

$$\begin{bmatrix} 0 \\ \hline \mathbf{y}_{unloading} \end{bmatrix} = \mathbf{N}_a^t \, \mathbf{Q}^{el} - \mathbf{A}_{aa} \begin{bmatrix} \bar{\mathbf{x}} \\ \hline 0 \end{bmatrix} - \mathbf{A}_{aa} \begin{bmatrix} \bar{\mathbf{p}} \\ \hline 0 \end{bmatrix} \tag{5.27}$$

The procedure to solve equation (5.27) is summarized as follows:

(1) solve the first set of equations for $\bar{\mathbf{p}}$,

(2) for $\bar{\mathbf{p}} \neq 0$ compute $\mathbf{x} = \bar{\mathbf{x}} + \bar{\mathbf{p}}$,

(a) if x is still positive, solve for y from the second set of equations.

(b) otherwise, calculate the (maximum) coefficient α ($\alpha \leq 1$) such that $\mathbf{x} = \bar{\mathbf{x}} + \alpha \, \bar{\mathbf{p}} \geq 0$. Under this condition, another component of x will become zero. This implies that another yield surface might be unloading. Therefore, it is necessary to rearrange the components of x and y to include the new unloading yield surface, and reinitiate the problem from step 1.

(3) for $\bar{\mathbf{p}} = 0$, solve for y from the second set of equations,

(a) if $\mathbf{y} \leq 0$, then the solution is found;

(b) otherwise, the largest positive component of y is removed from the set of

unloading yield modes, and the problem is reinitiated from step 1.

The method presented here is called the active set method. For a detailed discussion of this method read references 14 and 15.

5.3.2 Updating the Inverse of the Hessian Matrix $\mathbf{A}_{aa}$

It is obvious from the flow diagram of Fig. 5.2, that the solution to the elastoplastic problem (in particular, equations (5.8)) requires the inverse of the Hessian matrix $\mathbf{A}_{aa}$ to be computed. However, after each step of the analysis, the size of this matrix changes to reflect the current number of active yield surfaces. For example, when a new yield surface is activated, a new row and column are added to this matrix, and when a stress point unloads from an active yield surface, the row and column corresponding to the unloading yield surface are deleted. In either case, since the Hessian matrix $\mathbf{A}_{aa}$ is positive definite, the inverse of $\mathbf{A}_{aa}$ can be easily updated.

Consider the case when a new yield surface is activated and the inverse of $\mathbf{A}_I$ is to be computed from $(\mathbf{A}_{I-1})^{-1}$:

$$\mathbf{A}_I = \begin{bmatrix} \mathbf{A}_{I-1} & \mathbf{a}_k \\ \mathbf{a}_k^t & a_{kk} \end{bmatrix} \qquad \mathbf{A}_I^{-1} = \begin{bmatrix} \mathbf{D} & \mathbf{d}_k \\ \mathbf{d}_k^t & d_{kk} \end{bmatrix} \tag{5.28}$$

If the relation $\mathbf{A}_I^{-1}\,\mathbf{A}_I = \mathbf{I}$ is enforced, the inverse of matrix $\mathbf{A}_I$ can be easily determined and in the process the determinant of matrix $\mathbf{A}_I$ is computed:

$$\det|\mathbf{A}_I| = \frac{1}{d_{kk}} = a_{kk} - \mathbf{a}_k^t\,\mathbf{A}_{I-1}^{-1}\,\mathbf{a}_k$$

$$\mathbf{d}_k = -\left[\mathbf{A}_{I-1}^{-1}\,\mathbf{a}_k\right] d_{kk} \tag{5.29}$$

$$\mathbf{D} = \mathbf{A}_{I-1}^{-1}\left[\mathbf{I} - \mathbf{a}_k\,\mathbf{d}_k^t\right]$$

Similarly, if $\mathbf{A}_{I-1}^{-1}$ is to be computed from $\mathbf{A}_I^{-1}$, the last expression in equation (5.29) can be rearranged as follows:

$$\mathbf{A}_{I-1}^{-1} = \mathbf{D} \left[\mathbf{I} - \mathbf{a}_k \, \mathbf{d}_k^t \right]^{-1} \tag{5.30}$$

The inverse of $\left[\mathbf{I} - \mathbf{a}_k \, \mathbf{d}_k^t \right]$ (i.e. the identity matrix modified by a first rank matrix $\mathbf{a}_k \, \mathbf{d}_k^t$) is simply:

$$\left[\mathbf{I} - \mathbf{a}_k \, \mathbf{d}_k^t \right]^{-1} = \left[\mathbf{I} + \frac{\mathbf{a}_k \, \mathbf{d}_k^t}{1 - \mathbf{d}_k^t \, \mathbf{a}_k} \right] \tag{5.31}$$

$$\text{therefore,} \qquad \mathbf{A}_{I-1}^{-1} = \mathbf{D} \left[\mathbf{I} + \frac{\mathbf{a}_k \, \mathbf{d}_k^t}{1 - \mathbf{d}_k^t \, \mathbf{a}_k} \right] \tag{5.32}$$

6. APPLICATION OF THE ELASTOPLASTIC ANALYSIS PROGRAM TO A REINFORCED CONCRETE FRAME-WALL STRUCTURE

In this chapter, the nonlinear static analysis program developed in the previous chapters is used to analyze a reinforced concrete frame-wall structure studied under the U.S.-Japan cooperative research program. Since the primary concern of this chapter is to correlate the experimental and analytical responses of the structure, it is necessary to begin with a description of the test structure and a summary of the experimental testing program. A mathematical model of the structure is then introduced with a complete description of the analytical models used for the individual elements of the structure. In the final sections of this chapter, the results of the nonlinear static analysis are presented followed by a general discussion regarding the degree of correlation obtained between the experimental and analytical responses of the structure.

6.1 Description of the Test Structure

The structure considered here is a 1/5-scale replica of the full-scale seven-story reinforced concrete frame-wall structure. The plan and elevation of the model are shown in Figs. 6.1-6.3 . The structure consists of a moment resisting space frame with a centrally-located shear wall. In the orthogonal direction, there are four end-walls that are provided to eliminate the possibility of dominant torsional modes. Since this model is designed to be an exact replica of the full-scale structure, a complete floor system consisting of reinforced concrete slabs with beams and girders spanning the distance between the columns is also provided.

6.2 An Overview of the Experimental Testing Program and the Experimental Response of the Model

The main objective of the experimental testing program [1,2,3] was to

evaluate the response of the test structure to earthquake ground motion of increasing intensity. Altogether, the structure was subjected to three series of simulated earthquake ground motions. The first series consisted of low-level excitation. The primary objective of this series was to test the response of the instrumentation and to evaluate the response of the model under low-level excitation. During this period of testing the serviceability limit state was exceeded, but the response of the model was still considered to be linear elastic.

The second series was intended to test the performance of the structure under damageability and ultimate limit states. During this series, the model was subjected to earthquake ground motion of increasing intensity until the flexural capacity of the first-story shear wall was exhausted. Since the principal reinforcements at the base of the shear wall were either fractured or yielded far beyond the yield strength of the material, the dominant mode of failure was identified as flexural failure. But the evaluation of the experimental data at the time of failure revealed that a shear failure in the web of the wall was also imminent.

The third series of tests was conducted to observe the behavior of the wall after repair and retrofitting. During these experiments, the model was subjected to several extreme excitations which resulted in another flexural failure at the base of the wall.

At every level of excitation, the response of the structure was dominated by the behavior of the shear wall. In the elastic range, the wall acted as a huge vertical cantilever beam that restrained the lateral displacement of the frame. Once the shear wall yielded at the base, the neutral axis of the wall moved toward the compression boundary element and the wall started to rock at its corner. This behavior of the wall led to a three dimensional mechanism of motion which involved an out-of-plane behavior of the floor diaphragm where all the longitudinal and the transverse girders framing into the wall deformed and restrained the motion

of the wall (see Fig. 6.4).

Besides the three dimensional response of the structure, the shear wall introduced other nonlinear behavior as identified in reference 3: (1) the nonlinear shear deformation of the wall; (2) the fixed end rotation at the base of the wall; and (3) variation in flexural and shear stiffness of the wall.

These response characteristics are not commonly included in mathematical models of this type of structure. However, since they represent the dominant response of the structure at the damageability and ultimate limit states, an attempt is made here to include these in the analytical studies.

In the remaining part of this chapter, an analytical model of the structure is introduced and a series of nonlinear static analyses are conducted with the primary objective of predicting both the local and the global responses of the structure at damageability and ultimate limit states.

6.3 Development of the Model for Nonlinear Static Analysis

The analytical model developed in this section is designed to predict the response of the structure at damageability and ultimate limit states. Because the structure is subjected to several low to moderate levels of excitation, before it is finally tested at its ultimate limit state, the modeling of individual elements is based on the assumption that all members are cracked.

Since the frame-wall structure of Fig. 6.5 has a plane of symmetry that passes through the main shear wall, it is only necessary to analyze half of the structure. The mathematical model of this structure is shown in Fig. 6.6. Both the gravity loading and the lateral loading on the structure are symmetrical with respect to the plane of symmetry. Therefore, the boundary conditions on this plane are such that only in-plane deformations are permitted.

In the mathematical modeling, the strength and stiffness properties of all

elements are modeled directly from the properties of the corresponding members of the structure. For those elements that lie on the plane of symmetry, the strength and the stiffness of each element represent half the properties of the corresponding members. Such an analysis accounts for only half the strength of the structure. Therefore, the strength of the analytical model has been doubled to correspond to that of the total structure.

The analytical model shown in Fig. 6.6 consists of both the frame elements and the finite elements. Only the main shear wall is modeled by finite elements; the remaining members are all modeled by frame elements. This model is restricted to only one lateral degree of freedom per floor level, simply because the floor system has been idealized as a rigid diaphragm. In the subsequent sections, the detailed analytical model of the individual members will be discussed.

6.3.1 Modeling of the Shear Wall

As mentioned earlier, the most important response characteristics of the shear wall have been identified [3] as: (1) rocking of the shear wall, (2) nonlinear shear deformation of the wall, (3) variation in flexural and shear stiffness of the wall, and (4) fixed end rotation at the base of the wall.

Since these response characteristics can not be modeled directly by a simple beam-column element, the most logical approach to take for modeling the shear wall is to use finite element methods. The particular advantage of this method is that it relies on the internal stresses of the element to compute the strength and stiffness of the member.

In order to model the shear wall with finite elements, the reinforced concrete section is considered to be a composite section. Basically, the concrete and the reinforcing bars are modeled separately by plane stress elements, and the full bond between the two elements is enforced through compatibility at the nodes. Figure

6.7 illustrates the cubic rectangular finite elements used for the analysis of the wall.

To model the reinforcing bars as plane stress elements, it is necessary to transform the uniaxial stress-strain relation of Fig. 6.8 according to the rules set forth in section 4.2.2 . For the elastic condition, the stress-strain relation for the horizontal reinforcing bar (with θ=0) becomes

$$\begin{bmatrix} \sigma_{xx} \\ \sigma_{yy} \\ \sigma_{xy} \end{bmatrix} = E \begin{bmatrix} 1 & 0 & 0 \\ 0 & 0 & 0 \\ 0 & 0 & 0 \end{bmatrix} \begin{bmatrix} \varepsilon_{xx} \\ \varepsilon_{yy} \\ 2\varepsilon_{xy} \end{bmatrix} \tag{6.1}$$

and for the vertical reinforcing bars (with θ=90), this relation is:

$$\begin{bmatrix} \sigma_{xx} \\ \sigma_{yy} \\ \sigma_{xy} \end{bmatrix} = E \begin{bmatrix} 0 & 0 & 0 \\ 0 & 1 & 0 \\ 0 & 0 & 0 \end{bmatrix} \begin{bmatrix} \varepsilon_{xx} \\ \varepsilon_{yy} \\ 2\varepsilon_{xy} \end{bmatrix} \tag{6.2}$$

Since these two orthogonal directions are completely independent, we can add the two stiffnesses and consider only one plane stress element to represent both types of reinforcement. In that case, the stress-strain relation becomes:

$$\begin{bmatrix} \sigma_{xx} \\ \sigma_{yy} \\ \sigma_{xy} \end{bmatrix} = E \begin{bmatrix} 1 & 0 & 0 \\ 0 & 1 & 0 \\ 0 & 0 & 0 \end{bmatrix} \begin{bmatrix} \varepsilon_{xx} \\ \varepsilon_{yy} \\ 2\varepsilon_{xy} \end{bmatrix} \tag{6.3}$$

Similarly, to establish the yield condition for the reinforcing bars in terms of the active stress resultant, equation (4.23), expressed as:

$$\phi = \pm \mathbf{N}^t \mathbf{Q} - R - H\,\lambda \leq 0 \tag{6.4}$$

$$\phi = \pm \begin{bmatrix} \cos^2\theta & \sin^2\theta & 2\sin\theta\cos\theta \end{bmatrix} \begin{bmatrix} \sigma_{xx} \\ \sigma_{yy} \\ \sigma_{xy} \end{bmatrix} - \sigma_{yield} - H\,\lambda \leq 0 \tag{6.5}$$

takes the following form for the yield surfaces in the horizontal and vertical steel,

respectively :

$$\phi = \pm \begin{bmatrix} 1 & 0 & 0 \end{bmatrix} \begin{bmatrix} \sigma_{xx} \\ \sigma_{yy} \\ \sigma_{xy} \end{bmatrix} - \sigma_{yield} - H_x |\varepsilon_{xx}|_p \leq 0 \tag{6.6}$$

$$\phi = \pm \begin{bmatrix} 0 & 1 & 0 \end{bmatrix} \begin{bmatrix} \sigma_{xx} \\ \sigma_{yy} \\ \sigma_{xy} \end{bmatrix} - \sigma_{yield} - H_y |\varepsilon_{yy}|_p \leq 0 \tag{6.7}$$

For a single finite element member to consist of both the horizontal and vertical reinforcements, the matrix **N** and the vectors **R** and **H** contain the corresponding vector for each individual yield surface. For example, if the horizontal and vertical reinforcements each have two yield surfaces (representing a yield in tension (+1) and a yield in compression (-1)), then the matrix **N** and the vectors **R** and **H** for the finite element member become:

$$\mathbf{N}^t = \begin{bmatrix} 1 & 0 & 0 \\ -1 & 0 & 0 \\ 0 & 1 & 0 \\ 0 & -1 & 0 \end{bmatrix} \qquad \mathbf{R} = \begin{bmatrix} \sigma_{x\,yield}^{+} \\ \sigma_{x\,yield}^{-} \\ \sigma_{y\,yield}^{+} \\ \sigma_{y\,yield}^{-} \end{bmatrix} \tag{6.8a,b}$$

$$\mathbf{H} = \begin{bmatrix} H_x^+ & 0 & 0 \\ H_x^- & 0 & 0 \\ 0 & H_y^+ & 0 \\ 0 & H_y^- & 0 \end{bmatrix} \tag{6.8c}$$

A final comment in regard to the finite element modeling of the reinforcement is that the reinforcing bars are assumed to be smeared or distributed uniformly across the section. Therefore, the strength and stiffness properties of steel must be multiplied by the reinforcement ratio ρ_s (which is defined as the ratio of the

reinforcement area to the cross-sectional area of the finite element).

Table 6.1 summarizes the properties of the horizontal and the vertical steel in both the panel and the edge member of the shear wall. The elastic stiffness of the steel is taken as 29000 ksi and the hardening stiffness is measured from the idealized yield surface that approximate the work-hardening behavior of the steel.

As mentioned earlier, during the inelastic response of the structure, a significant amount of fixed-end rotation is observed at the base of the wall. In order to model this phenomenon, the material property for the steel layer at the base of the wall has been chosen in such a way that the slip between the steel and the concrete is included in the stress-strain relationship of the reinforcing bars. This is illustrated in Fig. 6.8(b) where a stress-strain relationship has been calculated from the bending moment and axial force at the base of the wall, and the displacement of the reinforcing bars over a distance of 6 inches above the wall-foundation interface. This $\sigma - \varepsilon$ relationship is used to model the behavior of reinforcing bars (over a distance of 6 inches) at the base of the wall.

The concrete in the shear wall is modeled separately by a layer of plane stress elements. In the elastic range, concrete is assumed to obey Hooke's Law for isotropic homogeneous material:

$$\begin{bmatrix} \sigma_x \\ \sigma_y \\ \tau_{xy} \end{bmatrix} = \frac{E}{1 - \nu^2} \begin{bmatrix} 1 & \nu & 0 \\ \nu & 1 & 0 \\ 0 & 0 & \frac{1-\nu}{2} \end{bmatrix} \begin{bmatrix} \varepsilon_x \\ \varepsilon_y \\ \gamma_{xy} \end{bmatrix} \tag{6.9}$$

In the inelastic range, yield conditions are provided to define the initiation of cracking and crushing in the concrete. On the basis of biaxial experimental data on concrete specimens, Chen and Chen [11] have developed a model for the initial yield surface and the failure yield surface of concrete sections. The shape of these yield surfaces depends on the ratio of the biaxial compressive strength to the

uniaxial compressive strength of the concrete. This parameter depends to some extent on the degree of confinement of the concrete. For the unconfined concrete in the panel of the wall, the biaxial compressive strength of the concrete is not expected to be different from the uniaxial compressive strength. Hence, the ratio of biaxial to uniaxial strength is taken as unity. For the confined concrete in the edge member, however, the biaxial strength is expected to be higher in magnitude than the uniaxial strength. From experimental data on the biaxial strength of concrete [16], this ratio has been selected as 1.2 for the confined concrete.

The general shapes of the concrete yield surfaces are given in Fig. 6.9. The idealized yield surfaces obtained by inserting piecewise linearized yield planes in the original curved surfaces are also shown in Fig. 6.10. These surfaces are all normalized with respect to the uniaxial compressive strength of the concrete ($f_c^{'}$).

In order to model a concrete section, it is possible to define two (or more) yield surfaces; one which usually defines the initial yield surface of concrete (at 0.5 to 0.7 $f_c^{'}$), and a second surface that defines the ultimate or crushing limit of the concrete (at 0.9 to 1.0 $f_c^{'}$) (see Fig. 6.11). However, since the primary concern of this analysis is to predict the behavior of the structure at damageability and ultimate limit states and due to the fact that the finite element modeling of the wall is already a costly operation, only one set of yield surfaces is used to define the ultimate strength of the concrete at 1.0 $f_c^{'}$.

Figure 6.10 illustrates the properties of the confined and the unconfined concrete sections. In both cases, concrete is assumed to behave like an elastic-perfectly plastic material. The elastic stiffness of the concrete, which defines the behavior of the concrete prior to reaching the ultimate yield surface, is picked to be $0.5E_c$, where E_c is the initial uncracked stiffness of the concrete. This value has been selected based on the stress-strain relationship of a sample of concrete, taken

from the first story wall after the dynamic testing of the structure.

6.3.2 Modeling of the Longitudinal and Transverse Girders

The longitudinal and transverse girders of the structure are modeled by beam elements. The modeling parameters provided for these elements are based on the moment-rotation characteristics of the girders. In order to establish these properties, the cross-sectional behavior of the girders are determined and then the moment-rotational response of the girder is obtained by integrating the curvature along the length of the members.

For the cross-sectional analysis of the longitudinal girders, several moment-curvature relationships were computed in reference 17 (and illustrated in Fig. 6.12). The basic assumption in the cross-sectional analyses of the girders is that an effective width of slab (denoted by b_f) is contributing to the strength and stiffness of the girder section. Curves 1, 2, and 4 in Fig. 6.12(c) represent the moment-curvature relationship of the girder section when a uniform distribution of strain is considered across an assumed effective width of slab of 11.81, 23.62, and 39.37 inches, respectively. The third curve in Fig. 6.12(c) is obtained when a nonuniform distribution of strain (as illustrated in Fig. 6.12(a,b)) is considered across the width of the slab (39.37 inches).

Since the actual distribution of strain across the width of the slab is expected to be nonuniform, the third moment-curvature relationship of Fig. 6.12(c) is chosen for modeling the girders. This curve has been idealized in Fig 6.14(b) by two curves: the first curve is provided to model the behavior of the uncracked sections, while the second curve (shown by the dashed line) models the behavior of the cracked sections.

Given the sectional moment-curvature relationship of Fig. 6.14, the next phase of the analysis determines the moment-rotation characteristics of the member.

For this particular analysis, the longitudinal girders are modeled by a number of beam elements, as shown in Fig. 6.13 . Here, consideration is given to the fact that the girders are primarily subjected to end rotations. Therefore, the analytical model of the girders is highly discretized over the end zones, to allow for the spread of the inelastic deformation over the region. The parameters that define the behavior of each segment are then selected from the idealized moment-curvature relationship of Fig. 6.14(b).

After assigning the element properties, the member (shown in Fig. 6.14(a)) is loaded with vertical gravity load, followed by monotonically increasing end rotations. The results of the analysis are the moment vs rotation relationships of Fig. 6.14(c) for each end of the girder.

Given the moment-rotation relationships of Fig. 6.14(c), the longitudinal girders will now be modeled for the global analysis of the structure. A model of these girders must consist of at least two beam elements (as shown in Fig. 6.15(a)), simply because there are transverse beams that frame into the middle of the longitudinal girders. The moment-curvature relationships assigned to the elements are shown in Fig. 6.15(b). The elastic stiffness of the elements is taken to be the same as the cross-sectional stiffness, but the cracking and the yield moment are selected by trial and error in order to accurately model the moment rotation relationship of Fig. 6.14(c).

When this model is subjected to gravity loads followed by monotonically increasing end rotation, the moment-rotation relationship of Fig. 6.15(c) is obtained. This moment-rotation relationship fits closely the previous curve obtained for the highly discretized girder. Therefore, the two beam element model can be used successfully to represent the longitudinal girders in the global analysis of the structure.

A similar study is also carried out for the transverse girders. In this case, a

single beam element is used to represent each transverse girder. The element properties are shown in Fig. 6.16(b); the moment-rotation relationships generated for the these girders when subjected to gravity loads and equal end rotations are shown in Fig. 6.16(c).

6.3.3 Modeling of the Columns

The columns of the structure are modeled as biaxial beam-column elements. The modeling parameters provided for these elements consist of cross-sectional stiffness and the yield strength (which is generally expressed in terms of a moment-axial load interaction diagram).

Since the columns are presumed to have been cracked during the first series of tests, the flexural stiffness (for each principal direction) is based on the cracked section stiffness which is about 50 percent of the gross section stiffness. For the axial stiffness, the gross section stiffness is taken as the elastic stiffness of the element, simply because the columns are rarely subjected to a net tensile force and the average axial compressive stiffness of the columns calculated over a story height is very close to the gross section stiffness.

The yield surfaces specified for a biaxial beam-column element are generally expressed in terms of the biaxial bending vs axial load interaction diagram (see Fig. 6.17). However, a preliminary analysis of the structure indicated that the bending moment that developed about the longitudinal axis (M_y) never exceeded 25 percent of the yield moment. Hence, the only part of the analytical interaction diagram that is pertinent to the analysis is the interaction curve of Fig. 6.18 which shows bending moment about the lateral direction (M_z) vs axial load. In this figure, computed bending moment (M_z) vs axial load at first yield of steel and at maximum moment are illustrated. On the basis of this interaction diagram, the piecewise linearized yield surface shown in Fig. 6.18 is chosen for the analytical modeling of the

column. This idealized yield surface deviates considerably from the actual behavior of the section at around the balanced point. However, since the compressive axial load in the columns remains well below the balanced point, the error in the analytical interaction diagram can be ignored for this problem.

6.3.4 Modeling of the End Walls

The end walls are modeled by truss elements. When the structure is subjected to lateral loads, the end walls contribute only to the axial stiffness of the adjacent columns. Therefore, each end wall is modeled by two truss elements that are provided parallel to the adjacent columns. Each truss element represents half the strength and stiffness of the corresponding end wall.

The initial elastic stiffnesses of the end walls are taken as the gross section stiffnesses, and the yield strengths of the elements in tension and compression are taken as the tensile strength of the cracked section and the axial compressive strength of the uncracked section, respectively.

6.4 Analytical Response to Monotonically Increasing Lateral Loads

For the global analysis of the structure, the analytical model of Fig. 6.6 is subjected to gravity loads, followed by monotonically increasing lateral loads. The lateral loads represent the inertial forces developed by acceleration of the floor masses. In order to establish the upper bound, the lower bound, and the most probable analytical strength of the model, three different distributions of horizontal load along the height of the structure are considered (see Fig. 6.19). These include a uniform distribution, an inverted triangular distribution, and a parabolic distribution modeled after the pattern of inertial forces recorded at the time of maximum response of the structure during one of the high intensity excitations.

6.4.1 Global Analytical Response of the Model

The global analytical response of the structure when subjected to the three different lateral load patterns is given in Figs. 6.20 through 6.23. These figures show the roof displacement and the first story displacement vs the total base shear and the total overturning moment. Since the three analytical curves of Figs. 6.22 and 6.23 (corresponding to the three lateral load patterns) are almost identical, the three curves are represented by only one curve.

The inelastic response of the structure in terms of the sequence of plastic hinge formation is also illustrated in Figs. 6.24(a,b,c). The first group of elements to undergo plastic deformation is the longitudinal girders which reach their negative cracking moments at their right ends; and at the same time, the base of the shear wall begins to crack at its left end (see Fig. 6.24(c)). While the cracks extend further into the left side of the shear wall, the left ends of the longitudinal girders reach their positive cracking moments.

As the yielding of the model progresses, the longitudinal girders reach their positive and negative yield moments. Also, the transverse girders framing into the tension side of the wall yield at both ends (see Fig. 6.24(b)). Since the yielding of the transverse girders induces a considerable tension force in the columns of Frame A, the second row of columns in Frame A (see Fig. 6.24(a)) will eventually yield at both ends. This phenomenon occurs at a roof displacement of about 2.0 to 2.5 inches.

Besides the cracking and the inelastic deformations observed at the base of the wall (see Fig. 6.24(c)), there are isolated cracked zones at the sixth and seventh stories of the wall. The cracking in the sixth story is due to the reversal of the bending moment in the wall caused by the frame-wall interaction. But the one at the seventh story is due to local interaction between the frame and the wall (i.e., the large negative moment in the longitudinal girder induces local cracking in the panel

of the wall).

6.4.2 Comparison of Experimental and Analytical Responses of the Structure

In order to compare the analytical and the experimental responses of the structure, envelopes of peak experimental responses of the structure are given in Figs. 6.20 through 6.23. Since the analytical model of the structure is based on the assumption that the structure is in an initially cracked state, the experimental response curves shown in Figs. 6.20-6.23 correspond to tests conducted on an initially cracked structure.

Referring to Fig. 6.20 it can be seen that the experimental response curve for the base shear vs roof displacement is best matched with the analytical response curve obtained for the uniform load pattern. The other two analytical response curves (corresponding to the parabolic and triangular load distributions) match the initial slope of the experimental curve; but at high lateral load levels, they fall below the experimental curve. At this load level, for a given value of roof displacement, the analytical base shears obtained for uniform, parabolic, and triangular distributions are 101, 91, and 82 percent of the experimental value, respectively.

Basically, the same type of behavior is observed in Fig. 6.21, where the analytical and experimental response curves for base shear vs first story displacement are compared.

For the overturning moment vs roof displacement of Fig. 6.22, however, the analytical response curves obtained for the three different load distributions are almost identical, and they all fall short of the experimental response curve at high lateral load levels. It can be seen from Fig. 6.22, that the initial slope of the analytical curve matches that of the experimental curve. But, at high lateral load

levels, the two curves diverge with the analytical curve reaching up to 90 percent of the experimental curve. A similar type of behavior is also observed in Fig. 6.23, where the analytical and experimental response curves for overturning moment vs first story displacement are compared.

The differences in the analytical and the experimental responses of the structure can be due to either modeling errors or errors in interpretation of the experimental data. The main source of error in the analytical modeling of the structure is due to underestimating the strength and the stiffness of the individual element. A possible explanation for the higher strength observed in the real model is that during the dynamic excitation, the material is subjected to a maximum strain rate of the order of 0.1 in/in/sec [3]. Material tests have indicated that such a strain rate can increase the strength of the concrete and the reinforcing steel by about 15 and 25 percent, respectively [3].

A possible source of error in the experimental results is that even though the structure is excited horizontally, the interaction between the shaking table and the structure induces some vertical excitation in the structure. This vertical excitation results in a vertical inertia load which can possibly increase the strength of the vertical members. In particular, the bending moment and the shear strength of the shear wall increase with an increase in the axial load. This topic will be discussed further in the next section, where the analytical response of the shear wall is compared with the experimental response.

6.4.3 Local Response of the Shear Wall

In this section, the analytical and the experimental responses of the shear wall will be compared. The response of the wall in terms of the roof displacement and the first story displacement vs the wall base shear and overturning moment are given in Figs. 6.25 through 6.28. The three analytical curves shown in Figs. 6.25

and 6.26 correspond to the three different load patterns applied to the structure. Only one analytical response curve is shown for the roof displacement and the first story displacement vs wall overturning moment curves of Figs. 6.27 and 6.28, since the three analytical curves are almost identical.

It can be seen from Fig. 6.25 that the experimental response curve is best matched with the analytical response curve obtained for the uniform load distribution. The other two analytical response curves approximate the initial slope of the experimental curve, but, at high lateral load levels, they fall below the experimental curve. At these load levels, the analytical wall base shears obtained for the uniform, parabolic, and triangular load distributions are 99, 90, and 78 percent of the experimental values, respectively.

A similar conclusion can be drawn for the first story displacement vs the wall base shear of Fig. 6.26.

For the roof displacement vs the wall overturning moment of Fig. 6.27, the analytical and the experimental response curves have the same initial slope, but, as the yielding of the wall progresses, the two curves diverge with the analytical curve reaching up to only 90 percent of the experimental curve at a roof displacement of about 1.5 inches. Thereafter, the maximum moment capacity of the wall decreases because of the rupture of the main reinforcements.

Similar behavior is observed in Figs. 6.28 and 6.29, where the analytical and experimental response curves for the first story displacement and the fixed end rotation at the base of the wall vs the wall overturning moment are illustrated. In Fig. 6.29, the rupture of the wall reinforcements leads to a dramatic increase in the fixed end rotation from 5×10^{-3} to 10×10^{-3} radians.

The maximum difference between the analytical and the experimental response of the wall is seen in Fig. 6.30, where the axial force developed at the base of the wall is plotted as a function of roof displacement. It can be seen from this

figure that whereas the axial compressive force of the wall measured during the dynamic testing of the structure is as high as 60 kips, the compressive force developed in the analytical model of the wall is only 36 kips. The increase in the wall compressive force over the gravity loads (which is only 26 kips) is primarily due to the shear transferred to the wall from the longitudinal and transverse girders and slabs that frame into the wall. During the uplift and rocking of the wall, the girders framing into the wall restrain the motion of the wall and transfer a net compression force into the wall. This phenomenon is illustrated in Fig. 6.4.

A possible explanation for the difference in the experimental and analytical values for the wall axial force is that during the dynamic testing of the structure, the main reinforcement in the wall ruptures. Thereafter, the tensile force in the reinforcement is virtually eliminated and the net axial force in the wall is primarily due to the compressive force in the concrete. In order to measure the significance of the tensile force in the reinforcement, for the analytical model of the wall, the axial force developed at the base of the wall in the concrete and the reinforcement layers are plotted separately in Fig. 6.31. In this figure, it is clearly illustrated that while the compressive force in the concrete is of the order of 55 kips, the tensile force in the reinforcement is 19 kips resulting in a net axial force of 36 kips in the wall. Therefore, in the analytical model of the wall, if the tensile reinforcements had been ruptured, the axial force in the wall would have been of the order of 55 kips rather than 36 kips.

Other factors that contribute to the difference between the analytical and the experimental responses of the shear wall are experimental error in measuring the response of the wall and the vertical inertia force induced in the structure.

Since the test structure is designed to be statically determinate at the first story, the internal forces in the shear wall are determined by enforcing equilibrium at the bottom story of the structure. In particular, the internal forces in the columns

of the first story are determined from the internal force transducers that are provided in all first story columns and the internal forces in the end walls are determined by concrete strain gages. However, these gages are only monitored during the last series of tests and analytical techniques are developed to approximate the contribution of end walls during the earlier tests. This leads to some uncertainties in determining the experimental response of the wall.

Another source of discrepancy is due to the fact that when the experimental response of the wall is computed, all the effects of vertical inertia force induced in the structure are included in the response of the wall. In particular, the axial load in the shear wall is measured as the difference between the gravity loads and the axial force developed in the first story columns and end walls. Therefore, since the vertical inertia forces are not considered as an additional external force, their entire contribution is included in the wall axial load. The exact magnitude of the vertical inertial load is not known because of the lack of instrumentation of the building. But the maximum vertical acceleration on top of the shear wall has been measured to be of the order of 0.15g. This simply indicates that there is at most a 4 kip (26[kips]×0.15) increase in the wall axial load due to vertical excitation.

6.5 Crack Pattern and Type of Failure Observed in the Shear Wall

In order to fully understand the inelastic behavior of the shear wall, the crack pattern formed in the analytical model of the shear wall is compared with the ones formed in the walls of the test structures (i.e. considering both the 1/5-scale model tested at Berkeley and the full-scale model tested at Tsukuba, Japan).

Figure 6.24(c) shows the sequence of crack formation developed in the concrete layer of the shear wall. This figure clearly illustrates that because of the assumed low tensile strength of the concrete, cracking extends all the way to the third story of the wall, while the yielding of the reinforcing bars is primarily

concentrated in the first story of the wall.

To compare these results with the experimental response of the structure, the crack patterns of the 1/5- and the full-scale models at a roof displacement of 2.4 inches (1.4 percent roof drift) are shown in Fig. 6.32 . It can be seen from this figure, that while the crack patterns in the full-scale model consist of finely distributed diagonal cracking in the first three stories of the wall, the cracking in the wall of the 1/5-scale model is concentrated in the first story. Other cracks observed in the second, third, and fourth story of the wall panel of the 1/5-scale model are due to shrinkage of the concrete.

It is quite obvious that because of load reversal, similar crack patterns form on opposite sides of the wall panel in both the 1/5- and the full-scale models. This is in contrast to the analytical model where the applied loads are monotonically increasing and cracks are formed only on one side of the wall. Otherwise, the crack patterns formed in the analytical model are similar to those of the full-scale model, but are different from the ones formed in the 1/5-scale model.

One reason for the differences observed in the crack patterns is that the full-scale model is tested pseudo-dynamically, with a loading process so slow in nature that the load is almost sustained. But the 1/5-scale model is tested on the earthquake simulator with a model time which is $\sqrt{5}$ times faster than normal. Consequently, for the full-scale model (and also for the analytical model, since in both cases the loads are increased gradually) there is enough time for crack formation and propagation. But that is not the case for the 1/5-scale model.

Another reason for the different crack patterns is the difference in the tensile strengths of the concrete. For the 1/5-scale model, the original tensile strength of the concrete is twice that of the full-scale model. Also, since the analytical model of the structure is based on the properties of the cracked structure, the average tensile strength of the concrete is taken as one-half of the tensile strength of the

virgin specimen.

Besides the crack pattern formed in the wall, the type of failure sustained in the wall has been identified for both the analytical model and the test structures. In order to determine the type of failure in the analytical model of the wall, a set of criteria corresponding to the failure of the concrete and the reinforcing bars has been specified (see Fig 6.33). In particular, for the steel layer, the stress and strain at the tensile rupture and at the buckling compression of the reinforcing bars have been specified, and for the concrete layer, the failure of the material in the stress † and strain domains has been defined according to the Chen model [18].

Based on these criteria, the sequence of failure obtained in the concrete layer is shown in Fig. 6.34. The results can be summarized as follows: First, the cracks initiated on the tension side of the wall (1, 2) extend through the panel (3), and then, the concrete in the panel of the wall adjacent to the compression edge member (3^*) fails due to excessive shear-compression deformation. Finally, the failure in the wall panel extends all the way to the compression edge member (4), and the edge member itself (4^*,5) fails due to excessive compression deformation. This type of failure is characteristic of a shear-compression failure.

The stress and strain states in the concrete layer at the time of failure are shown in Fig. 6.35. It is interesting to note that the strain in the steel layer does not reach the ultimate strain of the material, and hence, the reinforcements are not ruptured.

Recall from section 6.2 that the failure in the 1/5-scale model is a flexural failure obtained from the rupture of the tensile reinforcing bars in the edge columns whereas the failure of the full-scale model is a shear-compression failure similar to the one obtained in the analytical model.

A possible explanation for the difference between the types of failure is that

† For the failure of the concrete in the stress domain refer to Fig. 6.10.

in the 1/5-scale model, because cracking is concentrated at the base of the wall, the principal reinforcements attain their ultimate strain. Whereas in the analytical model and the full-scale model, because of the distribution of cracking, the tensile reinforcements do not rupture; instead, most of the failure is concentrated in the compression side of the wall.

6.6 Conclusions

Although exact correlation between the analytical and the experimental responses of the structure is not obtained, the nonlinear static analysis of the structure predicts the local strength of the shear wall with the same accuracy that it can predict the global strength of the structure (90 percent of the experimental response).

The mathematical model of the structure is also capable of simulating the three dimensional response of the structure observed during the experiment. In particular the analytical modeling of the shear wall is capable of reproducing the behavior associated with rocking of the wall, fixed-end rotation at the base of the wall, and inelastic shear deformation observed in the wall.

7. SUMMARY, CONCLUSIONS, AND RECOMMENDATIONS

7.1 Summary

The primary objective of the studies reported herein was to develop analytical methods suitable for nonlinear analysis of reinforced concrete frame-wall structures. The analytical methods presented include a finite element model of the shear wall that is capable of simulating some of the physical characteristics of the wall.

Since analytical methods based on mathematical programming techniques are more efficient than classical nonlinear analytical methods, the method chosen for elastoplastic analysis of structures is based on mathematical programming techniques. In chapter 2, the solution strategy for this method is briefly described. It is clearly demonstrated that this procedure is considerably faster than most inelastic analysis programs, primarily because the introduction of a new plastic hinge does not require the stiffness matrix of the structure to be updated. Instead, after the introduction of every new plastic hinge, a pattern of self-equilibrating stresses that resists the corresponding plastic deformation is computed. Consequently, the nonlinear response of the structure can be computed from the superposition of the self-equilibrating stresses and the elastic stresses that resist the external loads.

In order to describe the analytical formulation and show its relation to mathematical programming, it is necessary to establish the constitutive laws as a function of two inherent parameters: the plastic multipliers and the plastic potentials. This is done in chapter 3, where the constitutive laws are introduced along with the compatibility and the equilibrium relations, and after some manipulation, the nonlinear response of the structure is presented in a mathematical form known as the linear complementarity problem.

Chapter 4 contains a description of the analytical models used to describe the nonlinear behavior of some typical members of the structure. In this chapter, the elastoplastic behavior of a selected group of frame elements and finite elements is presented. In particular, the discussion of finite elements is confined to the nonlinear behavior of plane stress elements that are useful in modeling reinforced concrete shear walls.

In chapter 5, the solution to the elastoplastic problems of chapter 3 is presented in terms of mathematical programming techniques. The analytical procedure is explained with the aid of an algorithm that works on an event-to-event basis. Generally, at the end of every event a new plastic hinge is formed. Therefore, for the next step of the analysis, a pattern of self-equilibrating stresses is computed, and the response of the structure to an increment of loading is computed by solving a linear complementarity problem. This process involves an elastic analysis (a forward reduction and a back substitution for computation of self-equilibrating stresses which basically requires NM numerical operations, where N and M denote the number of degrees of freedom and the band width of the structure stiffness matrix) and a pivot transformation on the Hessian matrix A for the solution to the linear complementarity problem of 5.6 (the number of operations in this case is of order n^2, where n denotes the number of active yield surfaces). In the event that this process is interrupted by the unloading of one of the active yield surfaces, then the solution to the quadratic programming problem of (5.10) (with the Hessian matrix A) is also required.

Since one of the objectives of the studies reported herein was to study the three-dimensional analytical response of the reinforced concrete frame-wall structure, a series of nonlinear static analyses are conducted and described in chapter 6. An analytical model of the structure consisting of both frame elements and finite elements is developed. When this model is subjected to gravity loads plus

monotonically increasing lateral loads, the global analytical response of the structure is found to be in good agreement with the envelope of the experimental response. Due to the nature of the analytical model chosen for the shear wall, both the analytical strength and the mode of failure of the wall can be predicted. In particular, the results obtained indicate that the analytical strength of the shear wall is 90 percent of the experimental value, and the mode of failure of the shear wall is similar to that of the pseudo-dynamically tested structure.

7.2 Conclusions

(1) The analytical model proposed for the three-dimensional inelastic analysis of a reinforced concrete frame-wall structure consists of frame elements for every member of the structure except for the shear wall which is modeled by finite elements. The primary reason for the finite element modeling of the shear wall is to incorporate some of the nonlinear behavior of the wall such as the nonlinear shear deformation, rocking and uplift of the wall.

(2) Applying the elastoplastic analysis computer program developed here to a three-dimensional analytical model of a 7-story reinforced concrete frame-wall structure (studied under the U.S.-Japan cooperative research program), the global analytical response of the structure was found to be in good agreement with the envelope of the experimental dynamic response of the structure.

(3) The local response of the wall, i.e. the shear and overturning moment resistance of the wall, is also predicted with the same accuracy (90 percent of the corresponding experimental results) as the global response of the structure.

(4) The analytical technique developed here can also predict the crack patterns

and the type of failure sustained in the wall. However, because of the sensitivity of the response of the wall to strain rate effects, the predicted crack pattern and mode of failure are not similar to the one observed in the dynamically tested structure. Instead, they appear to be a reasonable prediction of the behavior of the wall for the pseudo-dynamically tested structure.

(5) From the analytical studies, it can be concluded that the proposed program can be used reliably to estimate both the local and the global responses of reinforced concrete frame-wall structures.

(6) From the point of view of numerical efficiency it must be pointed-out that the elastoplastic analysis of the three-dimensional analytical model of the structure, consisting of 1396 degrees of freedom and 22734 yield surfaces, required 2.5 cpu hours on IBM 3090 computers. This is in light of the fact, that at ultimate limit load level, due to the extensive cracking of the shear wall, more than 800 yield surfaces were activated.

7.3 Recommendations for Future Research

(1) The analytical methods presented here were designed to determine the static nonlinear response of the structure. But as pointed out in chapter 6, some of the response characteristics of the structure (such as the mode of failure of the wall) are highly sensitive to the type of loading (dynamic vs static). Therefore, the analytical methods should be extended to include dynamic effects.

(2) Interaction between reinforcing bars and concrete (such as bond deterioration and slippage of the reinforcing bars) plays a crucial role in the behavior of reinforced concrete elements. In order to include these effects in the analysis

of the structure, elements such as those developed in reference 19, should be included in the analytical model of the structure.

(3) In the analytical techniques presented here, the hardening parameters were restricted to positive semi-definite matrices. To extend the analytical methods to solve any general hardening matrix (i.e., any negative hardening including the strain-softening behavior of elements), the mathematical programming techniques should be extended to solve nonconvex problems [9].

APPENDIX A

It is important to explain the difference between the hardening parameters H and the strain hardening stiffnesses k that are commonly used to describe a force-deformation relationship.

Consider the force-deformation relationship of Fig. A.1 . After the first yield surface is activated, the constitutive laws can be expressed either in terms of the strain hardening stiffness k_1:

$$\Delta M = k_1 \, \Delta\theta \tag{A.1}$$

or in terms of the hardening parameter H_1 and the elastic stiffness k_0:

$$\begin{aligned} \Delta M &= H_1 \, \lambda \\ \Delta M &= k_0 \, \Delta e \end{aligned} \tag{A.2}$$

The difference between the two relations is that in the first equation the parameter $\Delta\theta$ measures both the elastic and the plastic deformations, while in the second equation the elastic and the plastic deformations are measured separately by Δe and λ, respectively. Hence, the deformation quantities $\Delta\theta$, λ, and Δe are related through the following expressions:

$$\Delta\theta = \lambda + \Delta e \tag{A.3}$$

If we substitute for $\Delta\theta$, λ, and Δe from equations (A.1) and (A.2), equation (A.3) takes the following form:

$$\frac{\Delta M}{k_1} = \frac{\Delta M}{H_1} + \frac{\Delta M}{k_0} \tag{A.4}$$

Eliminating the force component ΔM from equation (A.4), leads to an expression that relates the stiffness parameters k_0 and k_1 to the hardening parameter H_1:

$$\frac{1}{k_1} = \frac{1}{H_1} + \frac{1}{k_0} \tag{A.5}$$

APPENDIX B

The usual representation of the plastic influence coefficient matrix **Z** is $\mathbf{Z} = \mathbf{k}\,\mathbf{c}\,\mathbf{K}^{-1}\mathbf{c}'\mathbf{k} - \mathbf{k}$. However, this matrix takes a different form when the force method of analysis is employed [20].

In the force method, the first step of analysis is to identify the redundancies (or the force degrees of freedom) and apply a set of redundant forces (**R**) at the selected cut sections. The behavior of the structure is then analyzed by setting up the equilibrium relationship that transforms any redundant force vector **R** into the internal stress vector **Q** at the critical sections:

$$\mathbf{Q} = \mathbf{A}\,\mathbf{R} \tag{B.1}$$

Furthermore, the relative displacement **r** at the cut section is generally obtained by integrating the elastic deformation along the length of the member

$$\mathbf{r} = \mathbf{E}\,\mathbf{R} \tag{B.2}$$

where **E** is the elastic compliance matrix.

If the structure is subjected to an imposed plastic deformation **p** at the critical sections, the compatibility relationship can be used to determine the direct contribution of concentrated deformation at the critical section to the relative displacement **r** at the cut section:

$$\mathbf{r} = \mathbf{A}'\mathbf{p} \tag{B.3}$$

Furthermore, the (B.2) relationship can be used to determine the contribution of any imposed elastic deformation (provoked by the concentrated plastic deformation at the critical sections) to the relative displacement of the cut section. Altogether, the relative displacement at the cut section is:

$$\mathbf{r} = \mathbf{A}'\mathbf{p} + \mathbf{E}\,\mathbf{R} = 0 \tag{B.4}$$

Therefore, the redundant forces are

$$\mathbf{R} = -\mathbf{E}^{-1}\,\mathbf{A}'\mathbf{p} \tag{B.5}$$

and the self-equilibrating moments induced by $\mathbf{p}$ in the critical sections are:

$$\mathbf{Q}^s = \mathbf{A}\,\mathbf{R} = -\mathbf{A}\,\mathbf{E}^{-1}\mathbf{A}'\mathbf{p} \tag{B.6}$$

Comparing this relationship to expression (3.59) it is obvious that the plastic influence coefficient matrix $\mathbf{Z}$ is:

$$\mathbf{Z} = -\mathbf{A}\,\mathbf{E}^{-1}\mathbf{A}' \tag{B.7}$$

Hence, $\mathbf{Z}$ is a negative definite matrix.

REFERENCES

[1] V.V. Bertero, et al, "U.S.-Japan Cooperative Earthquake Engineering Research Program: Earthquake Simulation Tests and Associated Studies of a 7-Story Reinforced Concrete Test Structure", Report No. UCB/EERC-84/05, Earthquake Engineering Research Center, University of California, Berkeley, 1984.

[2] R. Sause, and V.V. Bertero, "The Experimental Study of the Global Response and Distribution of Forces at the Base of A Seven-Story R/C Frame-Wall Structure Subjected To Simulated Earthquake Shaking", Earthquake Engineering Research Center, University of California, Berkeley, (in house report).

[3] F.A. Charney, "Correlation of the Analytical and Experimental Seismic Response of a 1/5-Scale Seven-Story Reinforced Concrete Frame-Wall Structure", Ph.D. Thesis, University of California, Berkeley, 1986.

[4] D.E. Grierson, and S.B. Abdel-Baset, "Plastic Analysis Under Combined Stresses", Journal of Engineering Mechanics Division, ASCE, Vol. 103, No. EM5, October 1977, pp. 837-853.

[5] A. Franchi and M.Z. Cohn, "Computer Analysis of Elastic-Plastic Structures", Computer Methods in Applied Mechanics and Engineering, Vol. 21, No. 3, 1980, pp. 271-294.

[6] ASCE Committee on Concrete and Masonry Structures, Task Committee on Finite Element Analysis of Reinforced Concrete Structures, "A State-of-the-Art Report on Finite-Element Analysis of Reinforced Concrete Structures", ASCE Spec. Publ. 1982.

[7] G. Maier, "Mathematical Programming Methods in Structural Analysis", Proceedings of International Conference on Variational Methods in Engineering, Vol. II, No. 8, Southampton University Press, 1973, pp. 8/1-8/32.

[8] O. De Donato, "Fundamentals of Elastic-Plastic Analysis", NATO-ASI on Structural Plasticity by Mathematical Programming, Waterloo, Aug. 1977, (Pergman Press, New York, 1979) 325-349.

[9] G. Maier, "A Matrix Structural Theory of Piecewise Linear Elastoplasticity with Interacting Yield Planes", Meccanica, Vol. 5, No. 1, 1970, pp. 54-66.

[10] G. Maier, "A Quadratic Programming Approach for Certain Classes of Nonlinear Structural Problems", Meccanica, Vol. 3, No. 2, 1968, pp. 121-130.

[11] A.C.T. Chen, and W.F. Chen, "Constitutive Relations for Concrete", Journal of Engineering Mechanics Division, ASCE, Vol. 101, No. EM4, August 1975, pp. 465-481.

[12] P. Wolfe, "The Simplex Method for Quadratic Programming", Econometrica, Vol. 27, No. 3, 1959, pp. 382-398.

[13] G. Maier, D.E. Grierson, and M.J. Best, "Mathematical Programming Methods for Deformation Analysis at Plastic Collapse", Computers and Structures, Vol. 7, 1977, pp. 599-612.

[14] P.E. Gill, W. Murray, and M.H. Wright, "Active Set Methods for Linear Inequality Constraints", Practical Optimization, Academic Press, London, 1981, pp. 167-174.

[15] D.G. Luenberger, "Active Set Methods", Linear and Nonlinear Programming, Addison-Wesley Publishing Co., Massachusetts, 1984, pp. 326-330.

[16] H.B. Kupfer, and K.H. Gerstle, "Behavior of Concrete Under Biaxial Stresses", Journal of Engineering Mechanics Division, ASCE, Vol. 99, No. EM4, August 1973, pp. 853-866.

[17] A.A. Chowdhury, "Mechanical Characteristics of Members of the 1/5-Scale Model of the Seven-Story R/C Test Building", Master of Engineering Thesis, University of California, Berkeley, 1983.

[18] W.F. Chen, "A Three-Parameter Model for Concrete Displaying Isotropic Hardening", Plasticity in Reinforced Concrete, McGraw-Hill Book Company, pp. 376-384.

[19] F.C. Filippou, "A simple model for reinforcing bar anchorages under cyclic excitations", Report No. UCB/EERC-85/05, Earthquake Engineering Research Center, University of California, Berkeley, 1985.

[20] O. De Donato, and G. Maier, "Mathematical Programming Methods for the Inelastic Analysis of Reinforced Concrete Frames Allowing for Limited Rotation Capacity", International Journal for Numerical Methods in Engineering, Vol. 4, 1972, pp. 307-329.

Table 6.1 Stress and strain response characteristics for the reinforcement in the edge member and the panel of the shear wall.

Reinforcement		E_s (ksi)	E_{SH} (ksi)	f_y (ksi)	f_u (ksi)	ε_u (in./in.)	ρ_s (in^2/in^2)
Edge member	Horizontal	29000	98.9	61.6	79.2	0.18	0.0060
	Vertical	29000	94.5	62.0	78.8	0.18	0.01082
Panel of the wall	Horizontal	29000	98.9	61.6	79.2	0.18	0.00394
	Vertical	29000	98.9	61.6	79.2	0.18	0.00394
Reinforcement at wall-foundation interface							
Edge member	Horizontal	29000	98.9	61.6	79.2	0.18	0.0060
	Vertical	12400	74.4	62.0	78.0	0.22	0.01082
Panel of the wall	Horizontal	29000	98.9	61.6	79.2	0.18	0.00394
	Vertical	12400	74.4	62.0	78.0	0.22	0.00394

E_s = Modulus of elasticity

E_{SH} = Strain hardening modulus

f_y = Yield stress

f_u = Maximum tensile stress

ε_u = Ultimate tensile strain

ρ_s = Reinforcement ratio

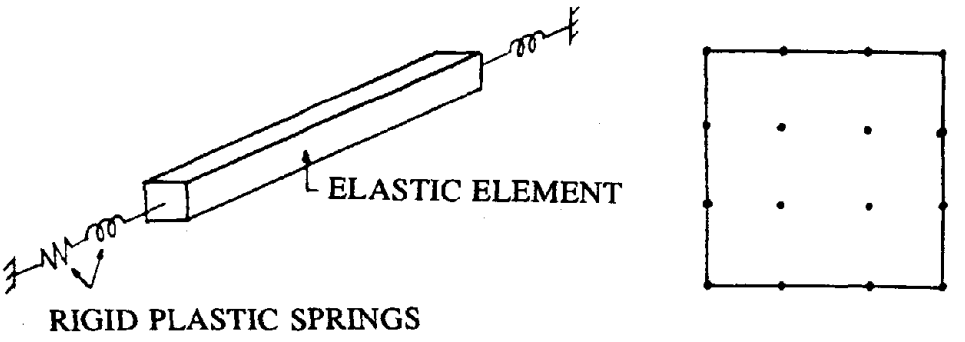

Fig. 2.1 - (a) Frame element and (b) finite element models

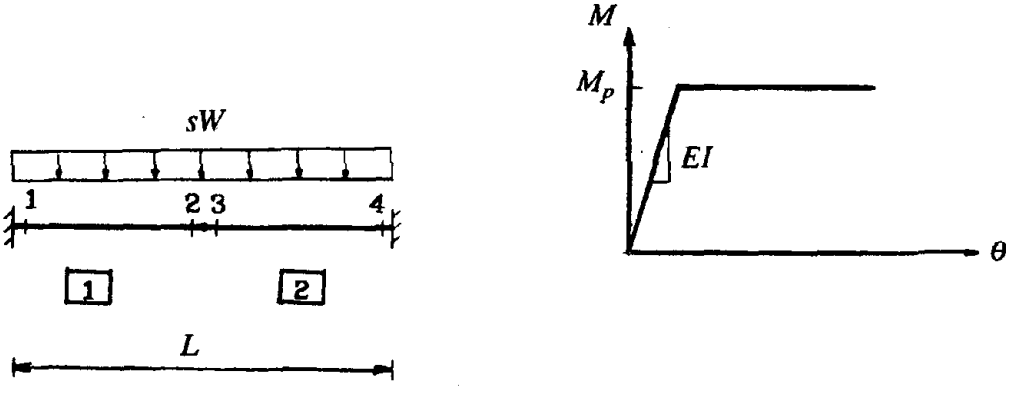

Fig. 2.2 - Beam example: geometry, loading, and material behavior.

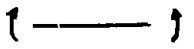

SIGN CONVENTION
FOR MEMBER FORCES

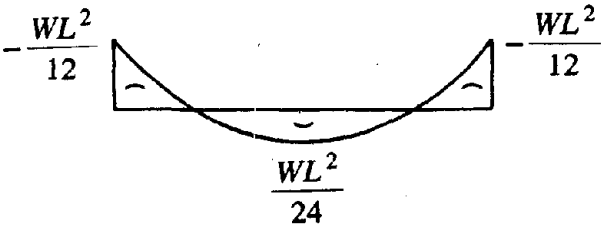

$$M^t_{elastic} = \left[-\frac{WL^2}{12} \quad \frac{WL^2}{24} \quad \frac{WL^2}{24} \quad -\frac{WL^2}{12} \right]$$

$$s_{elastic\ limit} = \frac{12M_p}{WL^2}$$

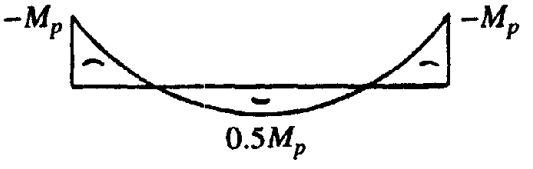

$$M^t_{elastic\ limit} = \left[-M_p \quad 0.5M_p \quad 0.5M_p \quad -M_p \right]$$

Fig. 2.3 - Elastic moment distribution and the elastic limit load

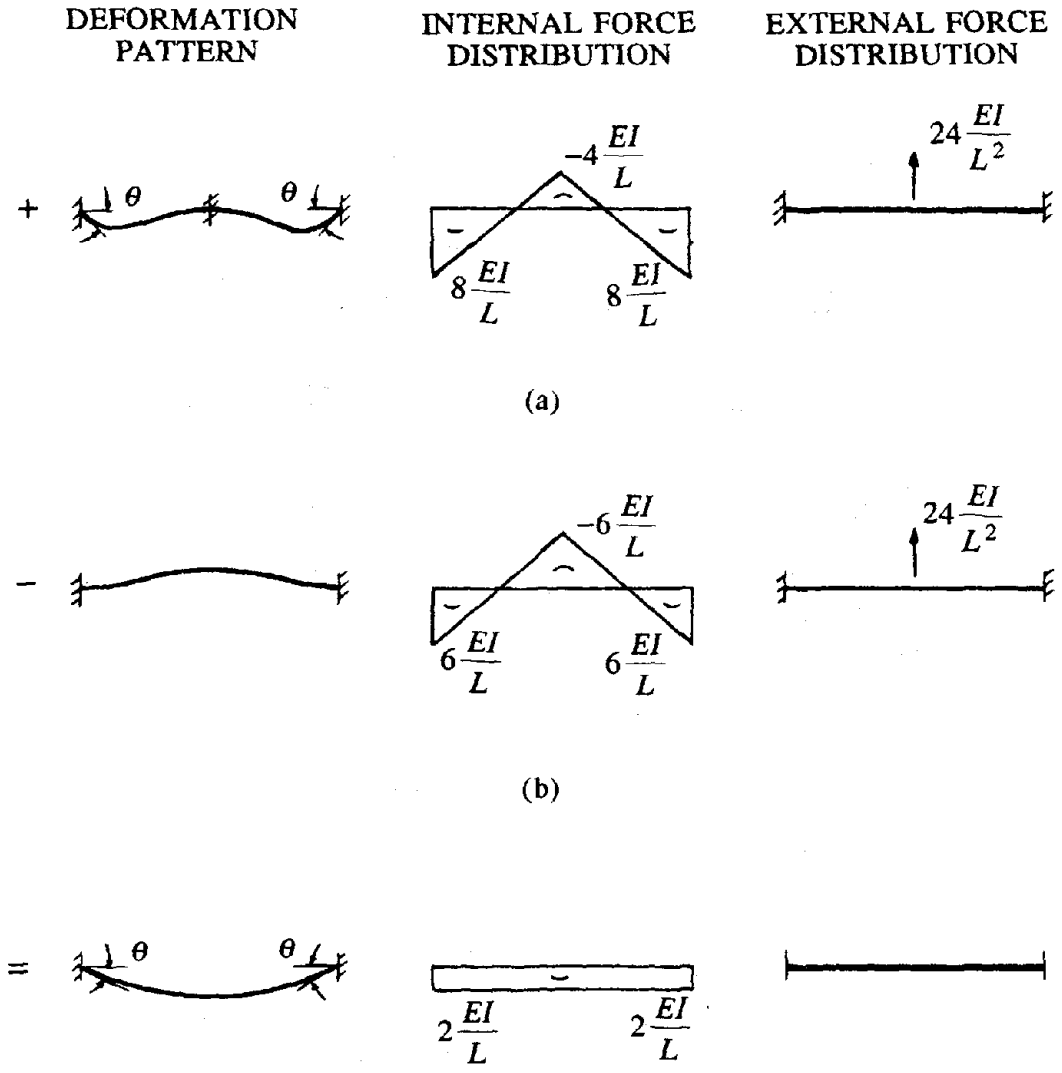

Fig. 2.4 - The pattern of self-equilibrating internal stresses that resists rotation at critical sections 1 and 4.

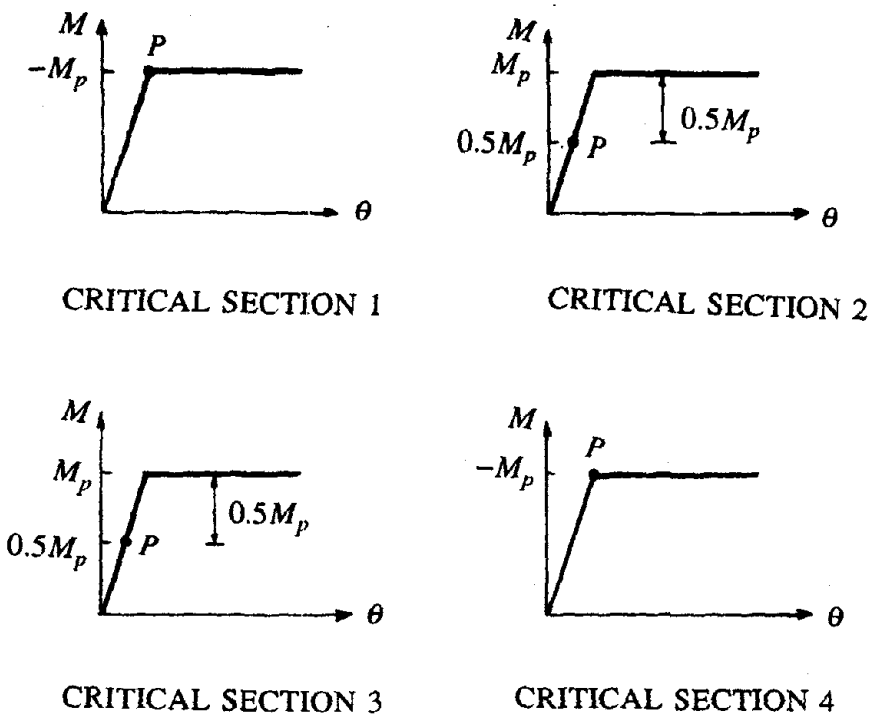

Fig. 2.5 - The state of stress at all critical section when elastic limit is reached.

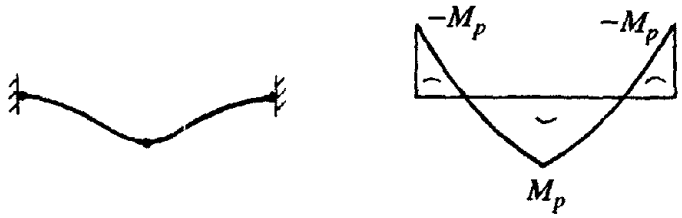

Fig. 2.6 - Deformation pattern and moment distribution at plastic collapse.

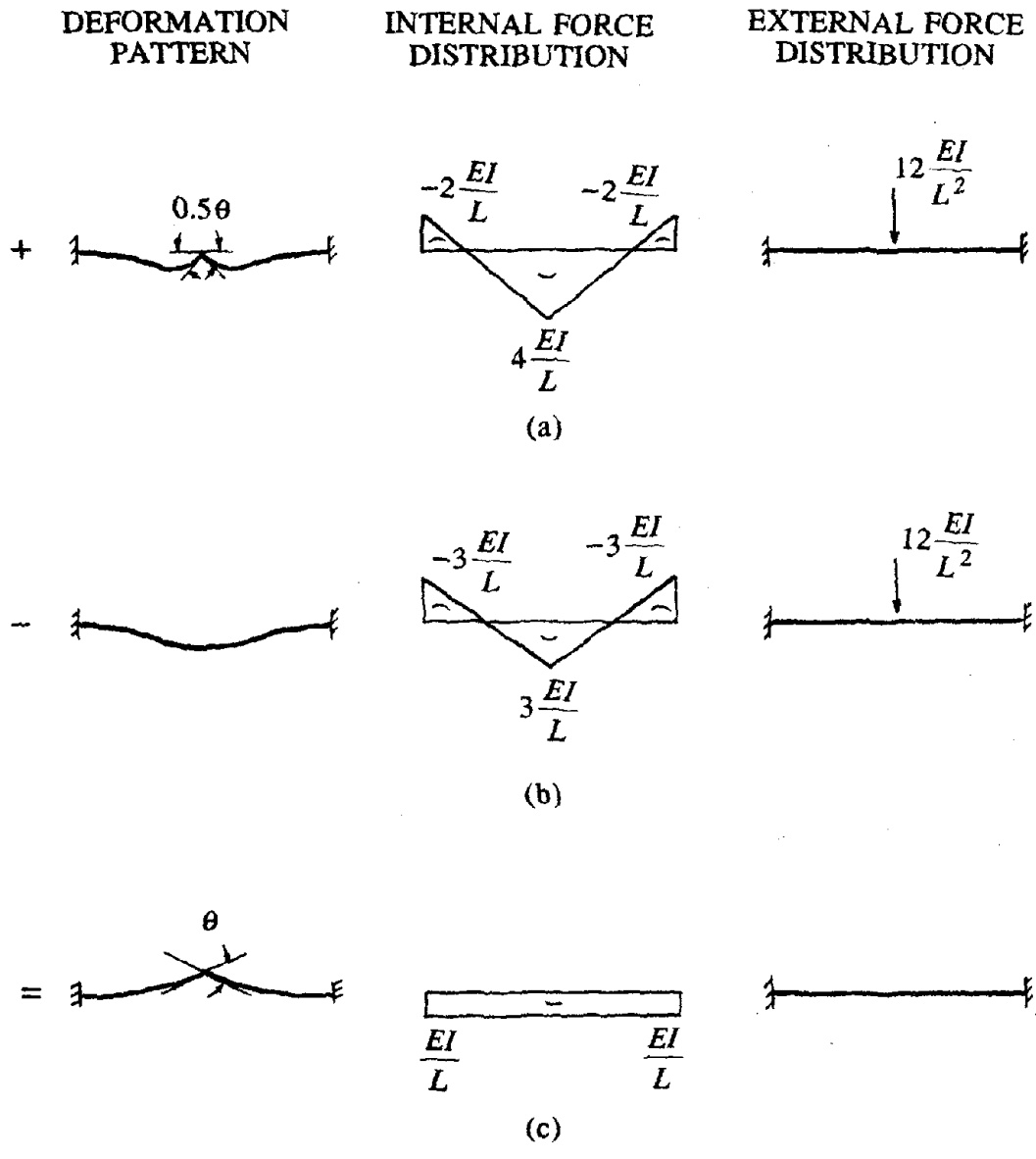

Fig. 2.7 - The pattern of self-equilibrating internal stresses that resists rotation at critical sections 2 and 3.

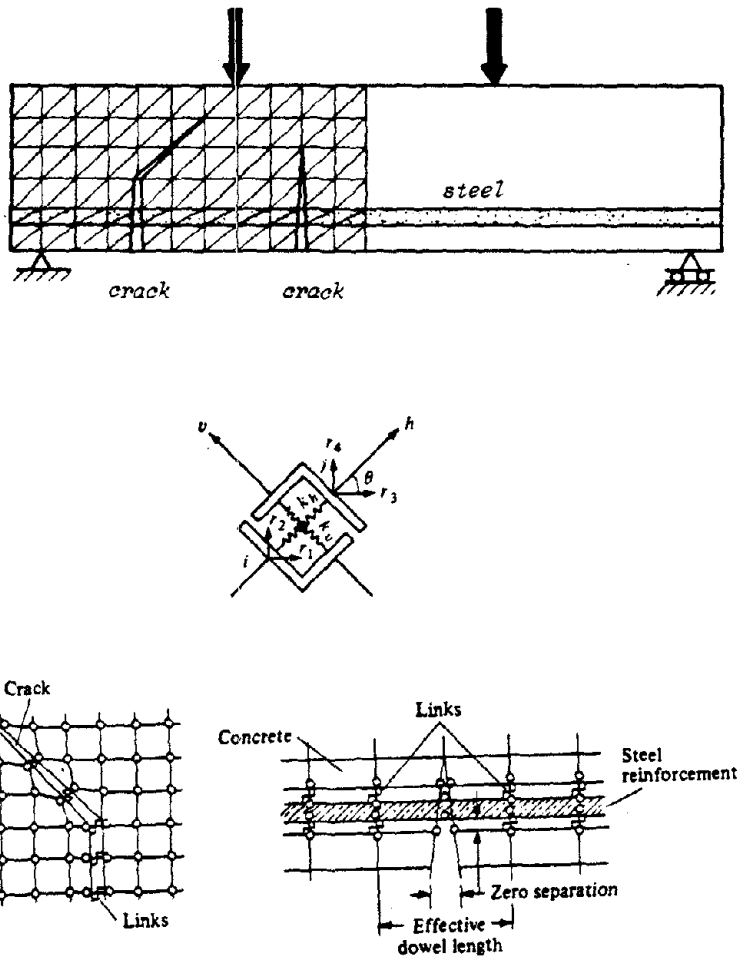

Fig. 2.8 - Discrete crack model for reinforced concrete model.

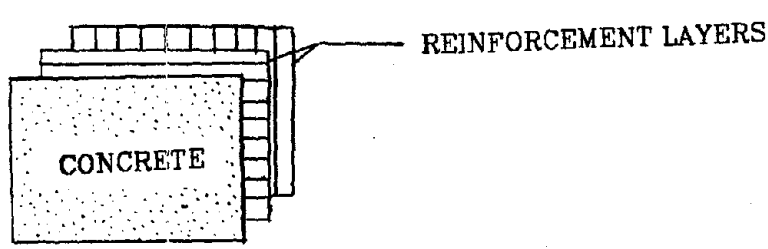

Fig. 2.9 - Distributed crack model for reinforced concrete model.

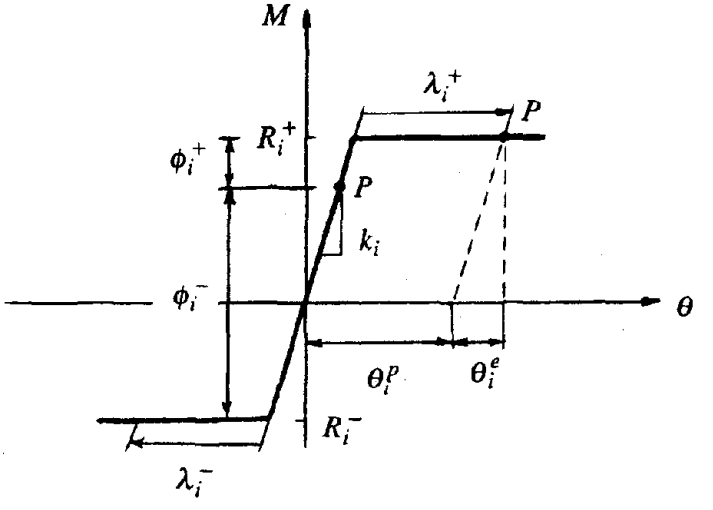

Fig. 3.1 - Elastic-perfectly plastic moment-curvature relationship of beam cross section i.

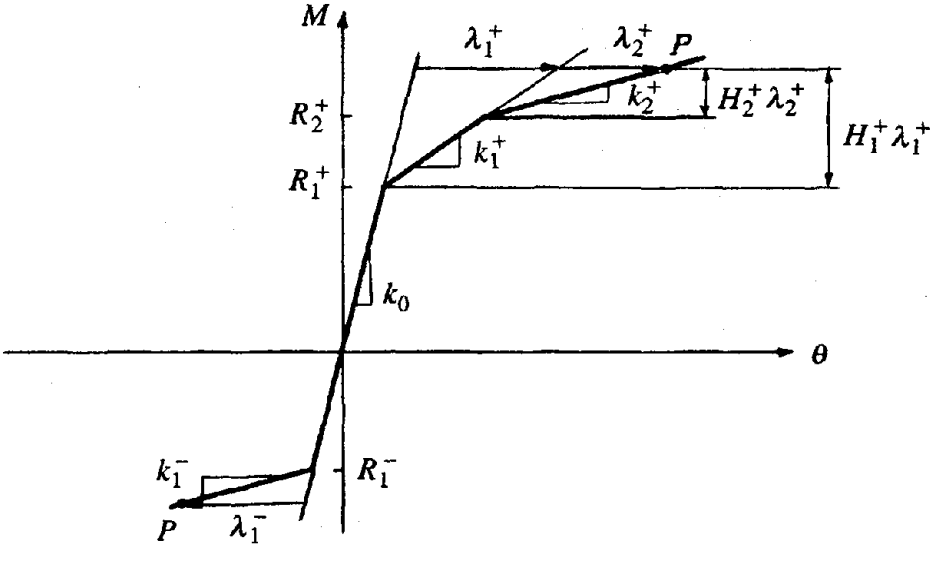

Fig. 3.2 - Elastic-linear workhardening moment-curvature relationship of beam cross section i.

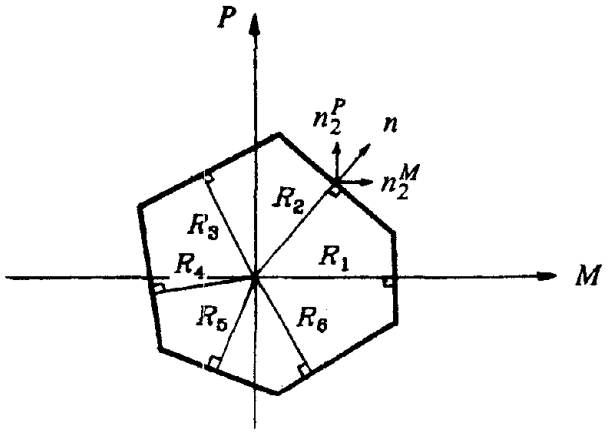

Fig. 3.3 - Elastic-perfectly plastic moment-axial load relationship of beam-column cross section i.

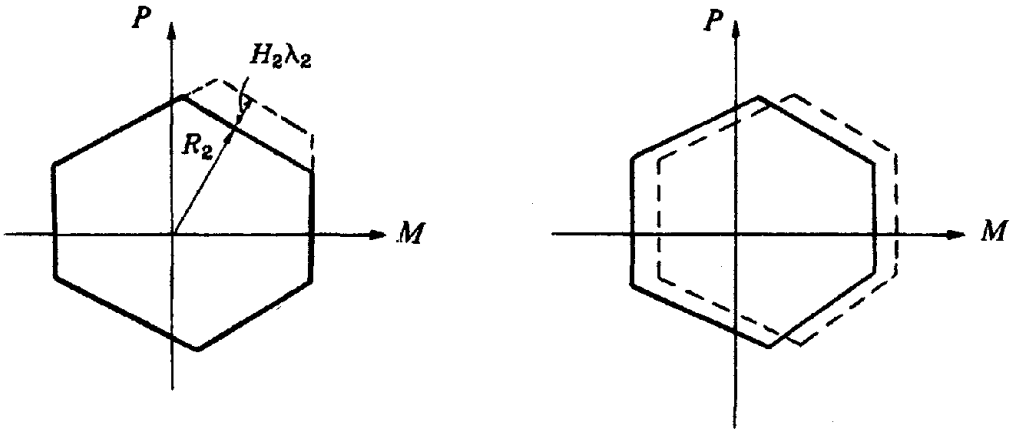

Fig. 3.4 - Elastic-linear hardening moment-axial load relationship of beam-column cross-section i.

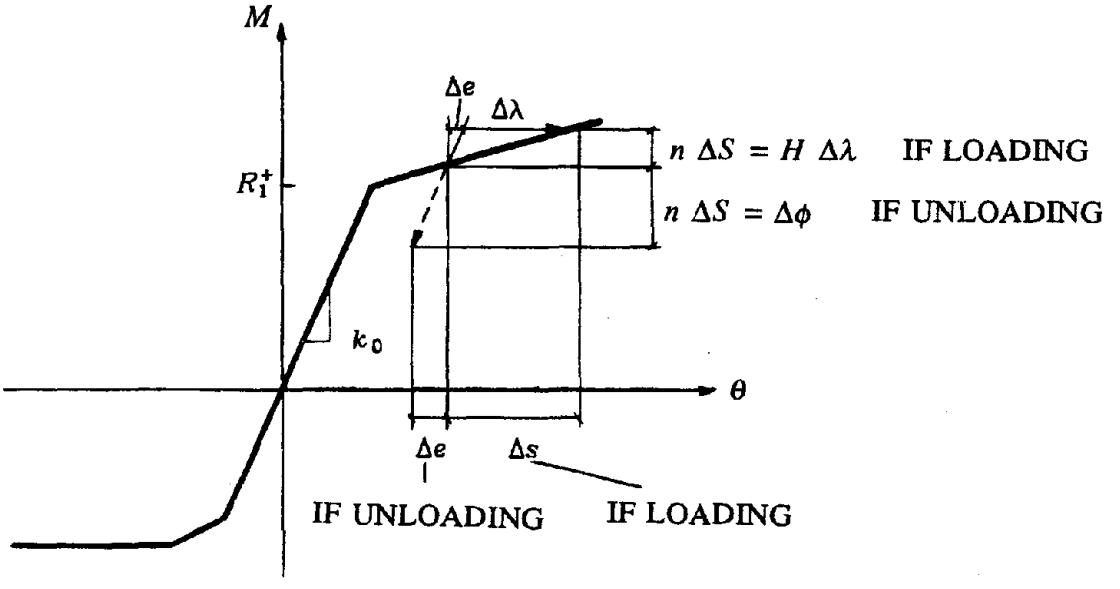

Fig. 3.5 - The nonholonomic elastic-linear workhardening behavior of beam cross section i.

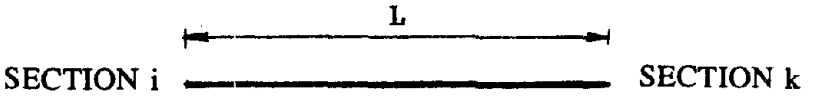

(a) Frame element e

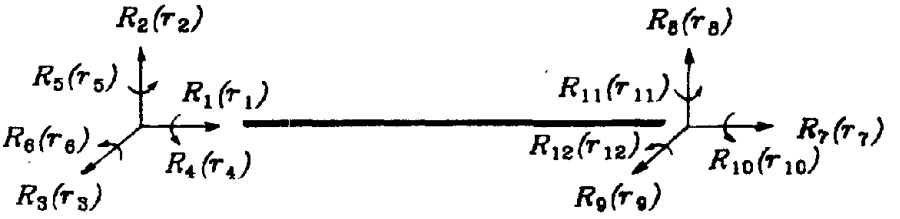

(b) Stress resultant - (deformation)

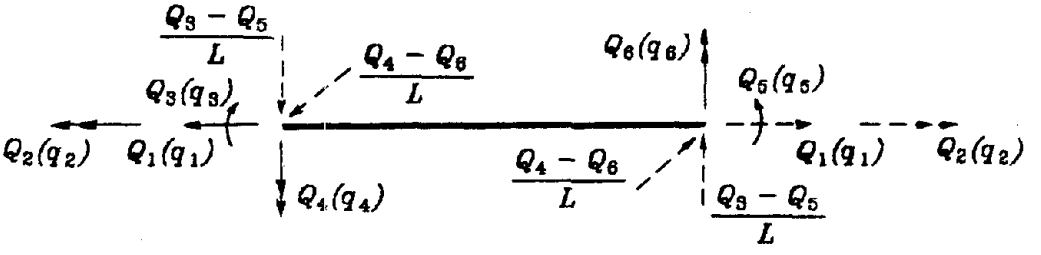

(c) Natural stress resultant - (natural deformation)

(d) Active stress resultant - (active deformation)

(e) Active stress resultant - (active deformation)

(f) Active stress resultant - (active deformation)

Fig 3.6 - Stress resultant vector for frame elements.

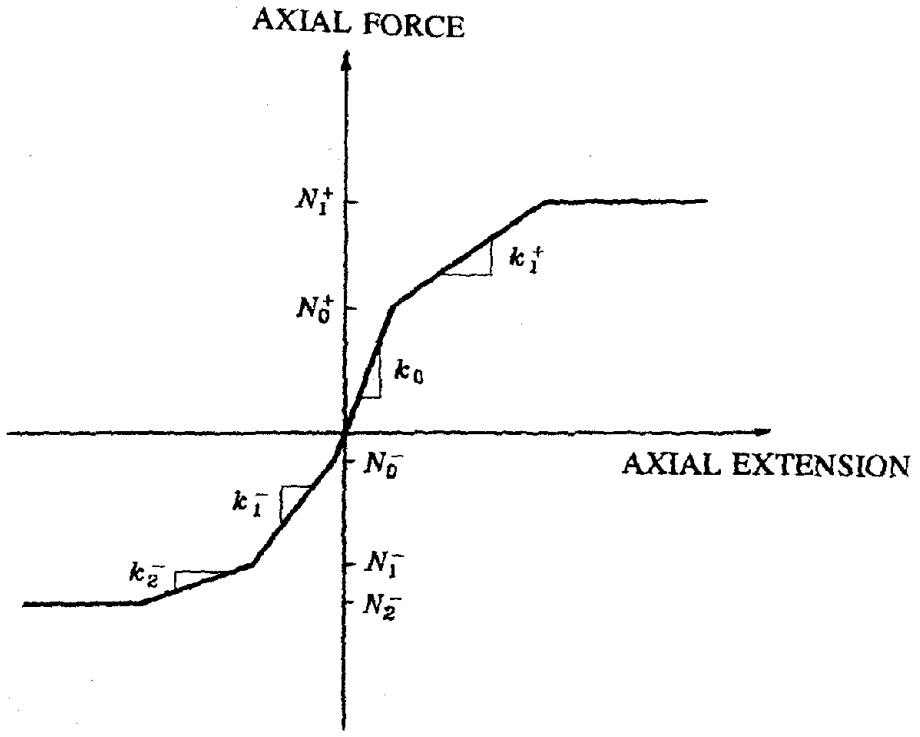

Fig. 4.1 - Multilinear force-deformation relationship for single stress component elements.

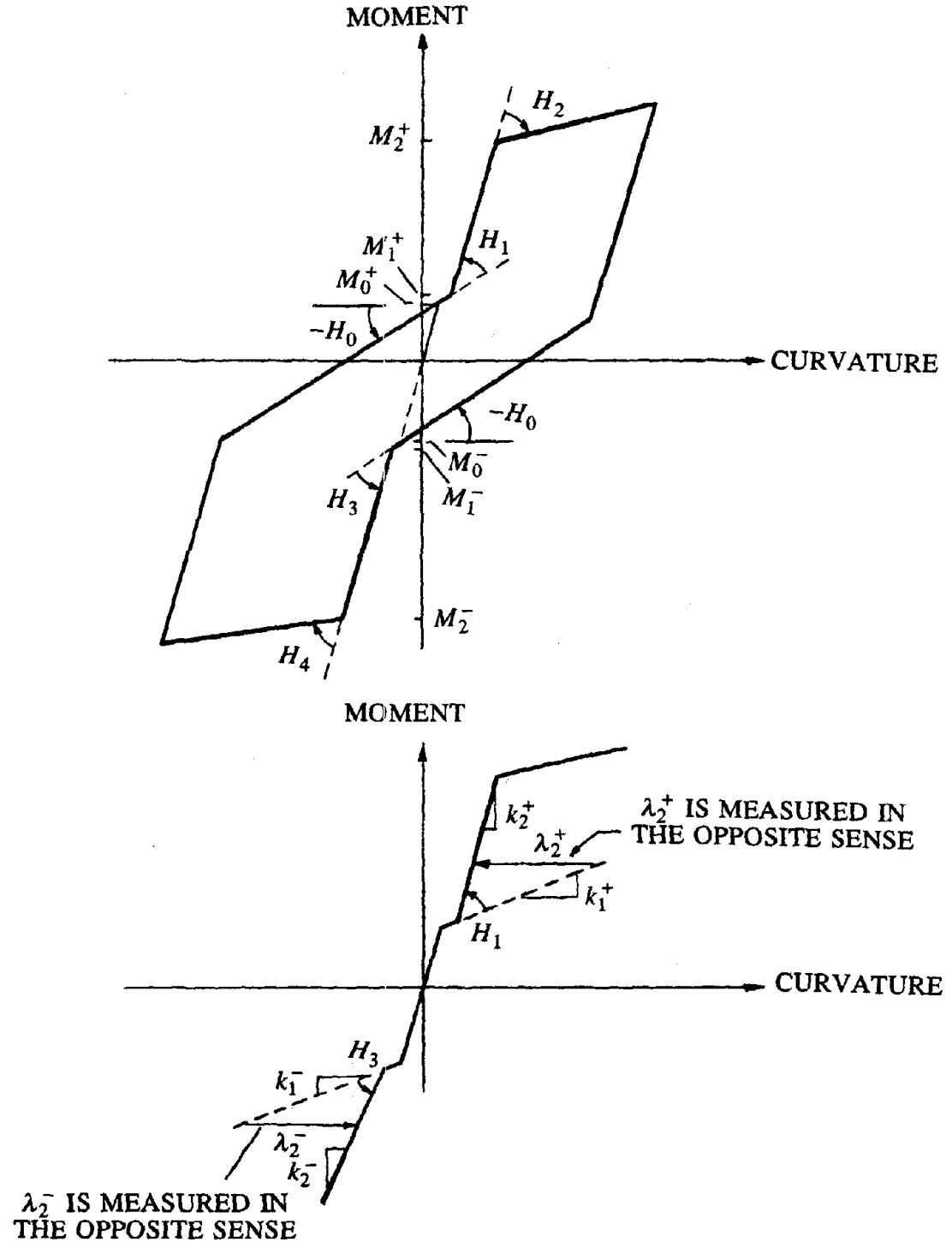

Fig. 4.2 - Modeling the pinching phenomenon for a reinforced concrete beam element.

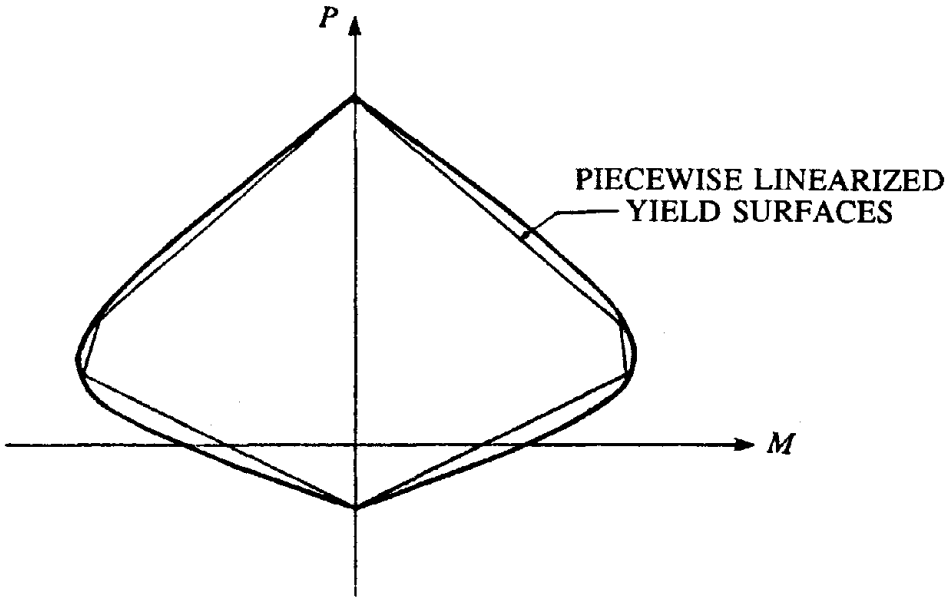

(a)

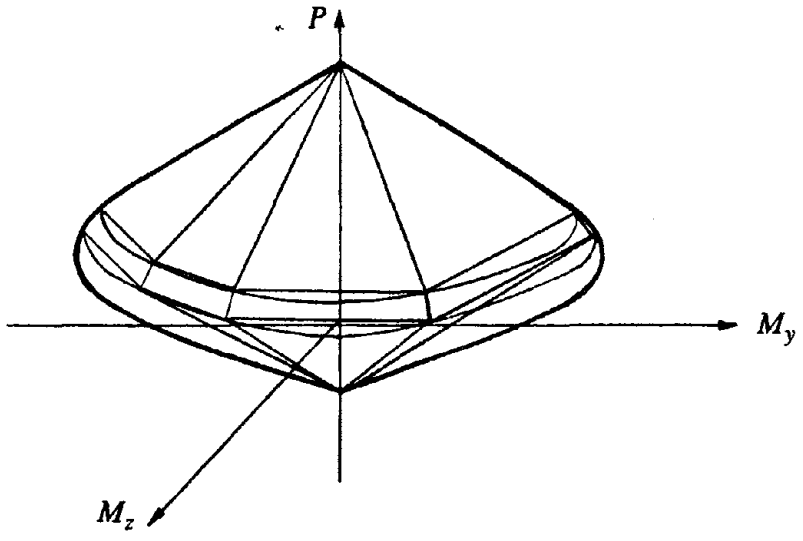

(b)

Fig. 4.3 - Uniaxial and biaxial interaction diagrams.

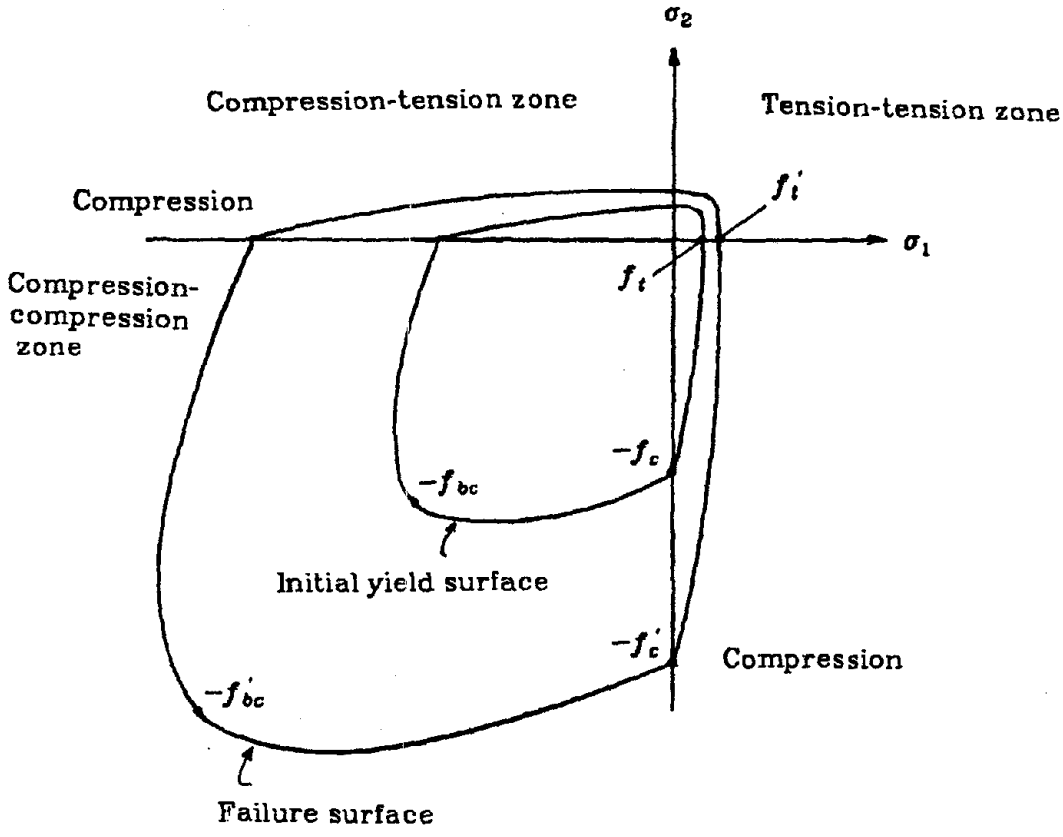

Fig 4.4 - Initial and failure yield surface of concrete in the principal stress plane.

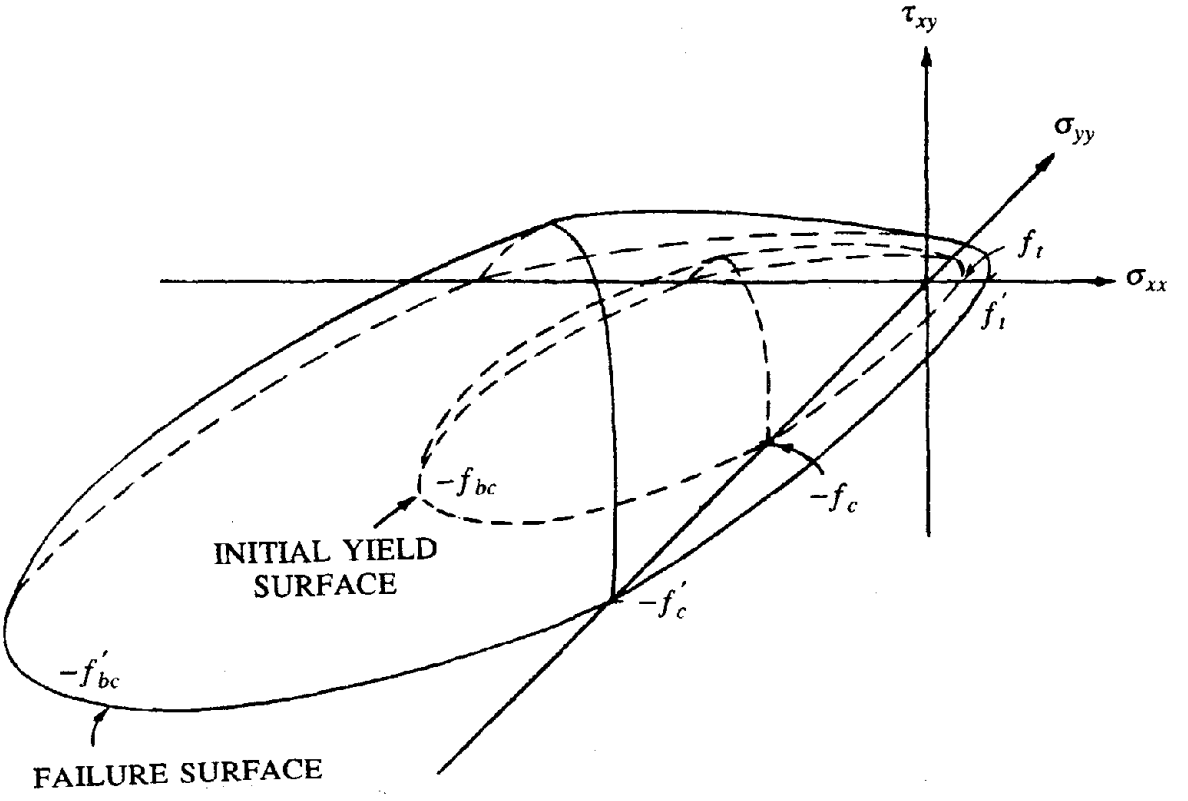

Fig. 4.5 - Initial and failure yield surfaces of concrete in the general stress space.

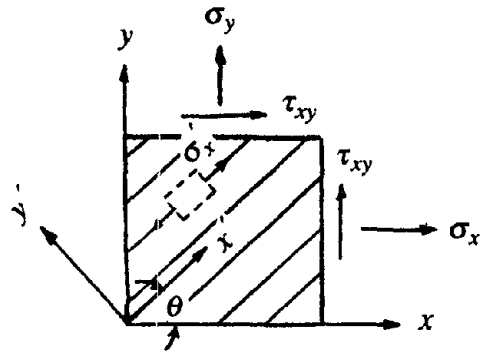

Fig. 4.6 - Stress components in the reinforcing bar elements.

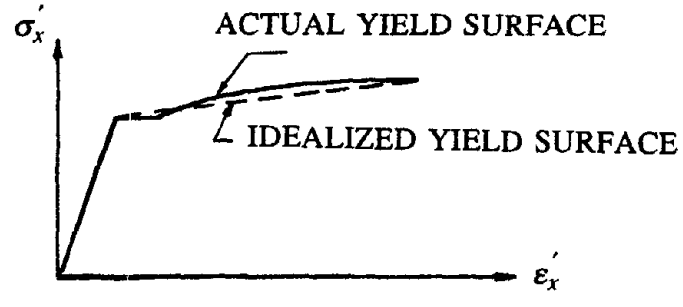

Fig. 4.7 - Uniaxial stress-strain relationship for the reinforcing bars.

x Integration points
• Nodal points

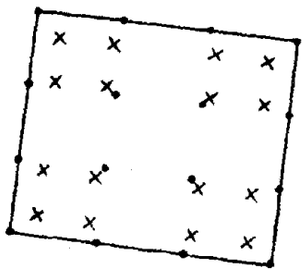

Fig 4.8 - Cubic rectangular plane stress elements.

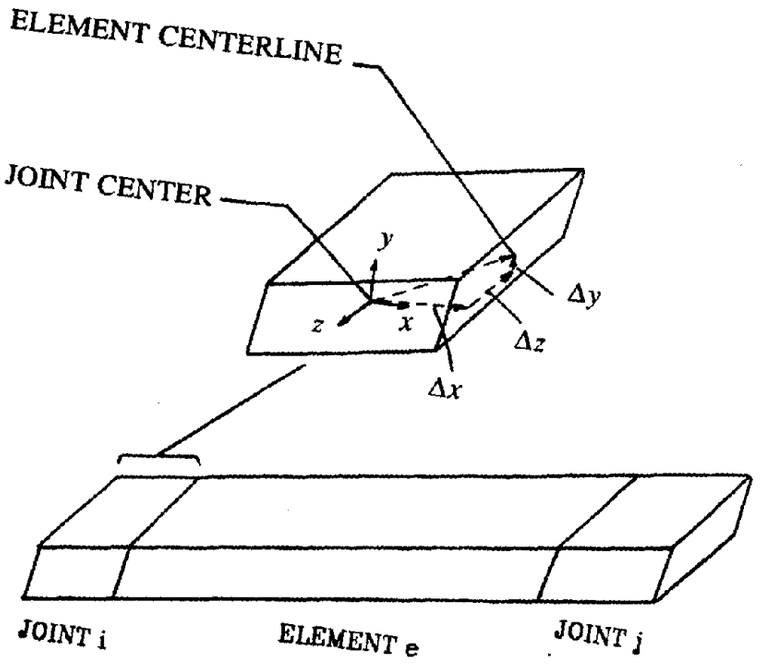

Fig. 4.9 - Joint element between frame elements.

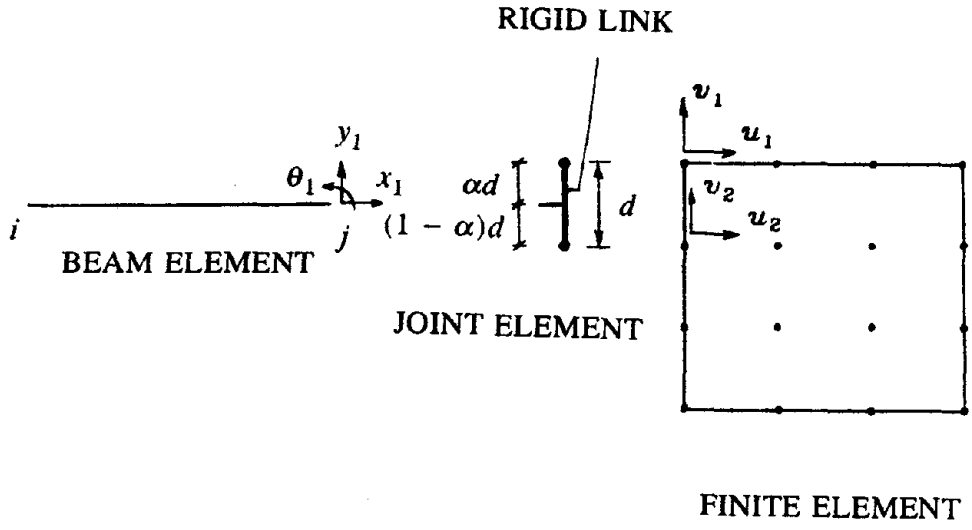

Fig. 4.10 - Joint element between a beam element and a finite element.

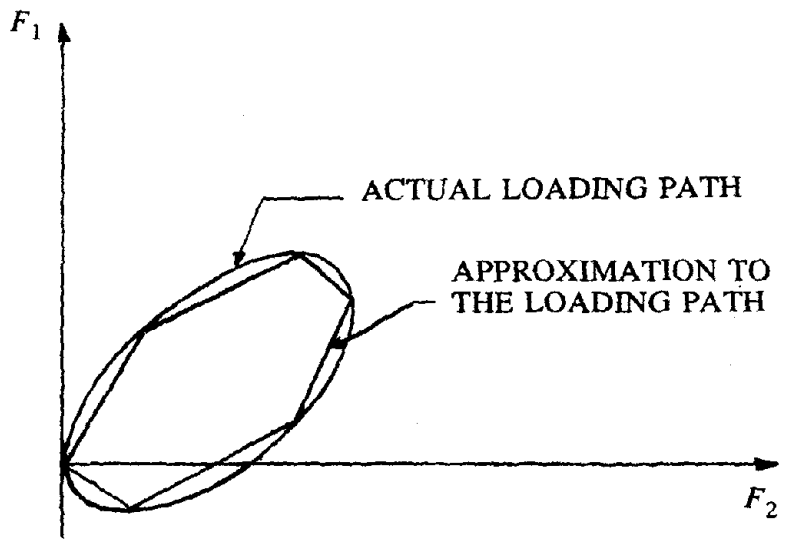

Fig 5.1 - A nonlinear loading path, approximated by several proportional loading stages.

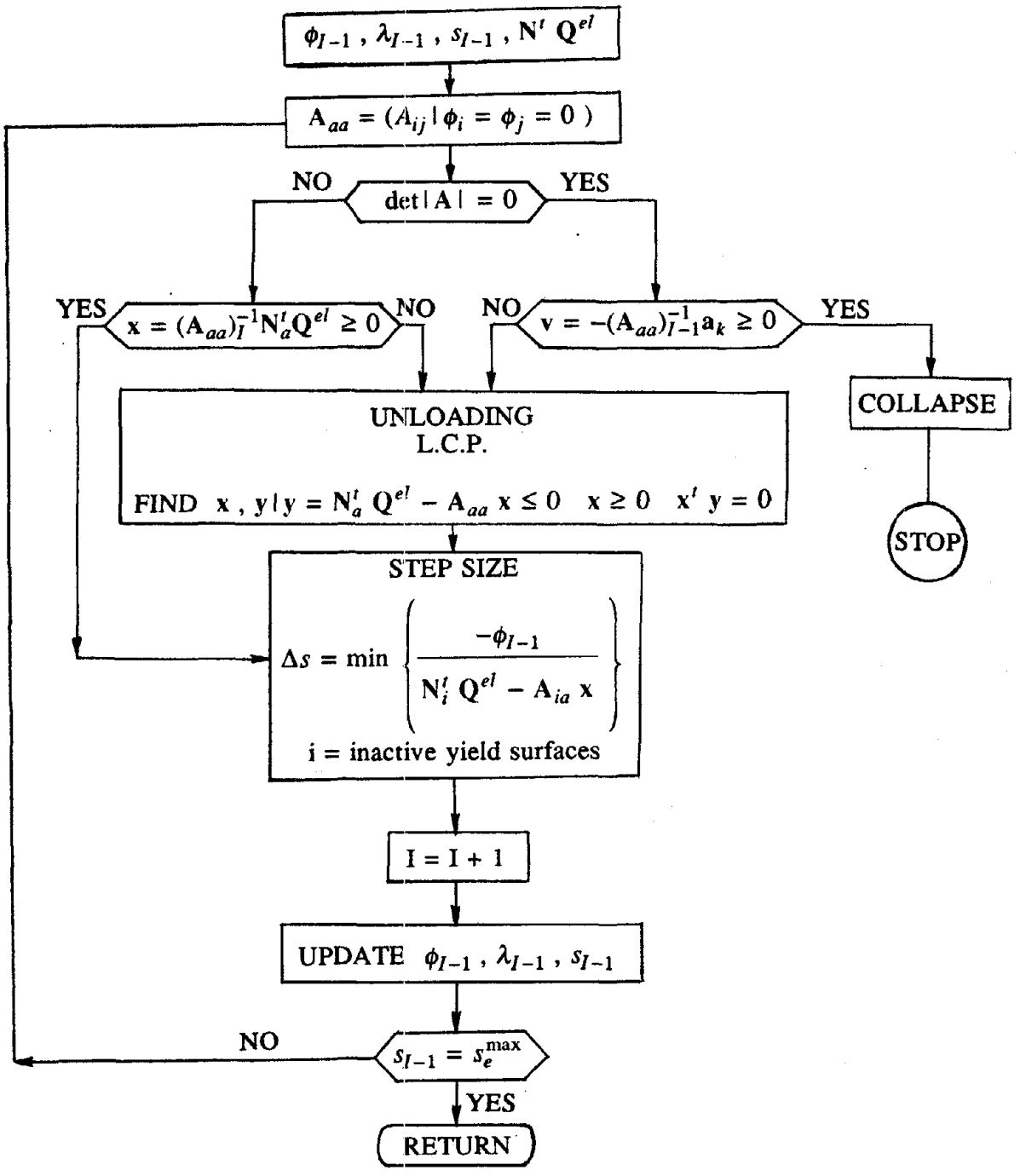

Fig 5.2 - Flowchart for the elastoplastic analysis procedure. This flowchart has been adopted from a procedure in reference 5.

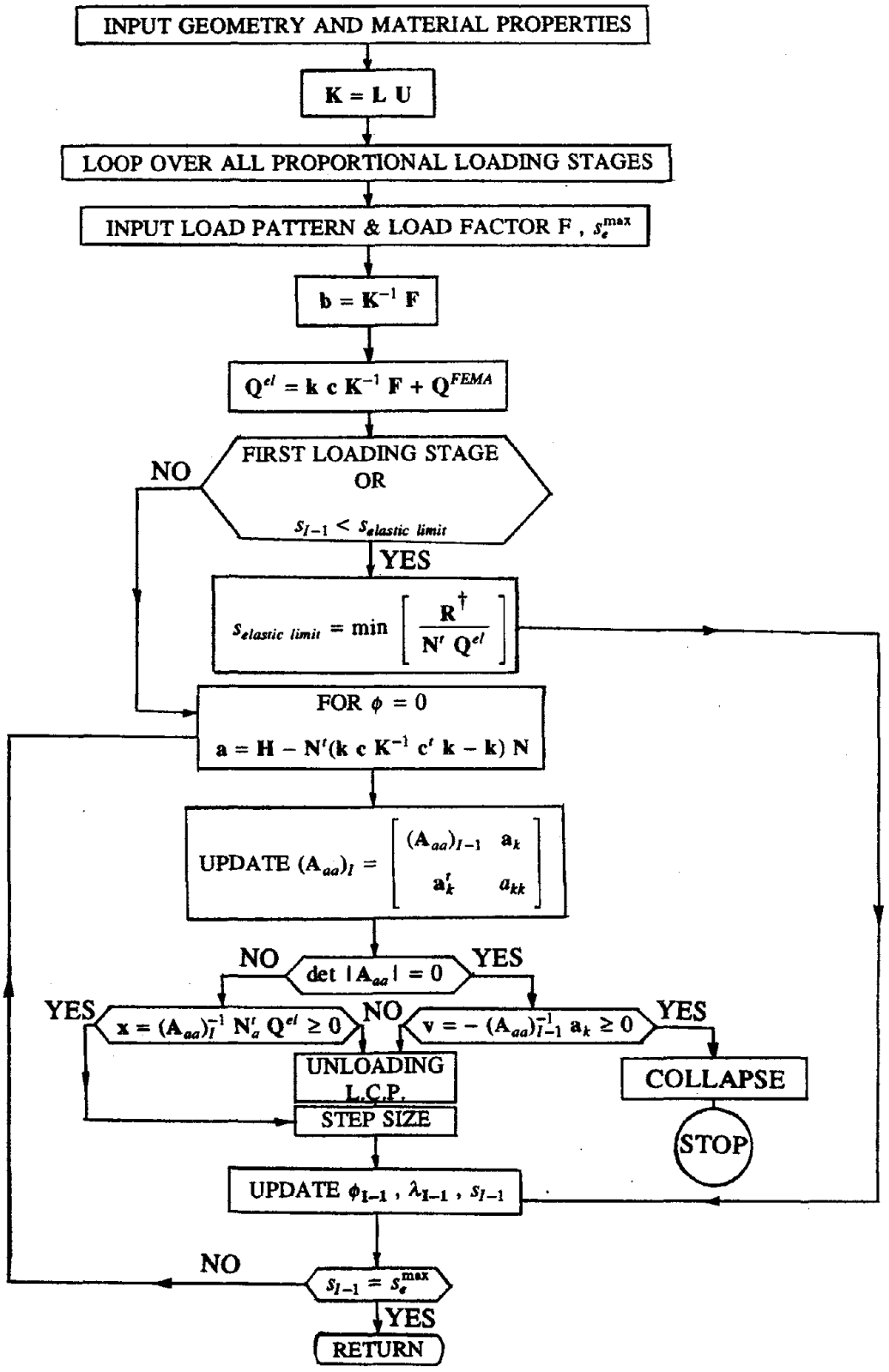

Fig. 5.3 - A flowchart for the complete analysis of the structure.

† If not the first loading stage, $R = -\phi$.

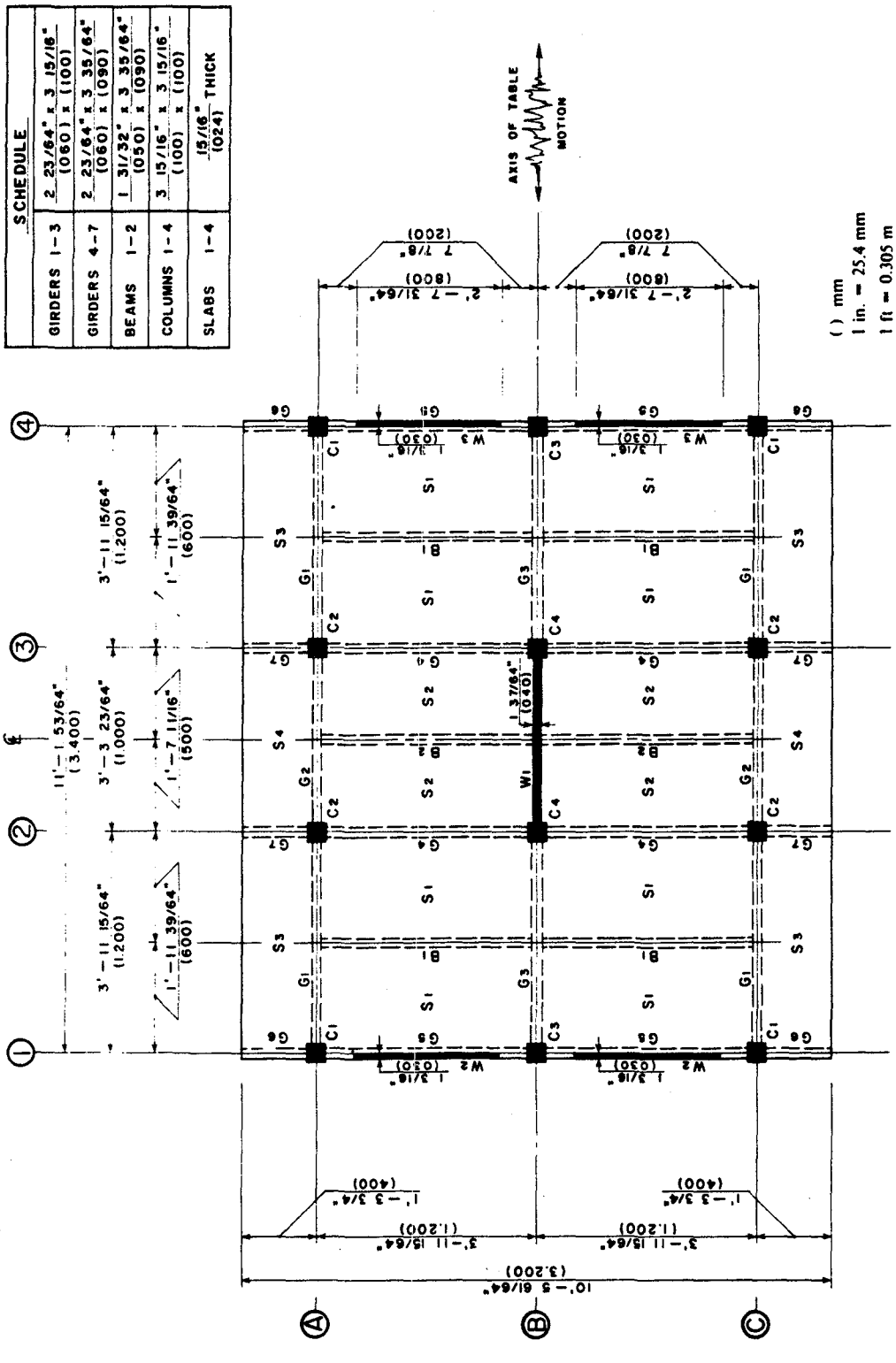

Fig. 6.1 - Typical floor plan of the 1/5-scale model

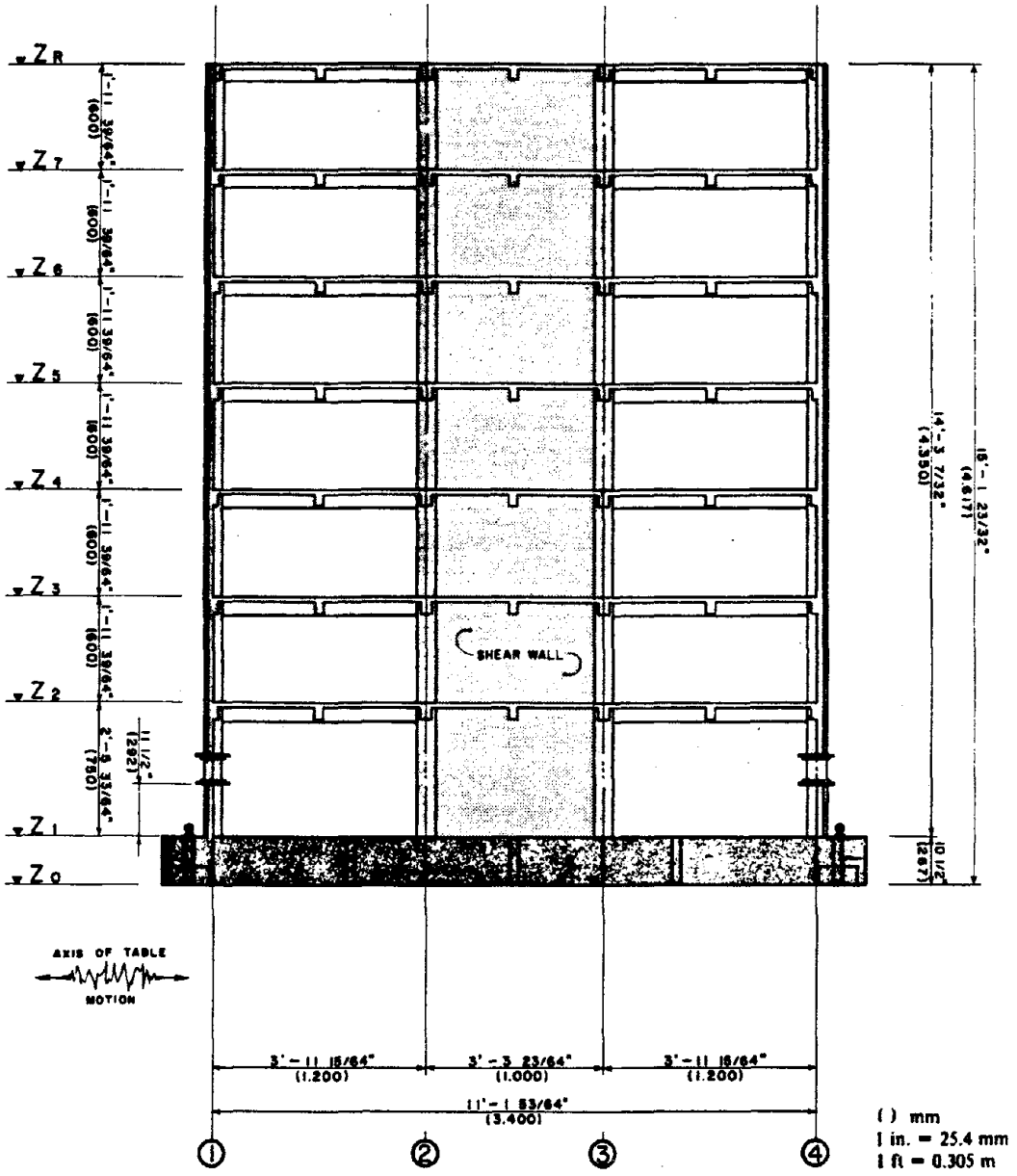

Fig. 6.2 - Elevation of the 1/5-scale model

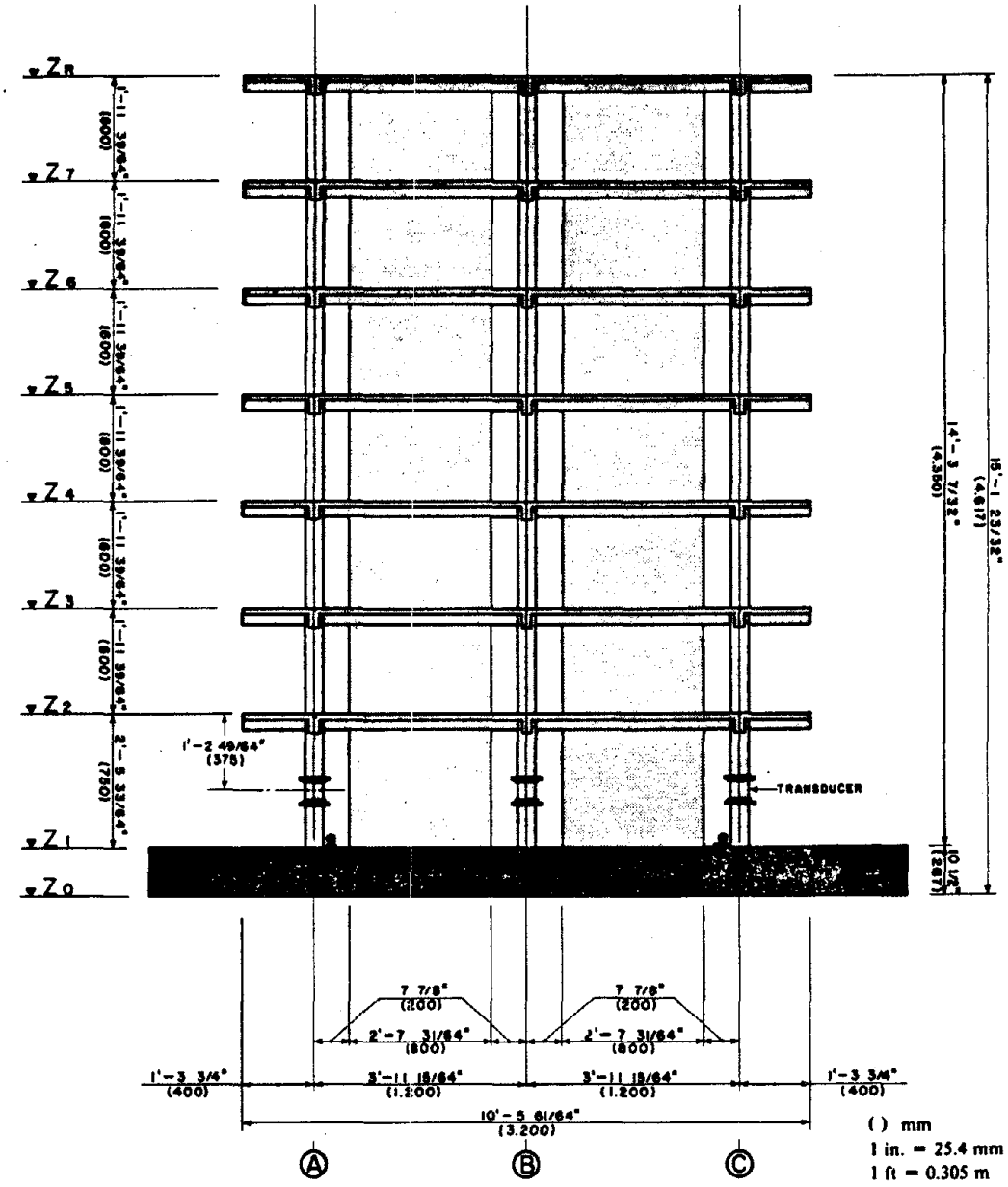

Fig. 6.3 - Section of the 1/5-scale model

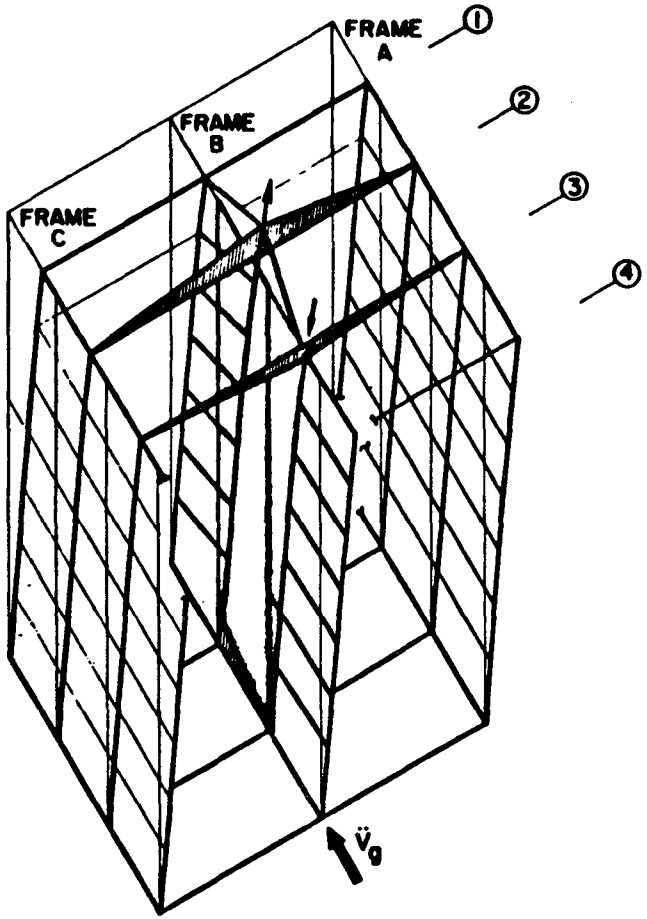

(a) Isometric view of wall rotation

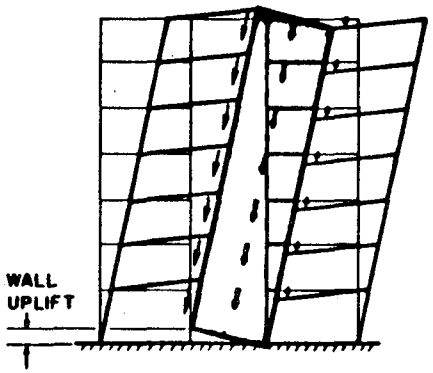

(b) Effect of wall uplift on connecting girders of frame

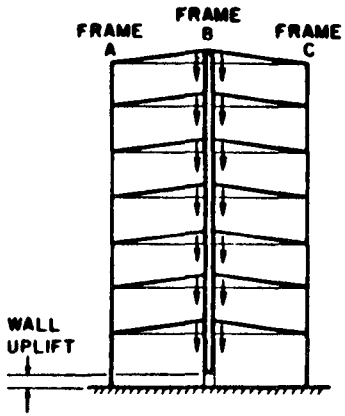

(c) Effect of wall uplift on girders framing into wall perpendicular to plane

Fig. 6.4 - Effect of outriggering action of frames on the shear wall

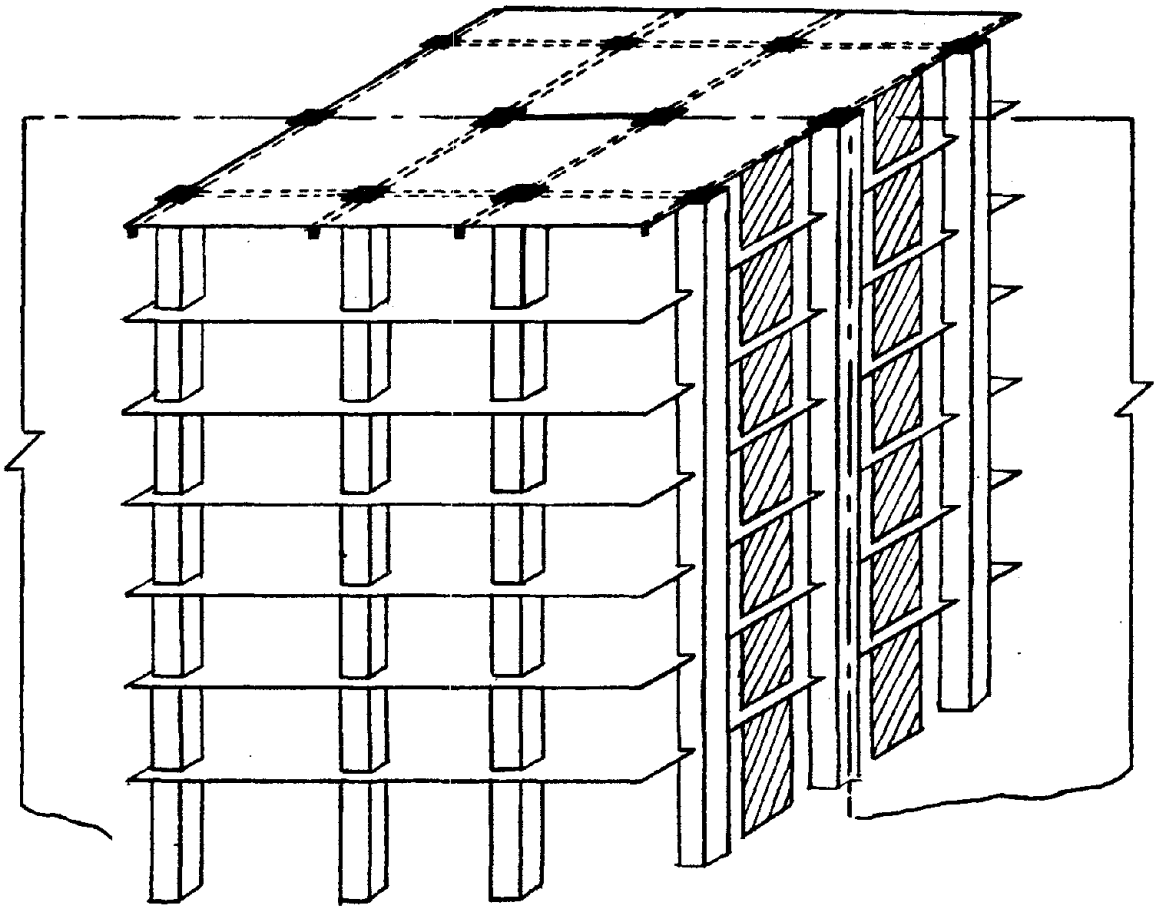

Fig. 6.5 - Three-dimensional view of the 1/5-scale model

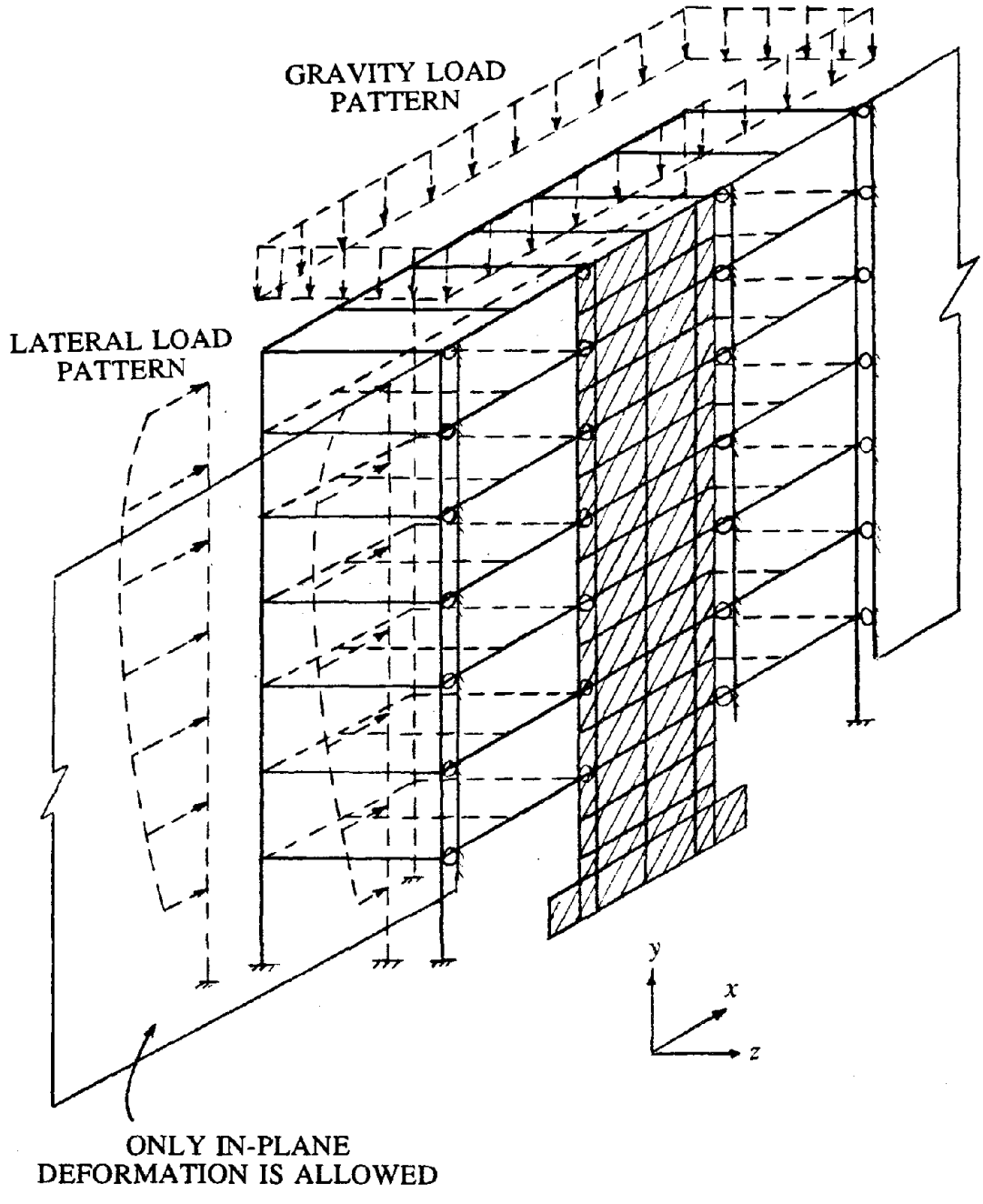

Fig. 6.6 - Analytical model used for the nonlinear analyses of the 1/5-scale structure

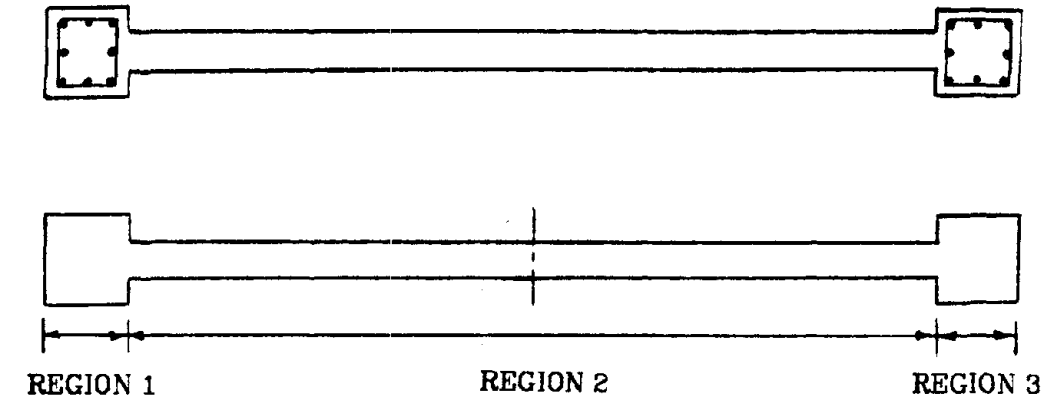

(a) Cross section

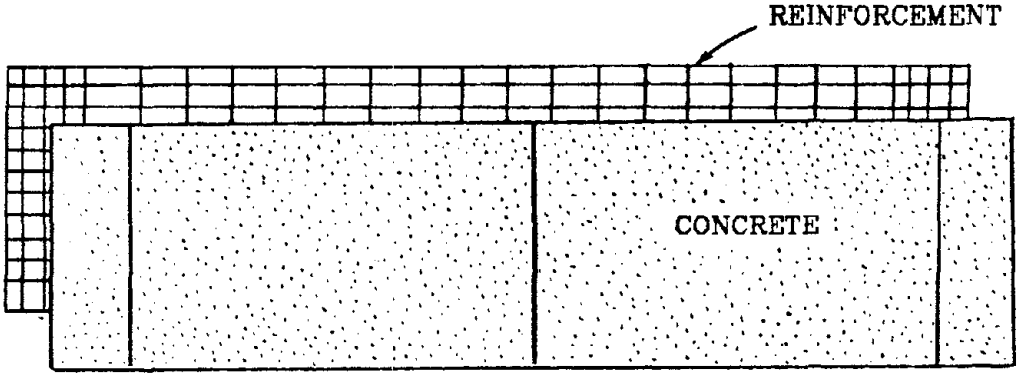

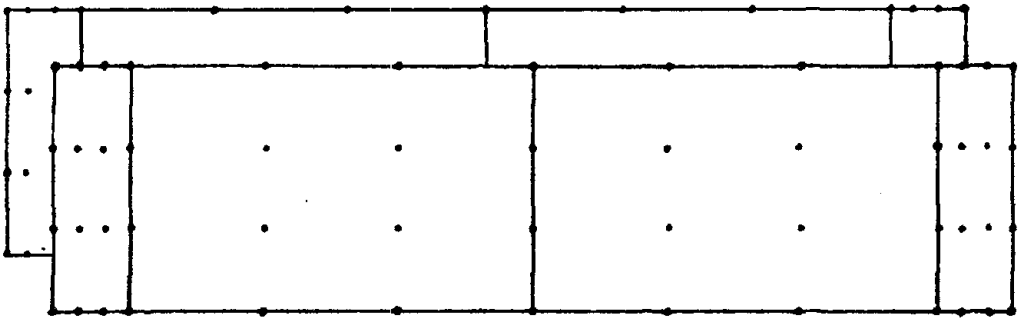

(b) Elevation

Fig. 6.7 - Finite element modeling of the shear wall

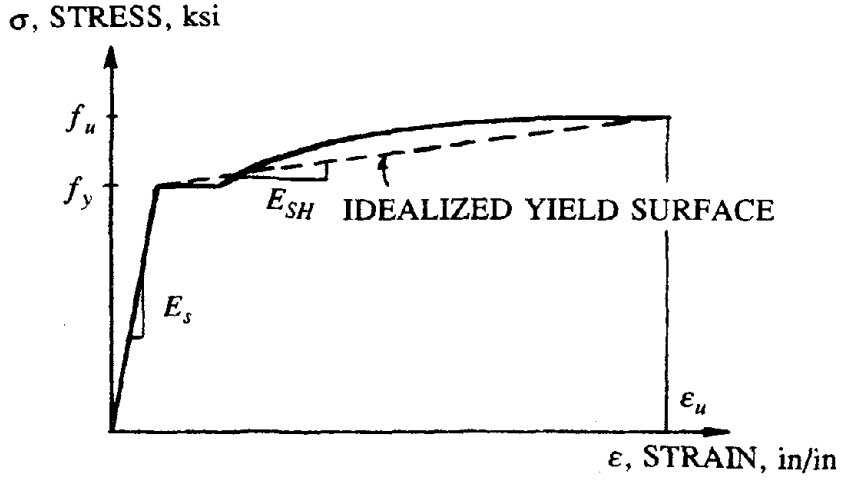

(a) Stress-strain relationship of reinforcing steel bars

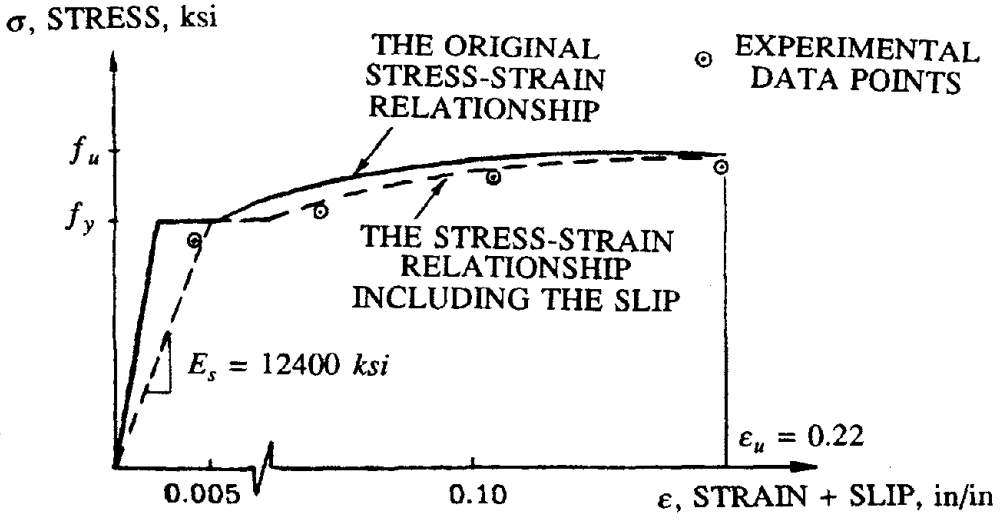

(b) Stress-strain relationship of the reinforcing bar modified to include the slip between the steel and the concrete

Fig. 6.8 - Material properties of the reinforcing steel bars

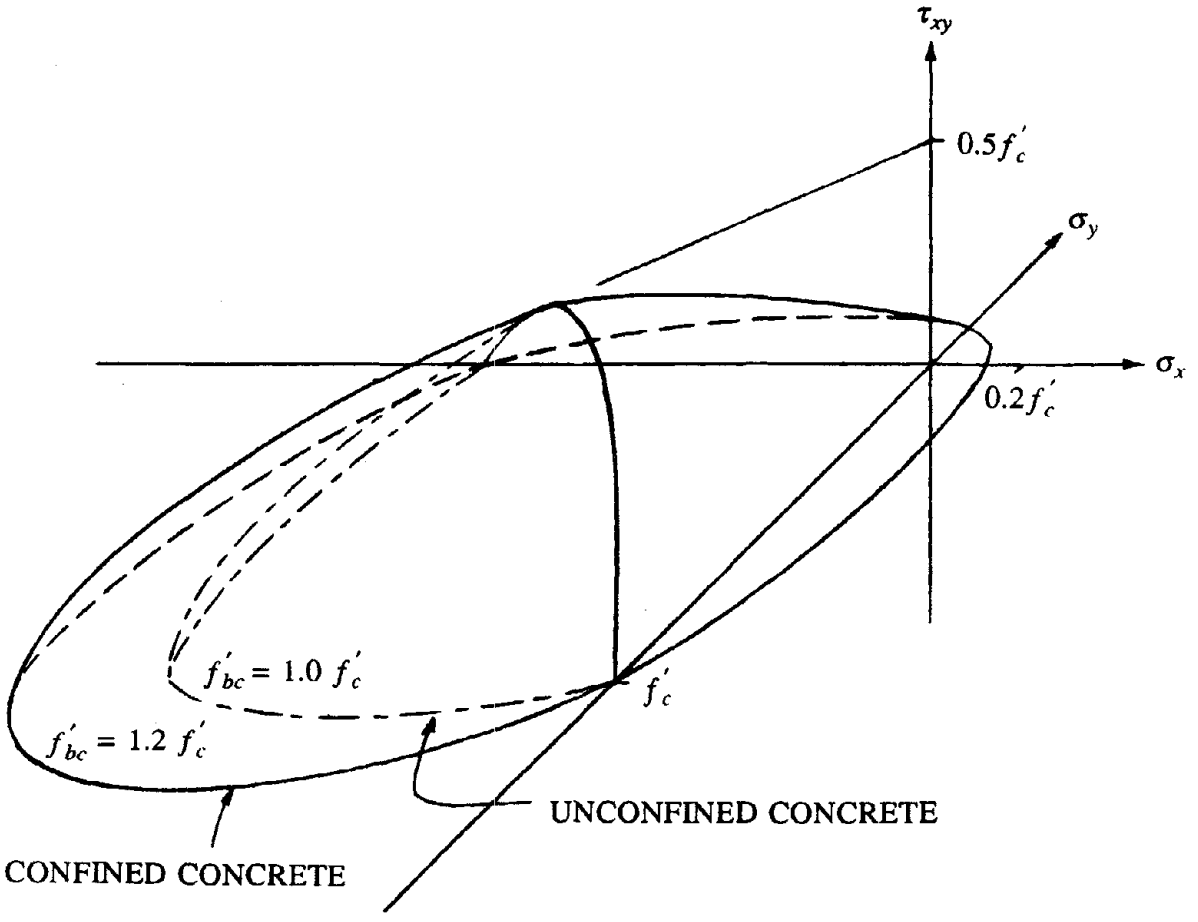

Fig. 6.9 - Yield surfaces defined for confined and unconfined concrete

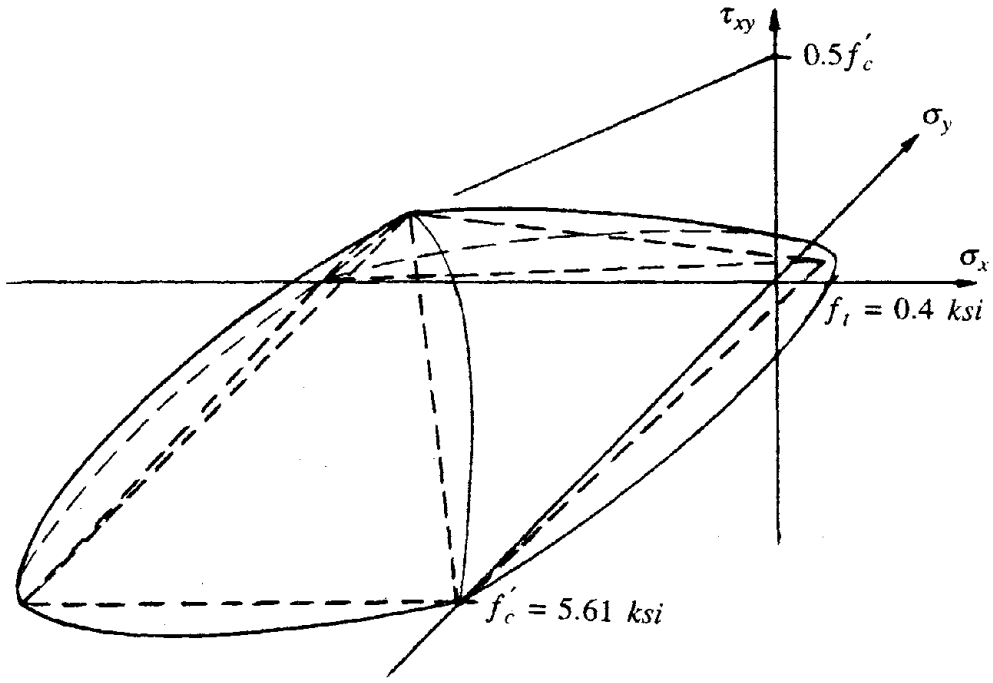

(a) Yield surfaces for unconfined concrete

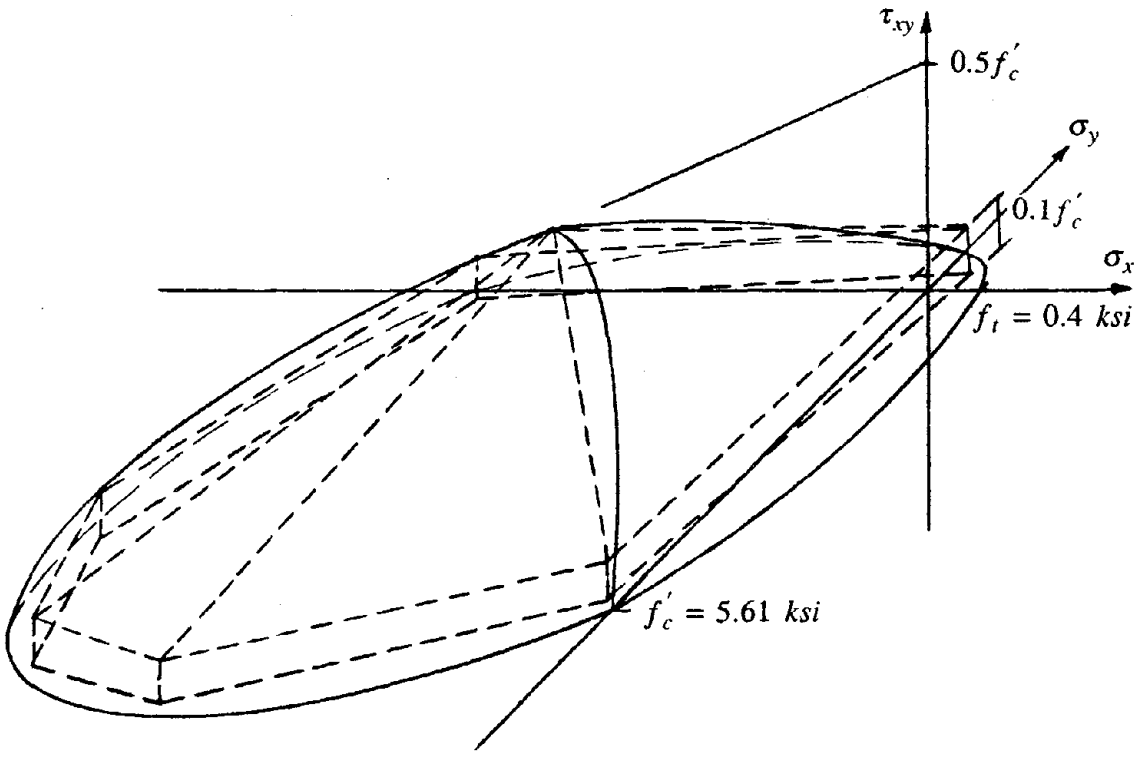

(b) Yield surfaces for confined concrete

Fig. 6.10 - Piecewise linearized yield surfaces for confined and unconfined concrete

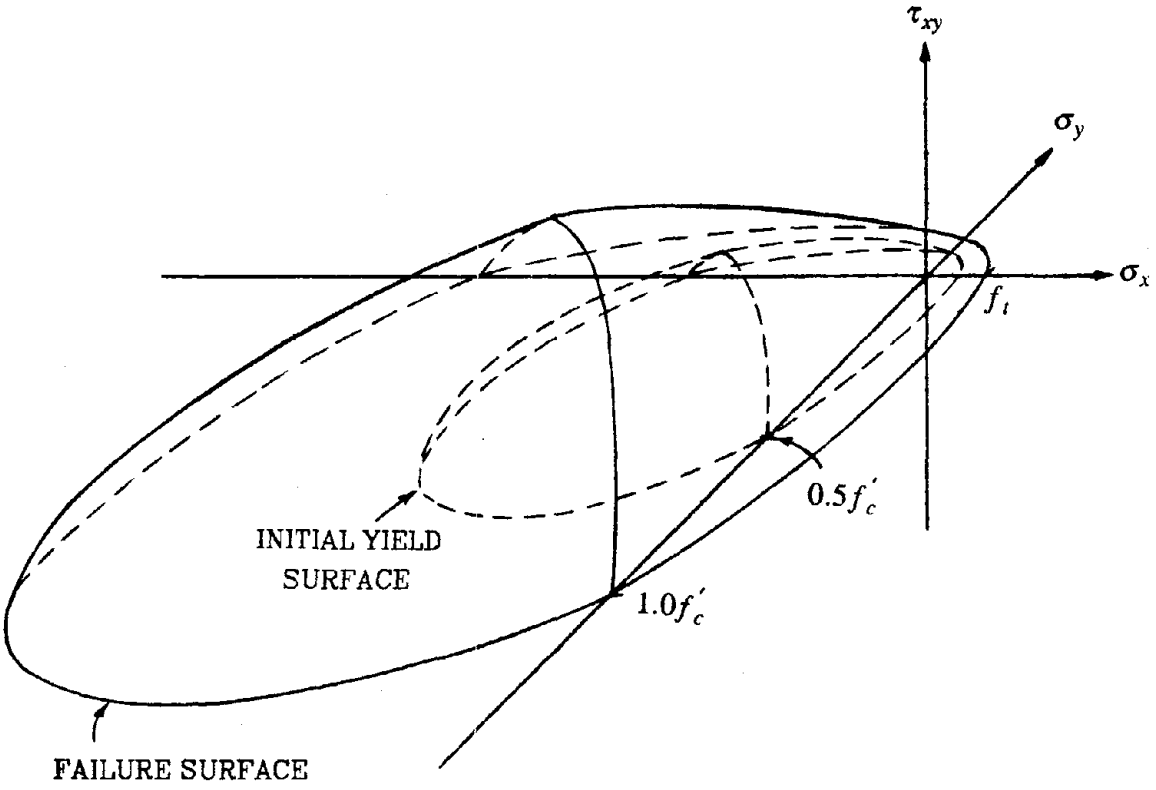

Fig. 6.11 - Initial and failure yield surfaces of concrete

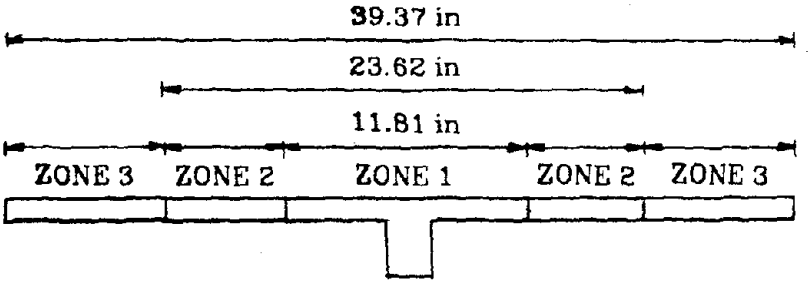

(a) Section detail showing different zones of slab steel where strain distribution is different

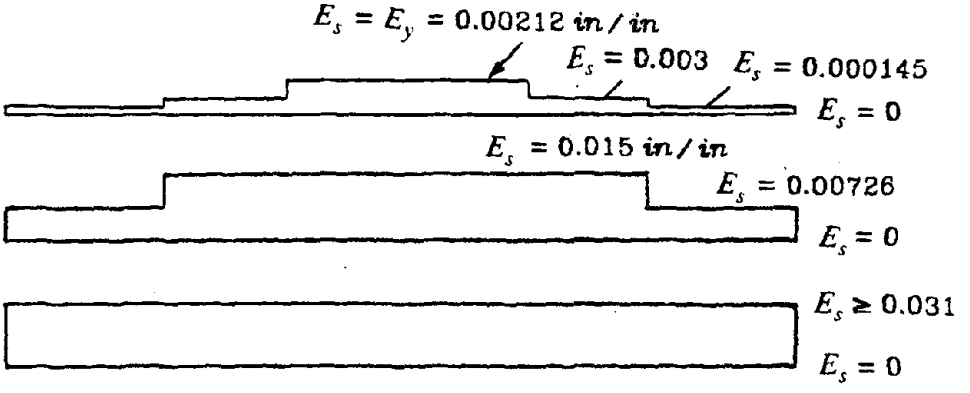

(b) A nonuniform distribution of strain in slab steel

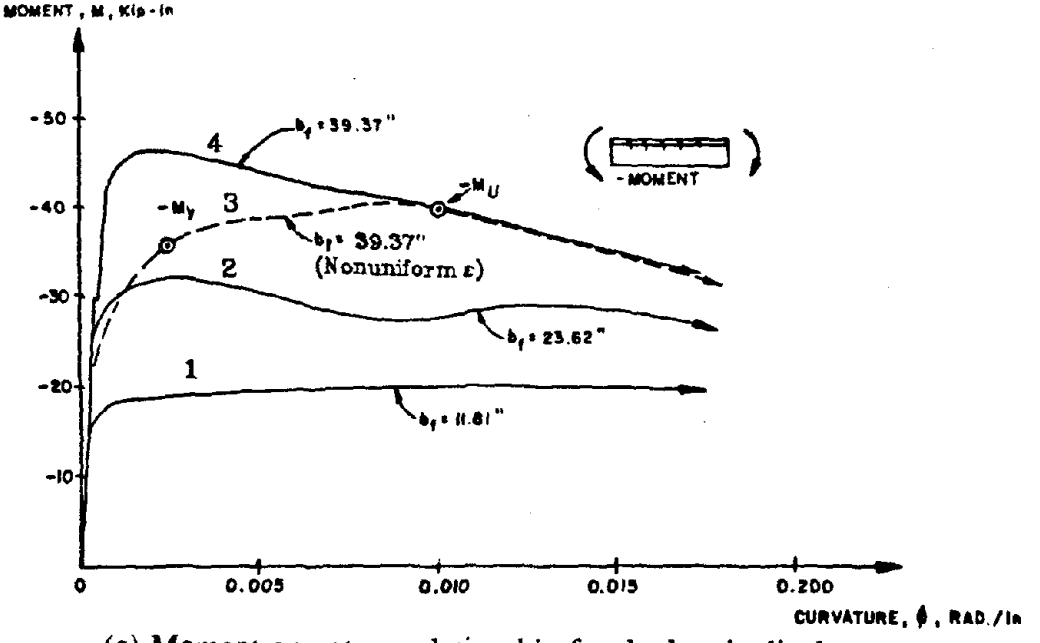

(c) Moment-curvature relationship for the longitudinal girder as based on the spread of yielding on the slab.

Fig. 6.12 - Effect of the spread of yielding through the width of the slab on the moment-curvature relationship of the longitudinal girders

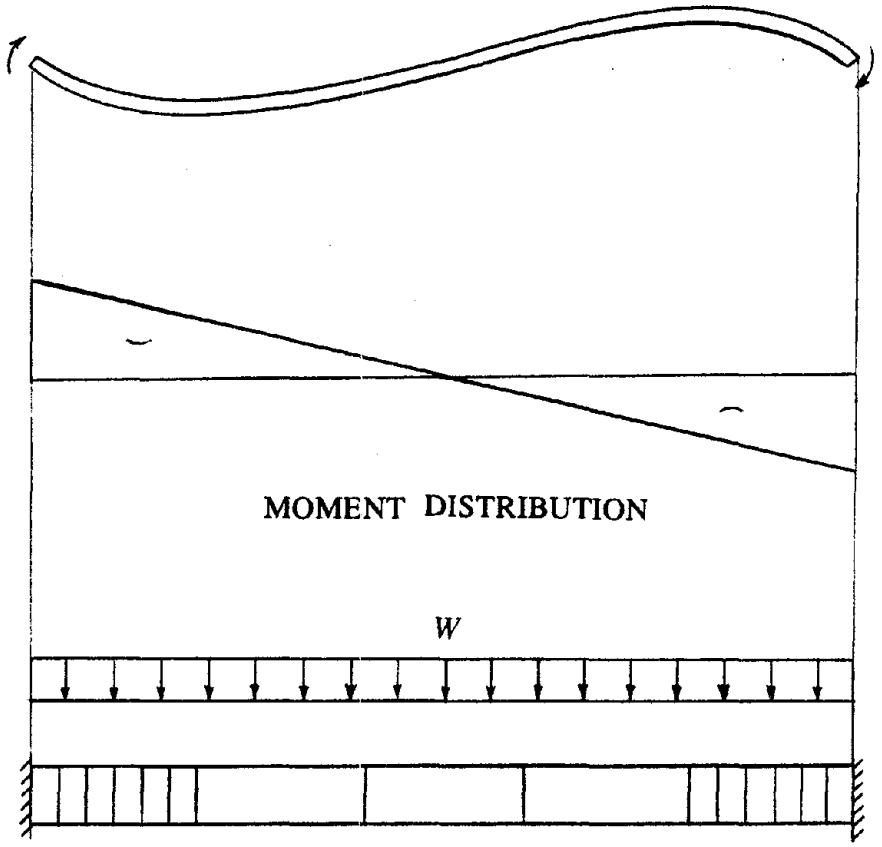

Fig. 6.13 - Discretizing girders to model the spread of plastic zone at the ends of girders

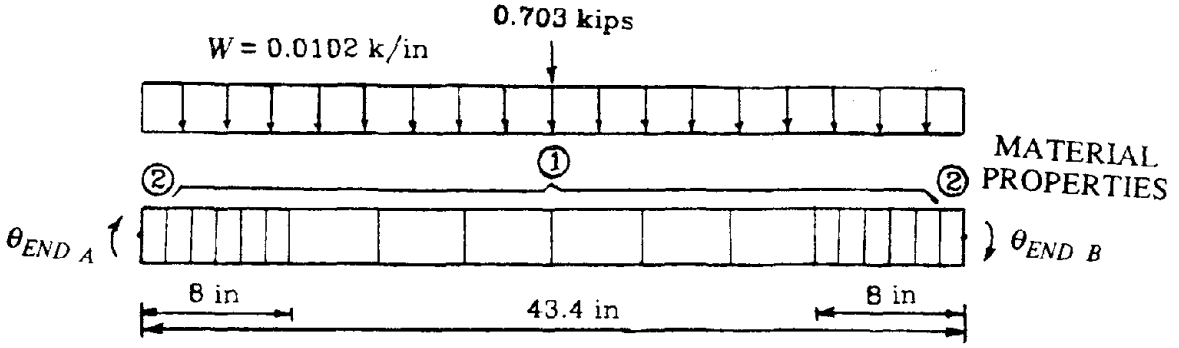

(a) Element discretization

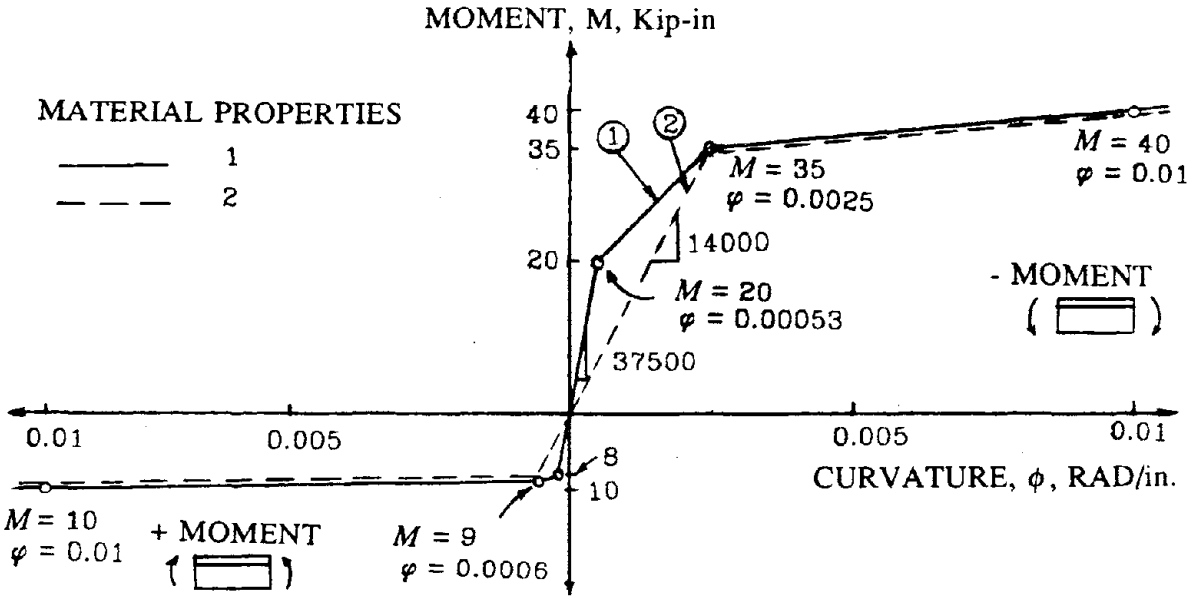

(b) Material properties assigned to the beam elements

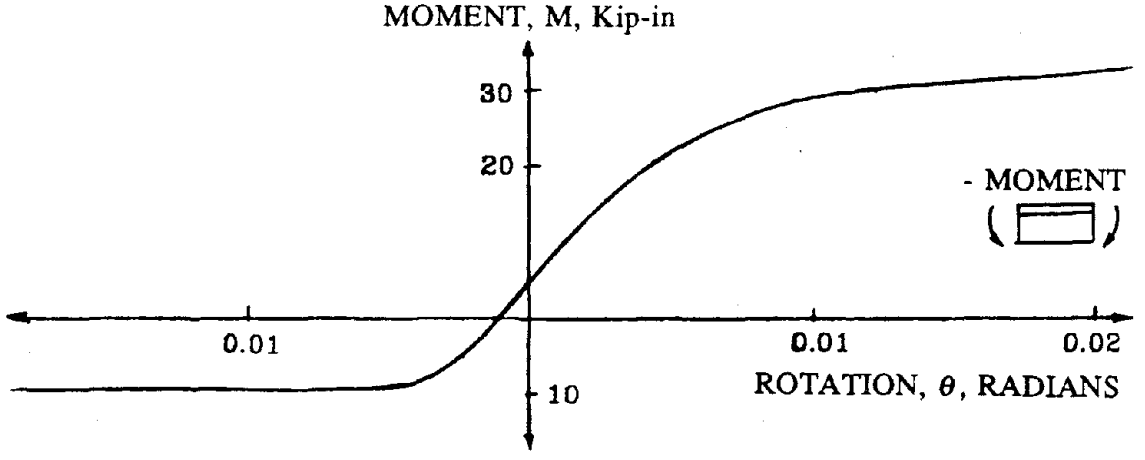

(c) The moment-rotation relationship obtained for the longitudinal girders

Fig. 6.14 - Modeling of the longitudinal girders

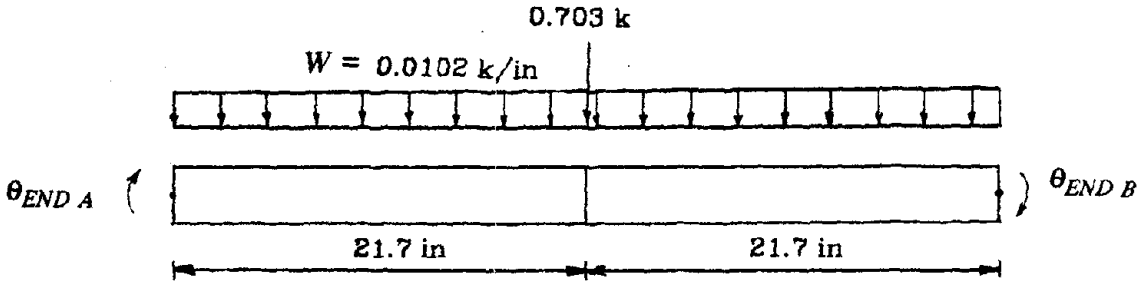

(a) Element discretization

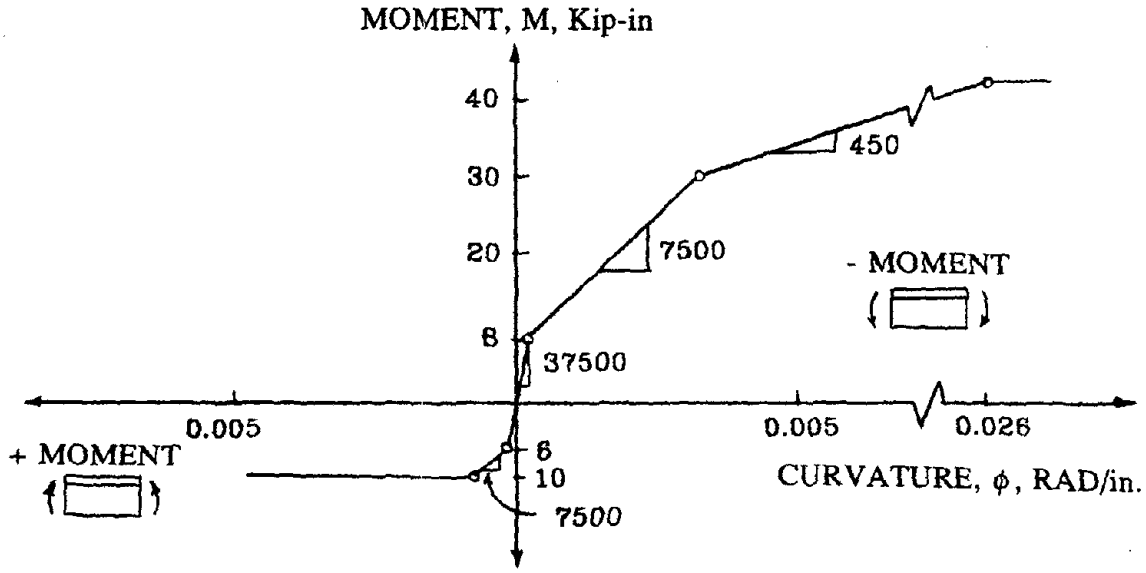

(b) Material properties assigned to the beam elements

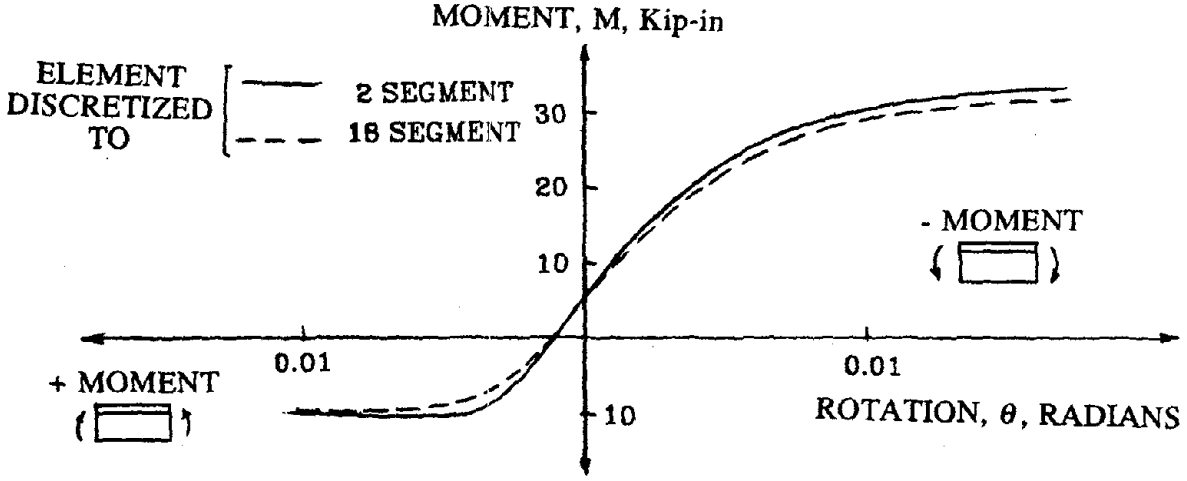

(c) The moment-rotation relationship obtained for the longitudinal girders

Fig. 6.15 - Modeling of the longitudinal girders for global analysis

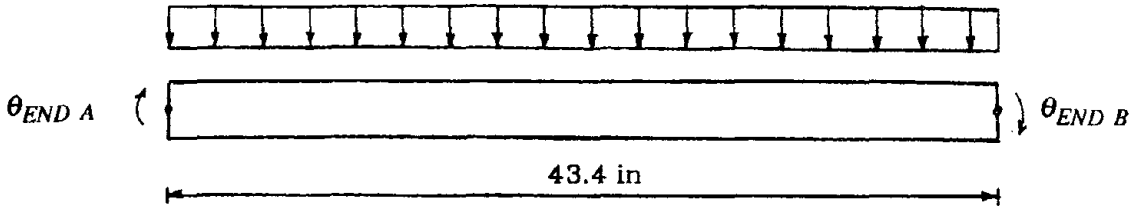

(a) Element modeling

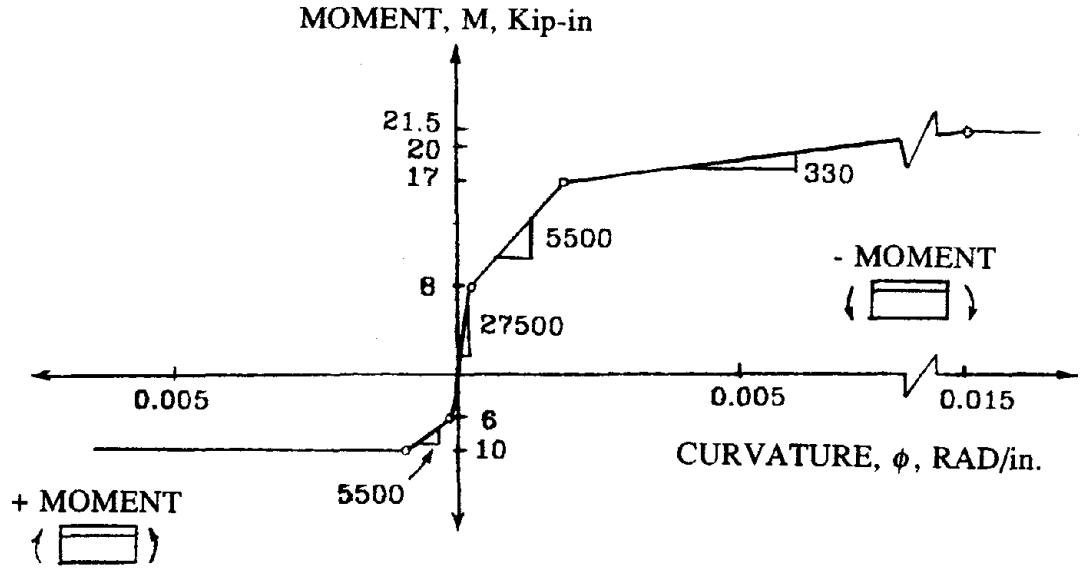

(b) Material properties assigned to the beam elements

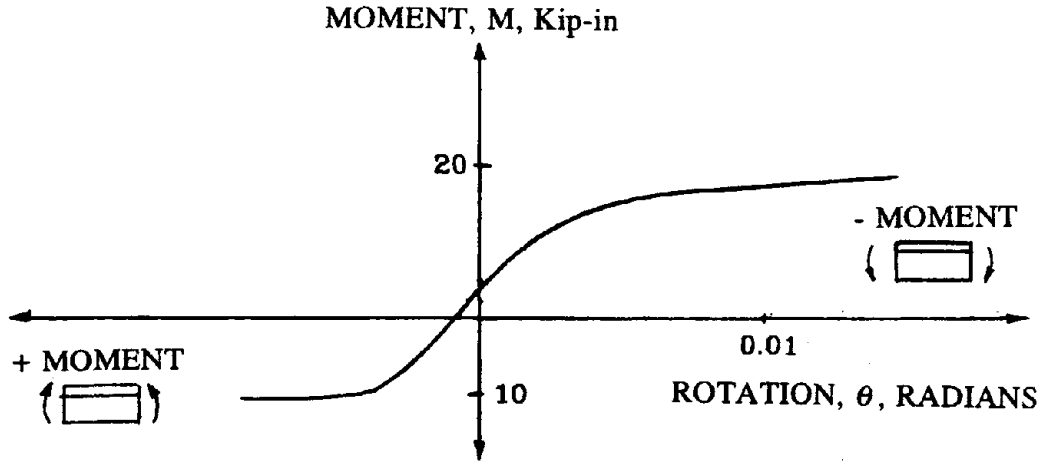

(c) The moment-rotation relationship obtained for the transverse girders

Fig. 6.16 - Modeling of the transverse girders

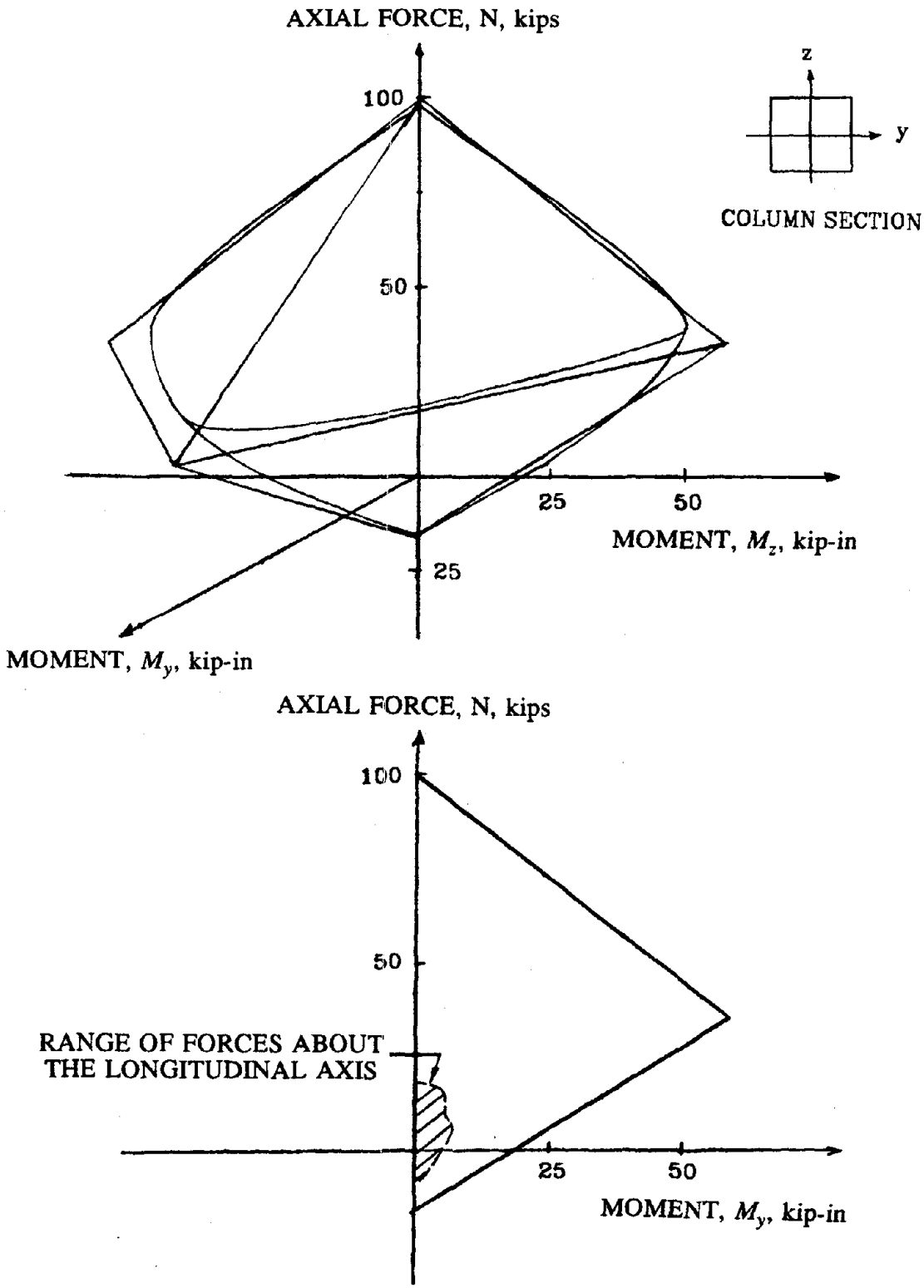

Fig. 6.17 - Biaxial interaction diagram for the columns of the test structure

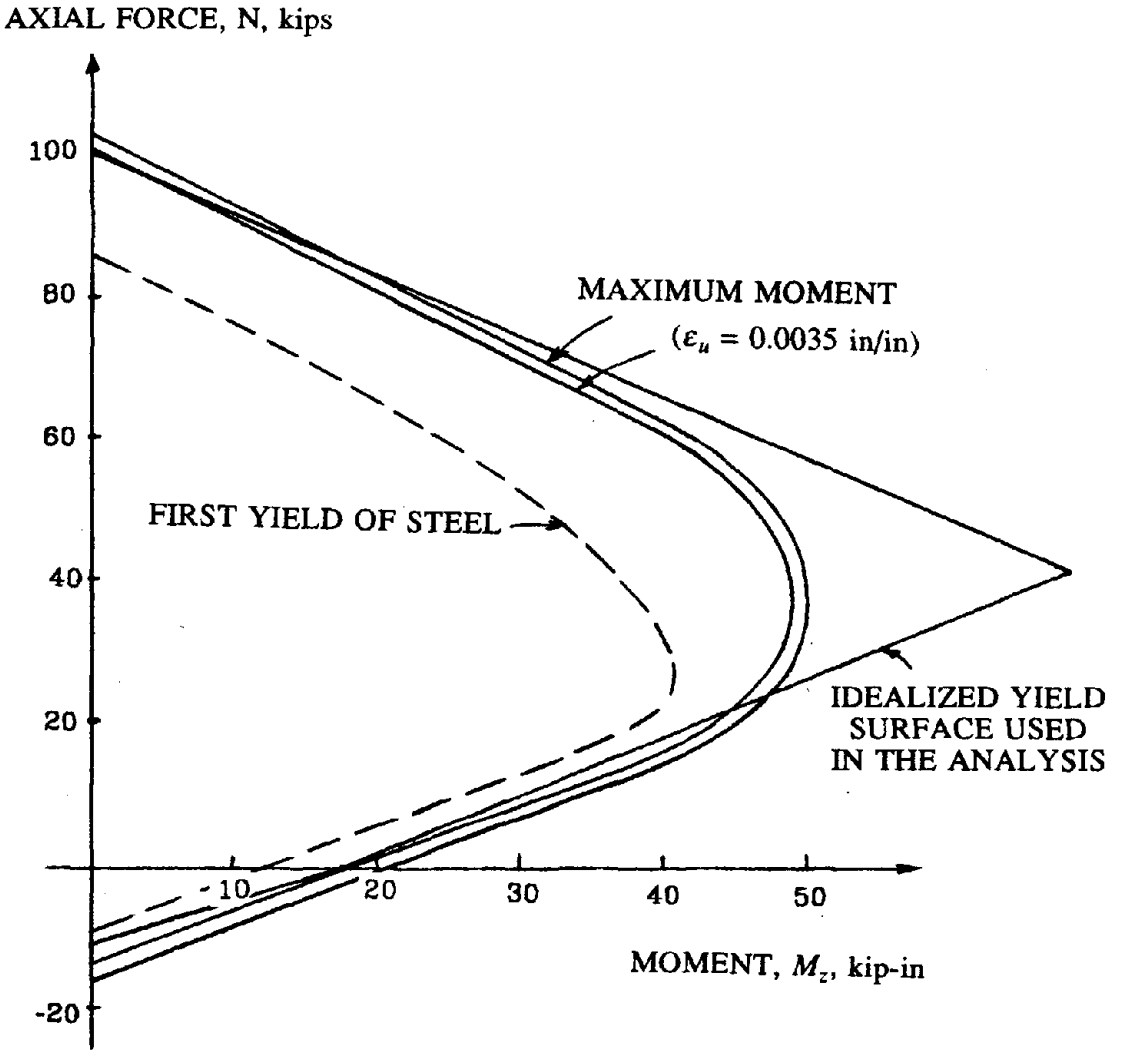

Fig. 6.18 - Uniaxial bending moment-axial load interaction diagram for the columns of the test structure

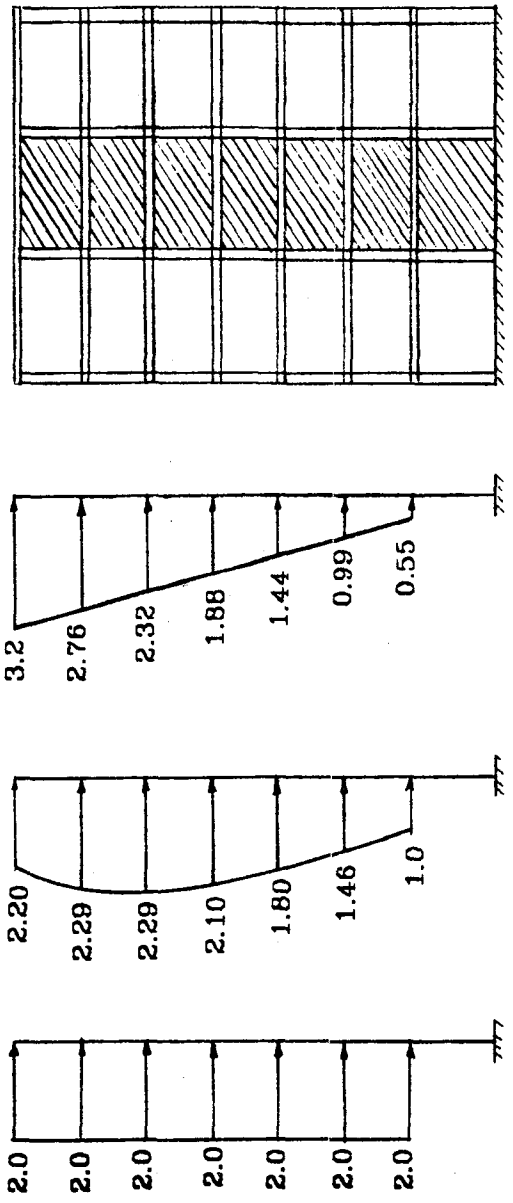

(a) Uniform (b) Parabolic (c) Triangular

Fig. 6.19 - Lateral force distribution

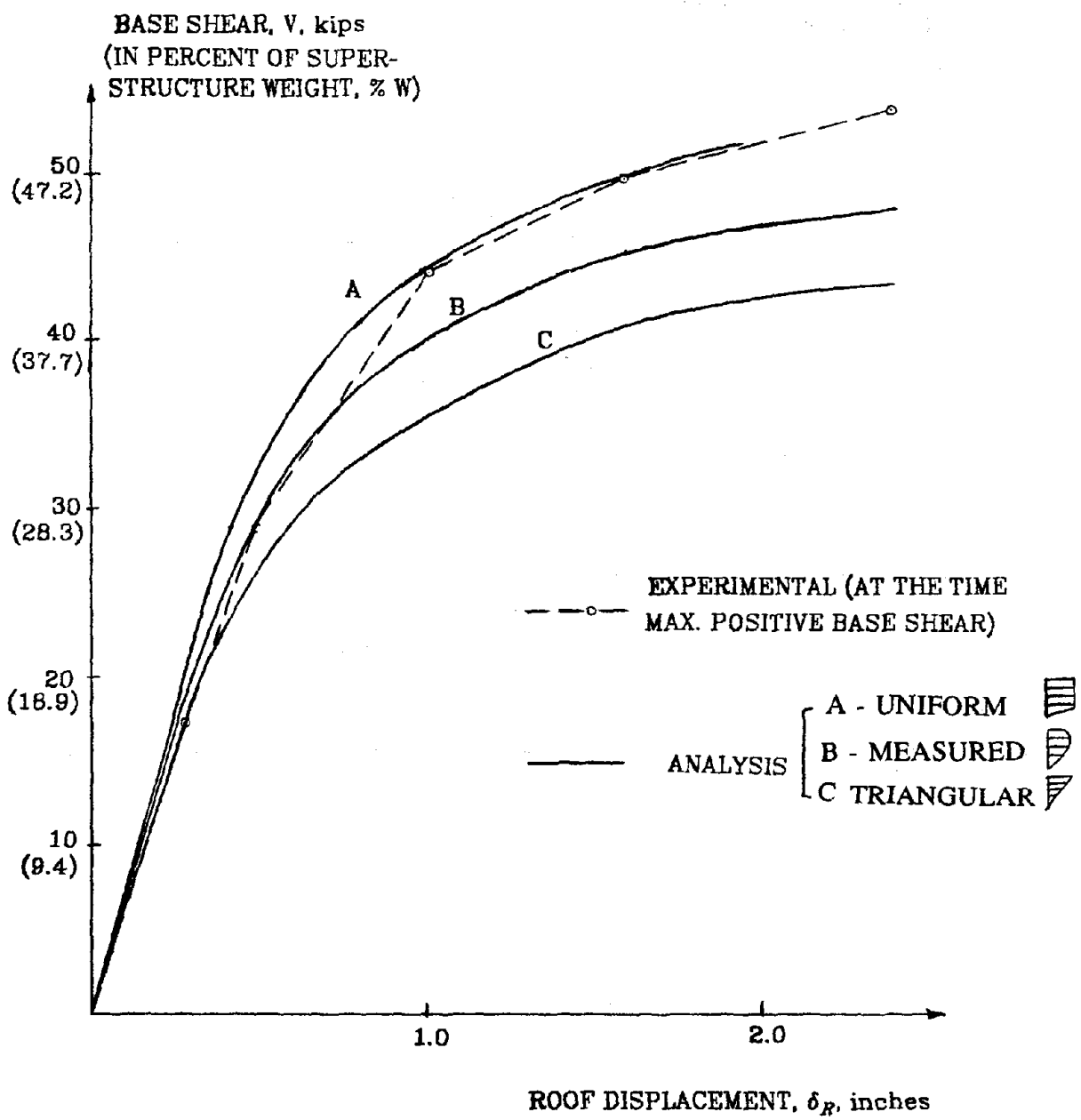

Fig. 6.20 - Roof displacement vs total base shear

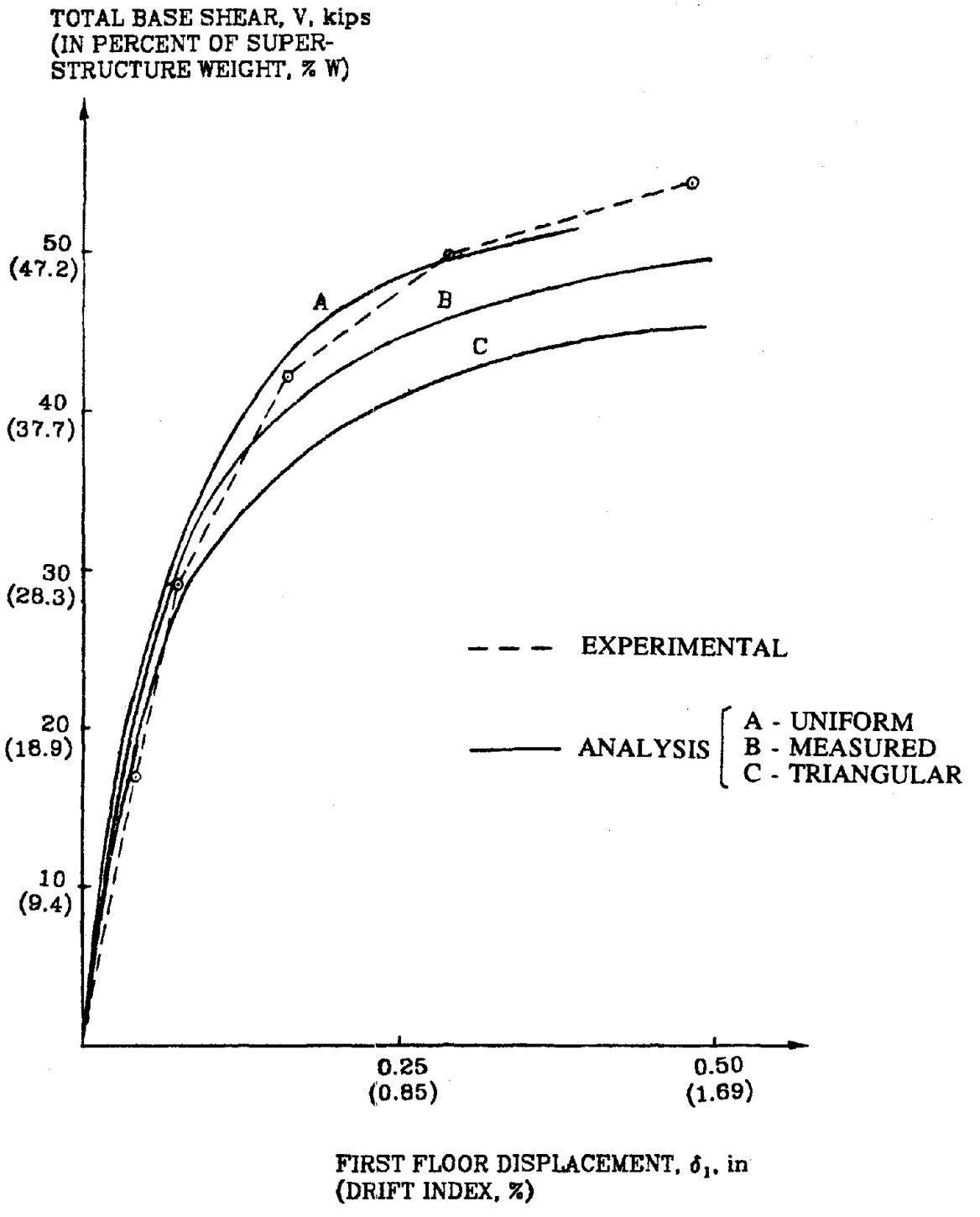

Fig. 6.21 - First floor displacement vs total base shear

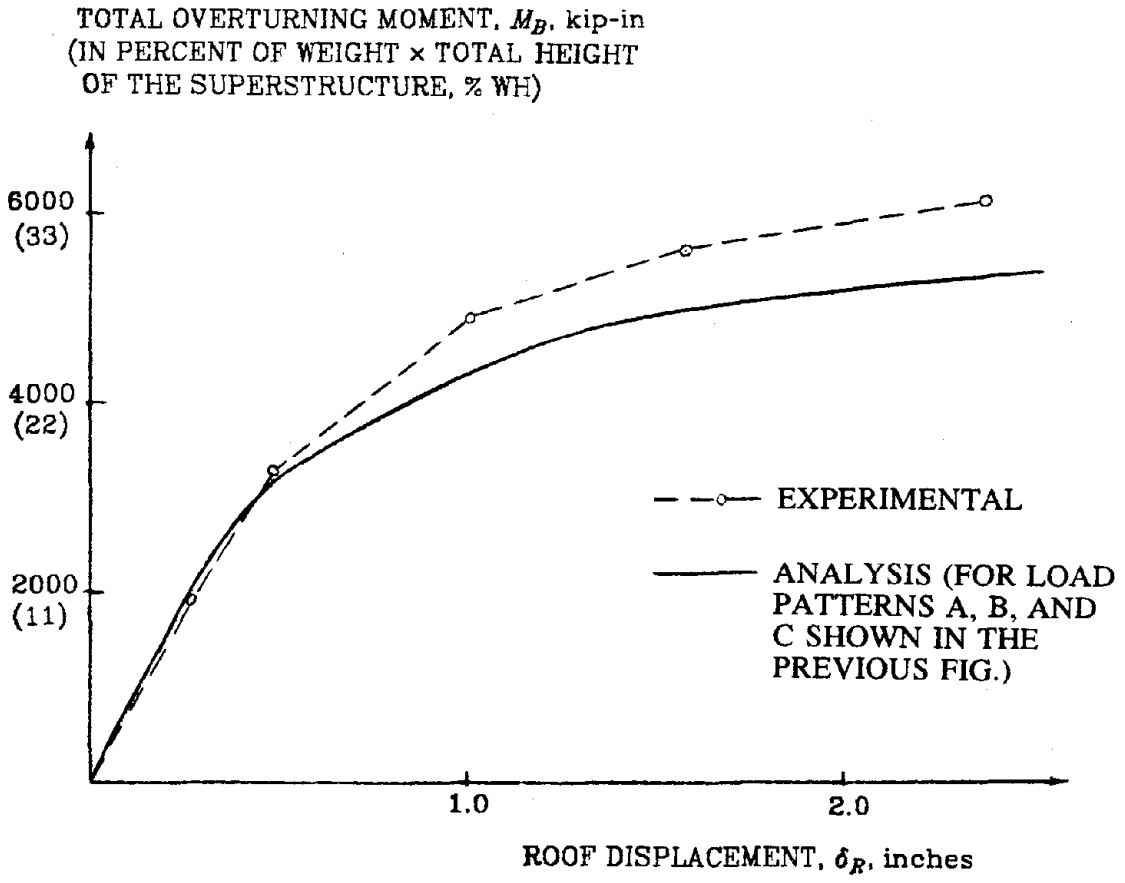

Fig. 6.22 - Roof displacement vs total overturning moment

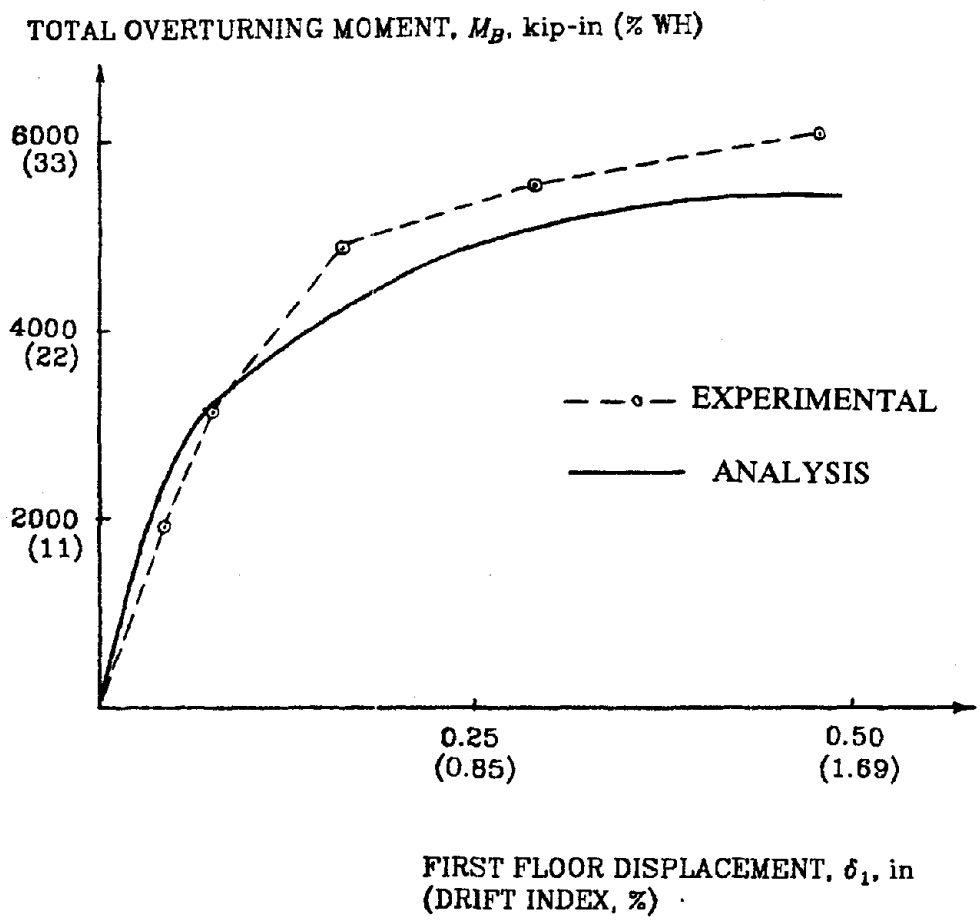

Fig. 6.23 - First floor displacement vs total overturning moment

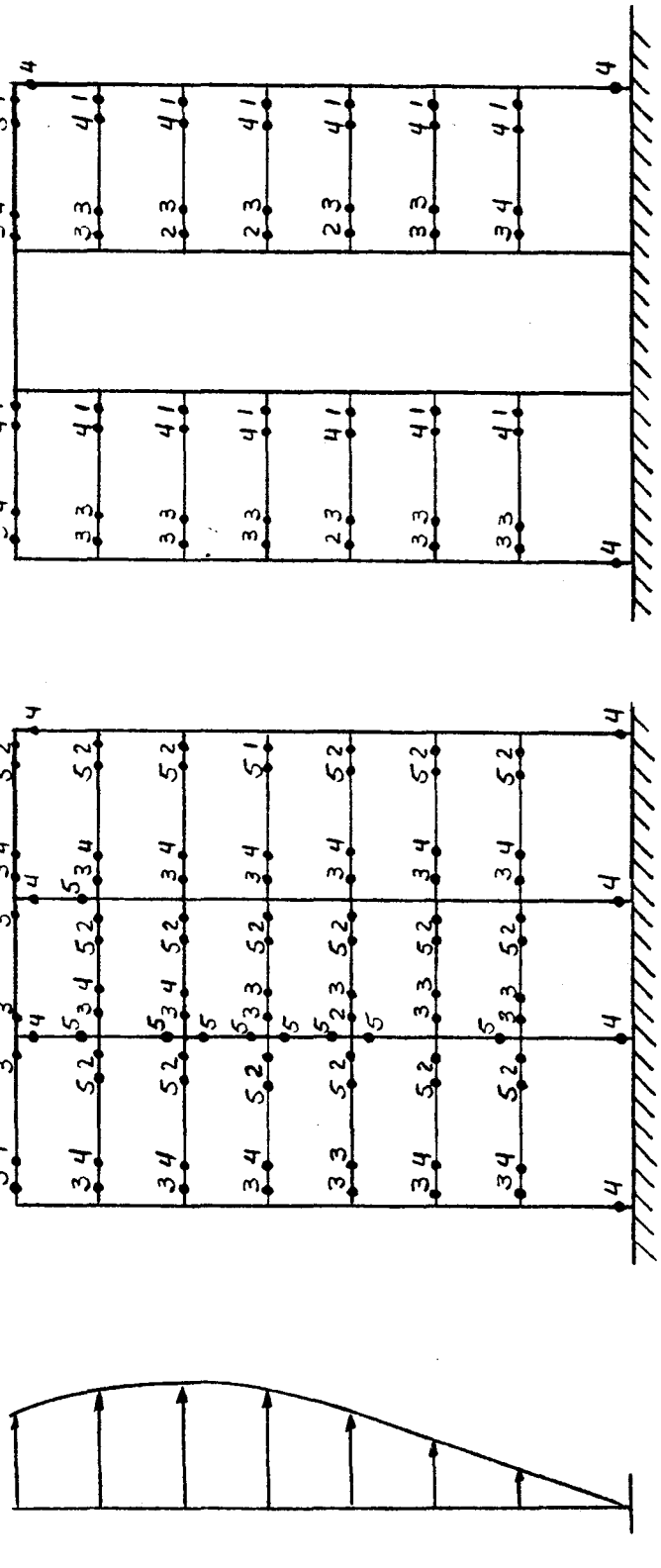

Fig. 6.24(a) - Sequence of plastic hinge formation in the longitudinal frames; double hinges indicate that the element has reached its cracking and yield moments.

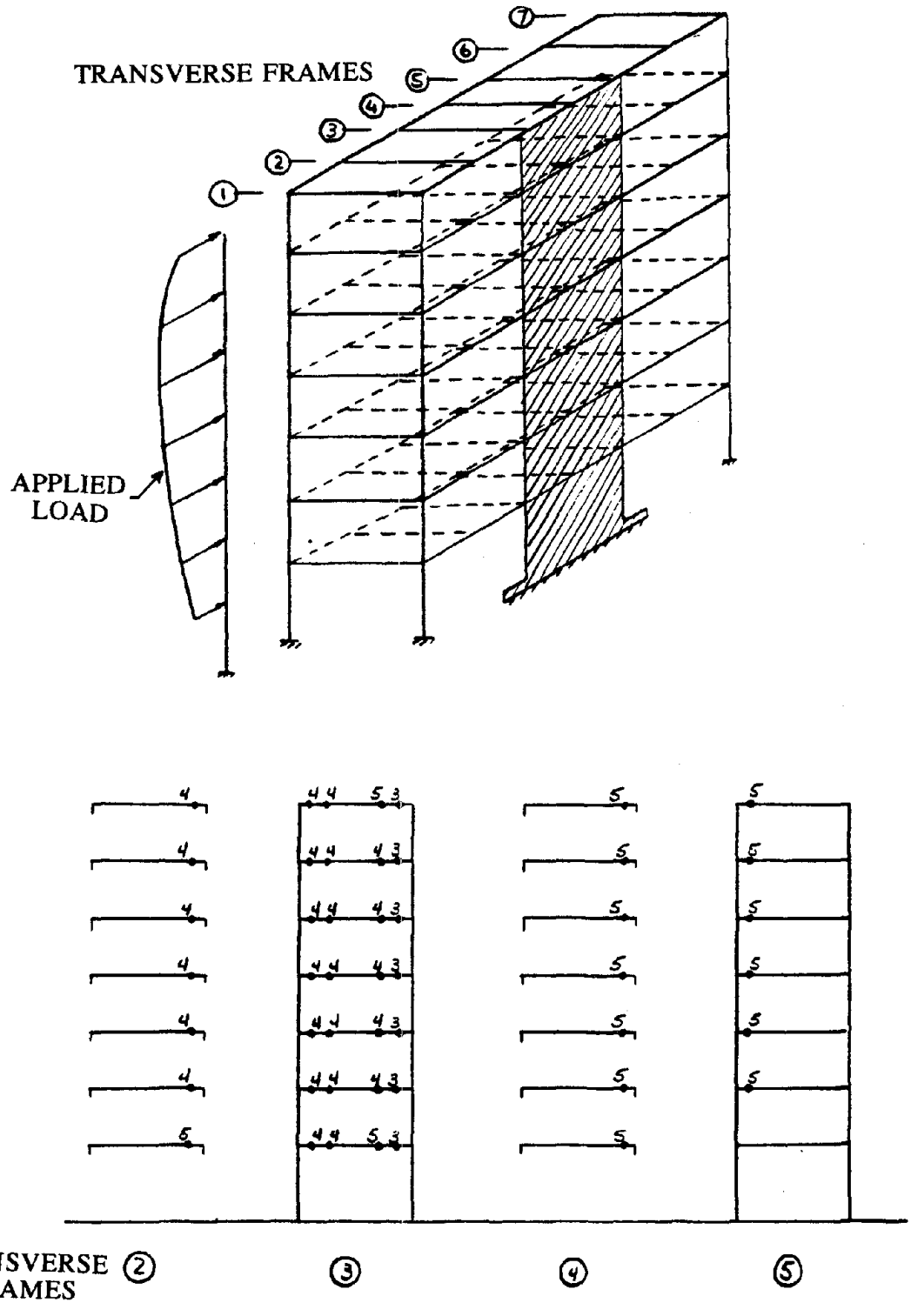

Fig. 6.24(b) - Sequence of plastic hinge formation in the transverse frames; double hinges indicate that the element has reached its cracking and yield moments.

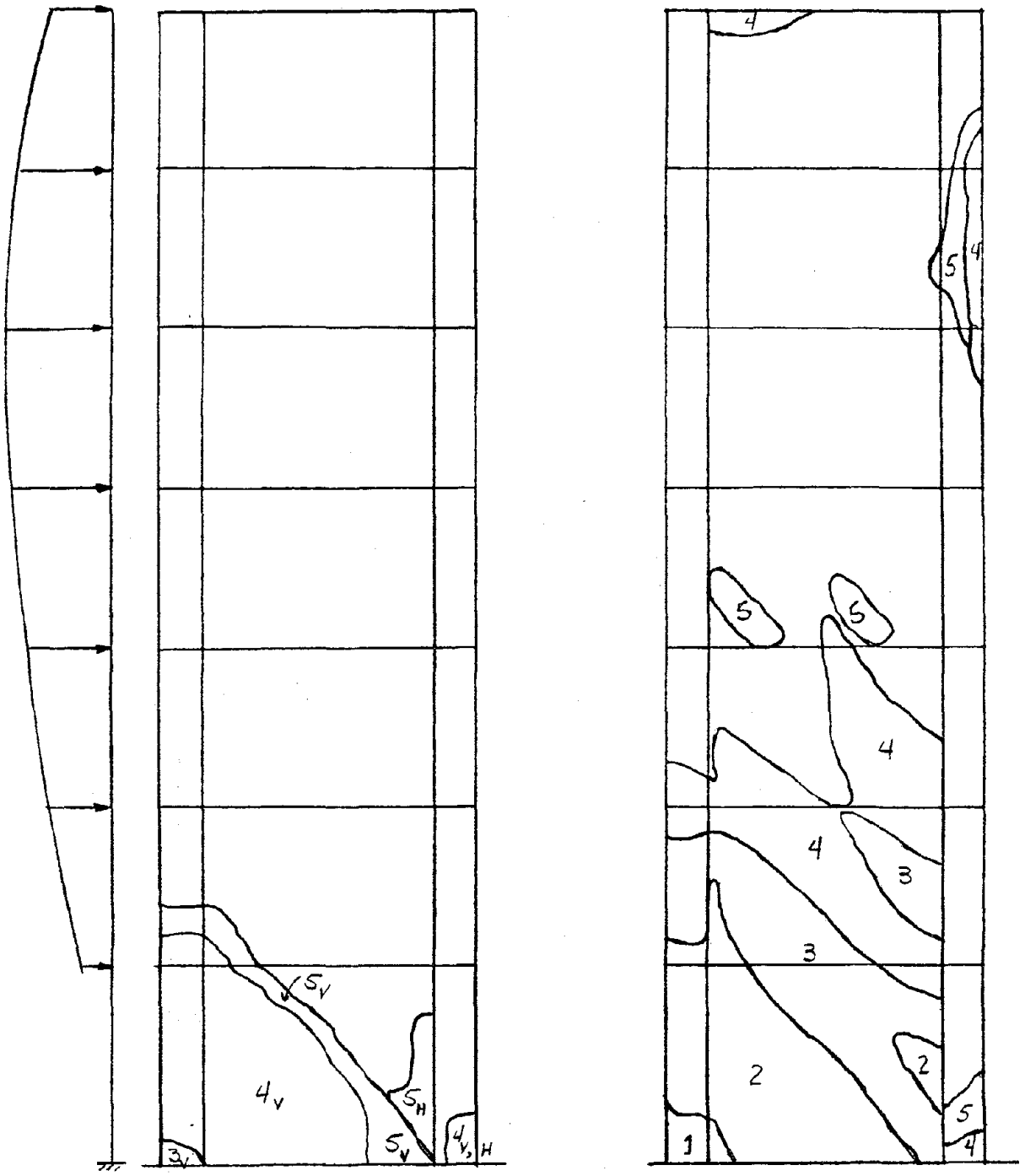

Fig. 6.24(c) - Sequence of crack formation in the concrete layer and plastic deformation in the steel layer of the shear wall

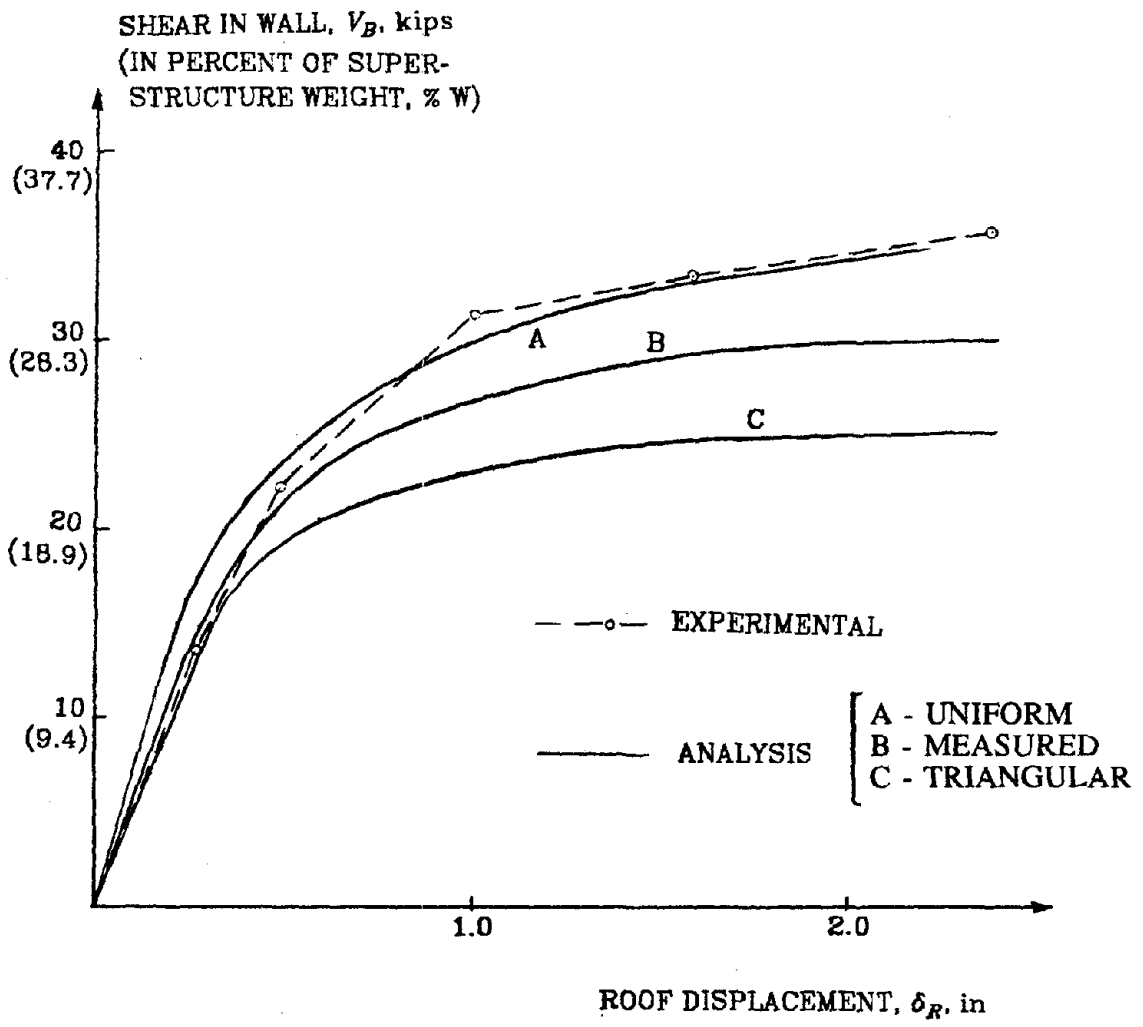

Fig. 6.25 - Roof displacement vs wall shear

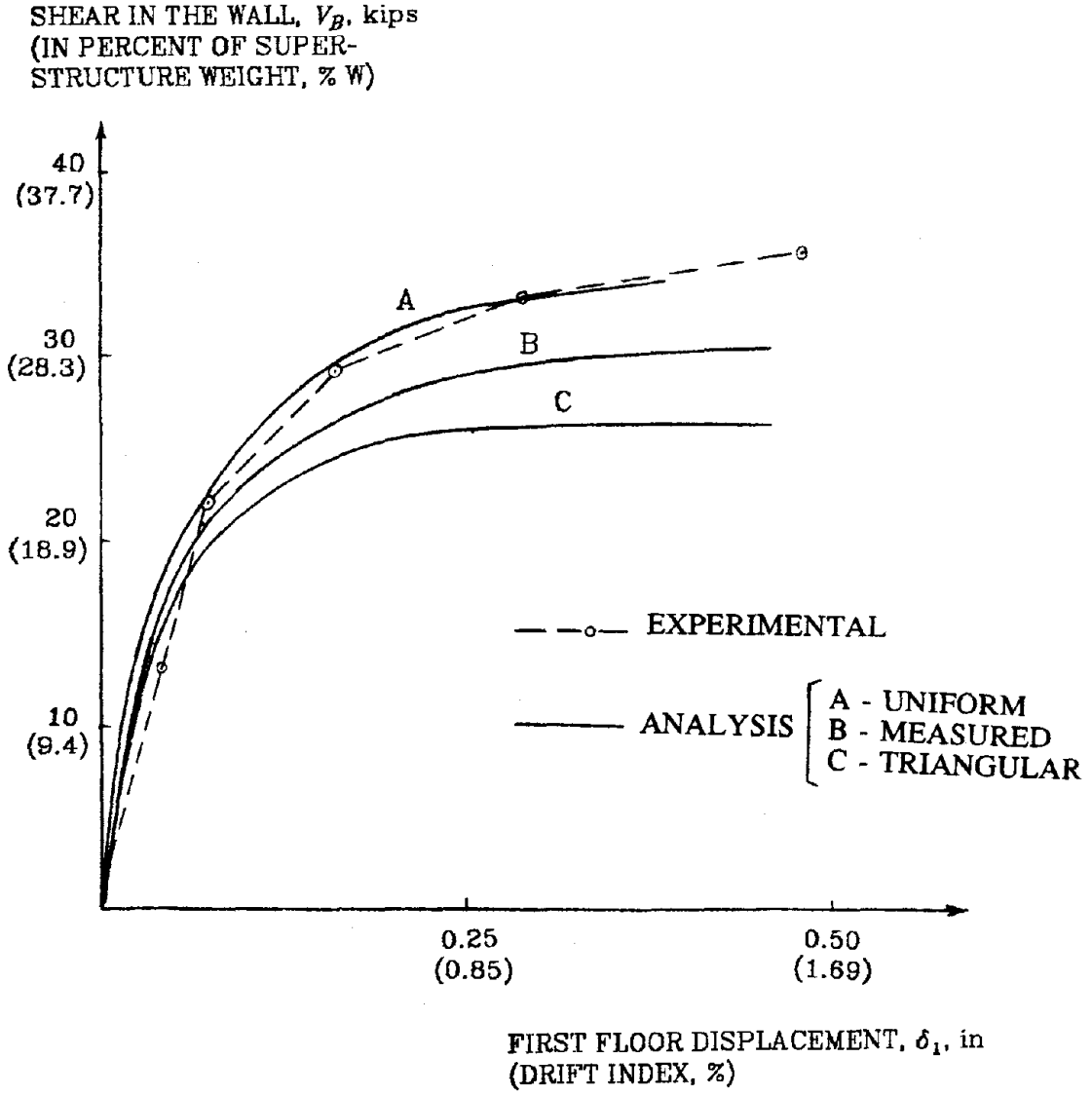

Fig. 6.26 - First floor displacement vs wall shear

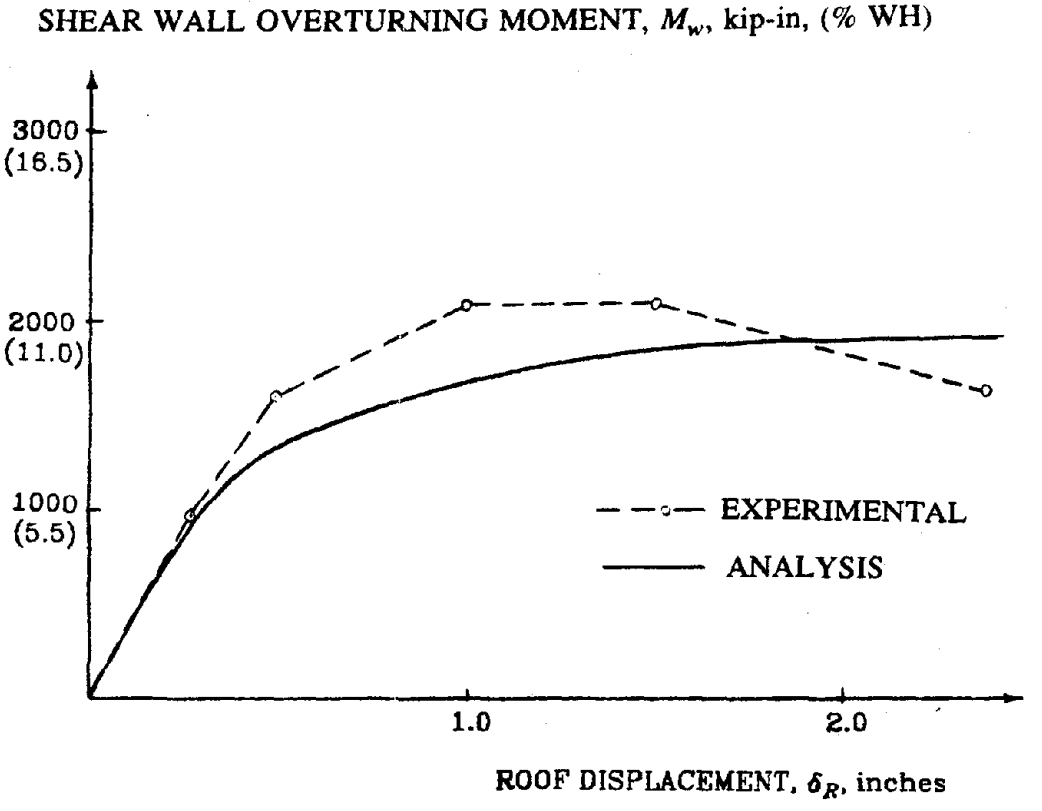

Fig. 6.27 - Roof displacement vs shear wall overturning moment

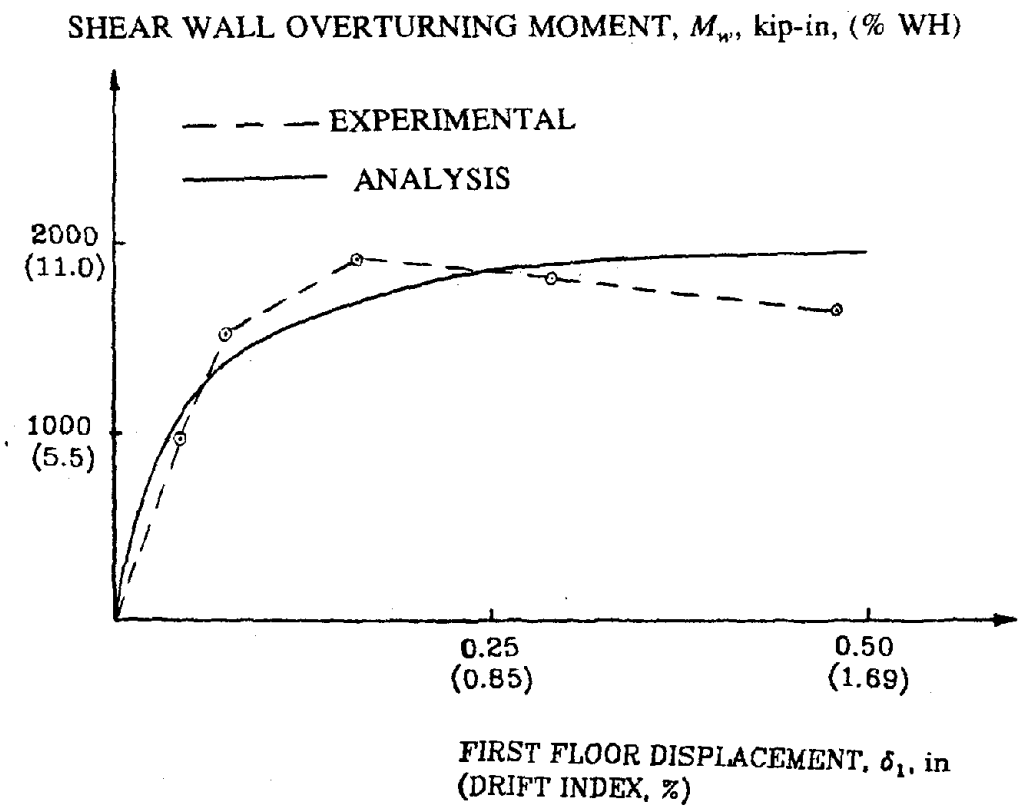

Fig. 6.28 - First floor displacement vs shear wall overturning moment

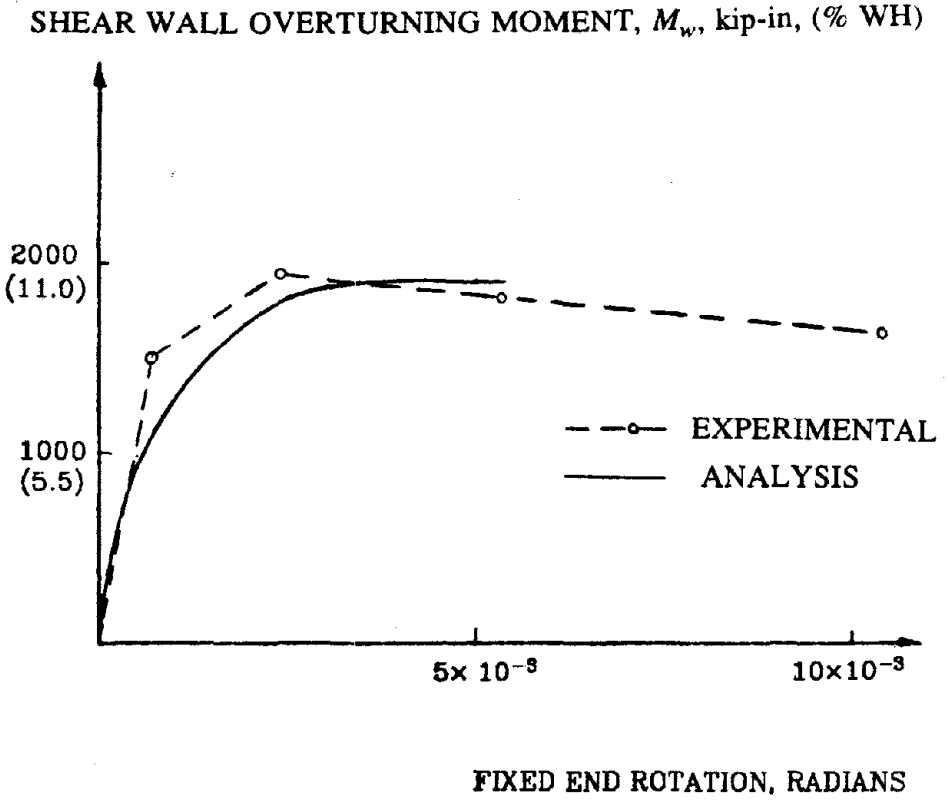

Fig. 6.29 - Fixed end rotation vs shear wall overturning moment

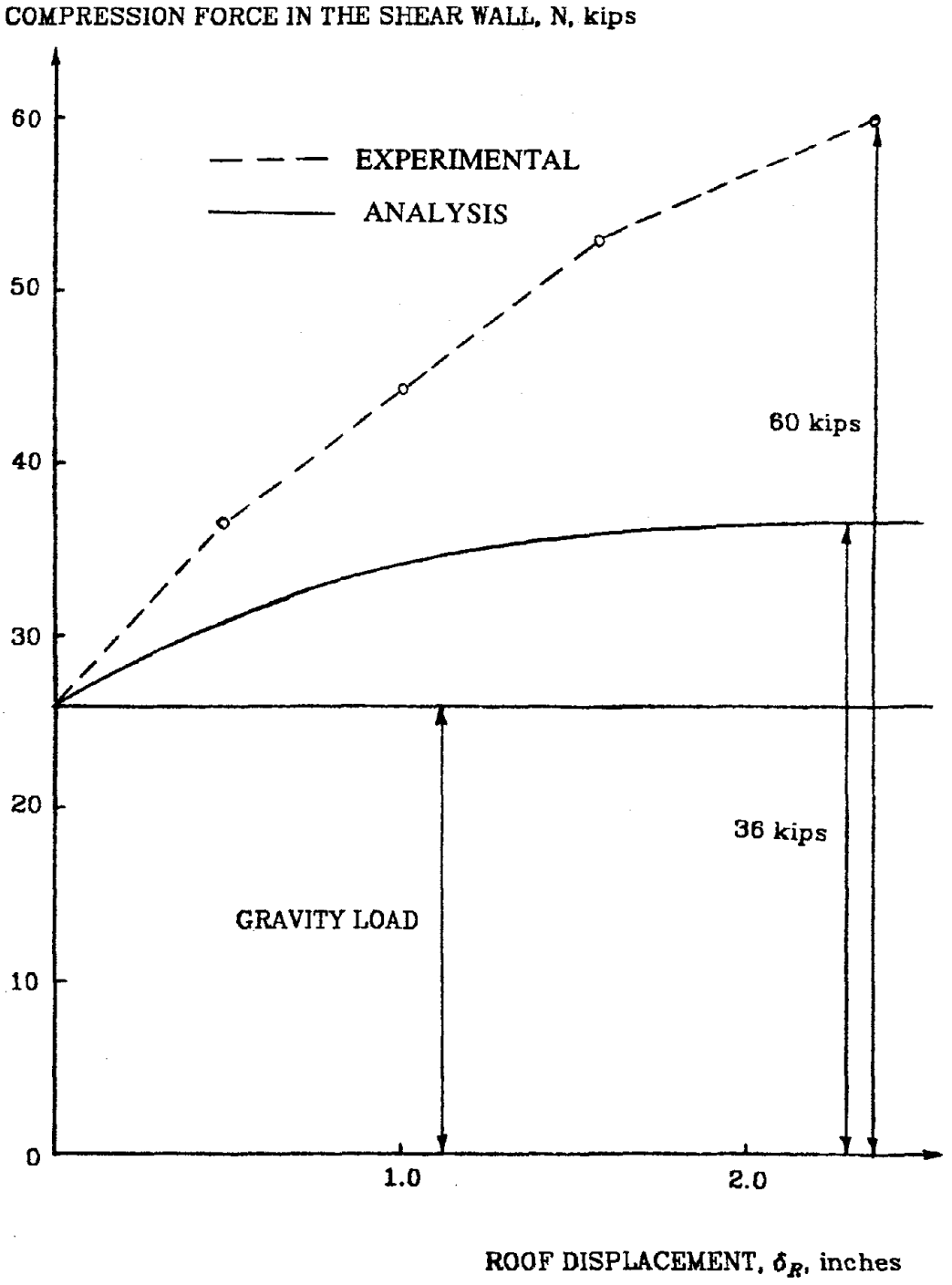

Fig. 6.30 - Roof displacement vs wall axial force

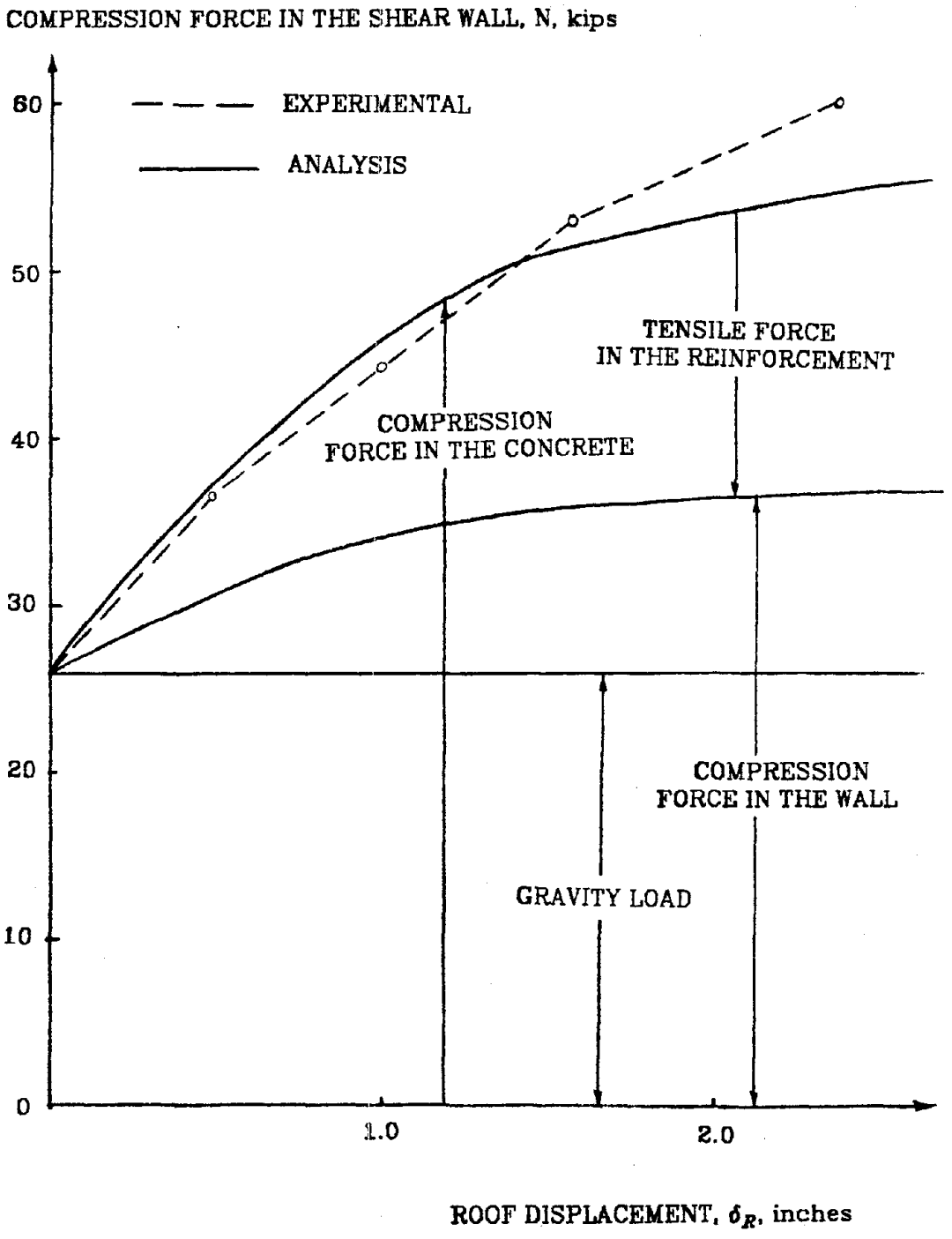

Fig. 6.31 - Roof displacement vs wall axial force showing the contribution of concrete and steel layers

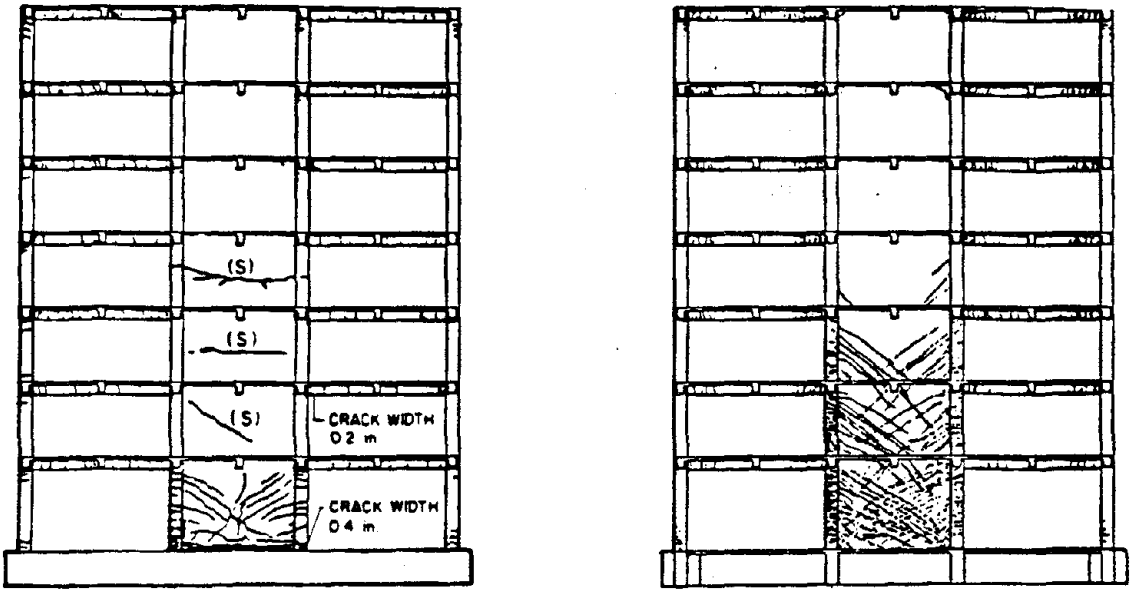

(a) 1/5-scale model after Taft 40.3 test

(b) Full-scale model after PSD-4 test (Hachinohe 35.7% G.)

Fig. 6.32 - Crack patterns in the 1/5-scale and full-scale models after 1.4% roof drift

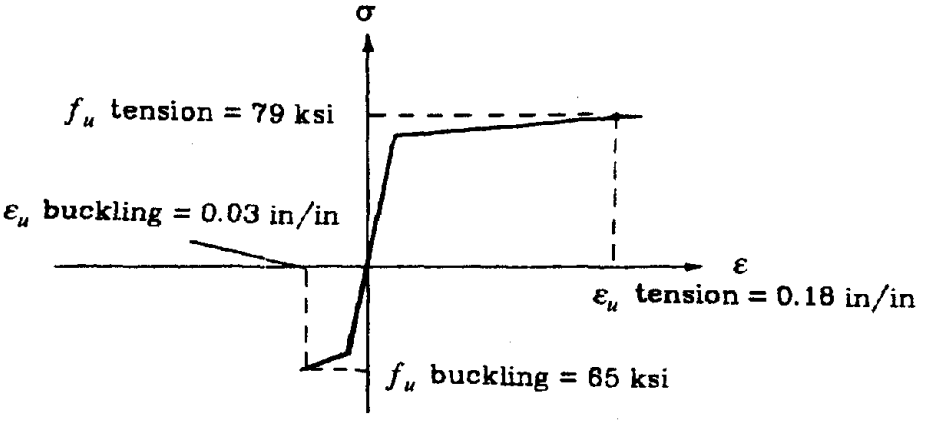

(a)

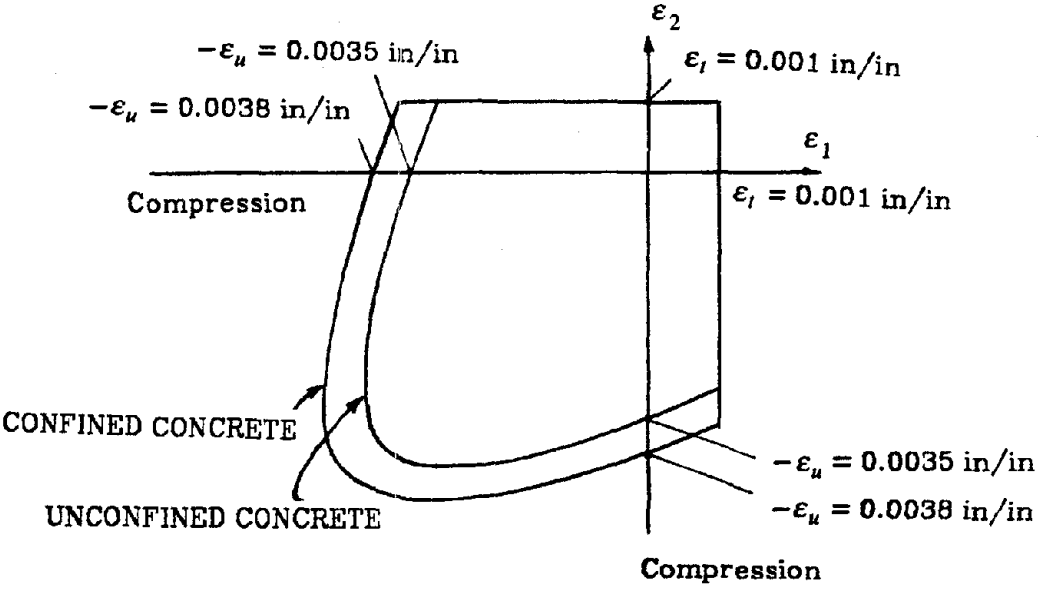

(b)

Fig. 6.33 - Failure criteria for the reinforcing bar and concrete

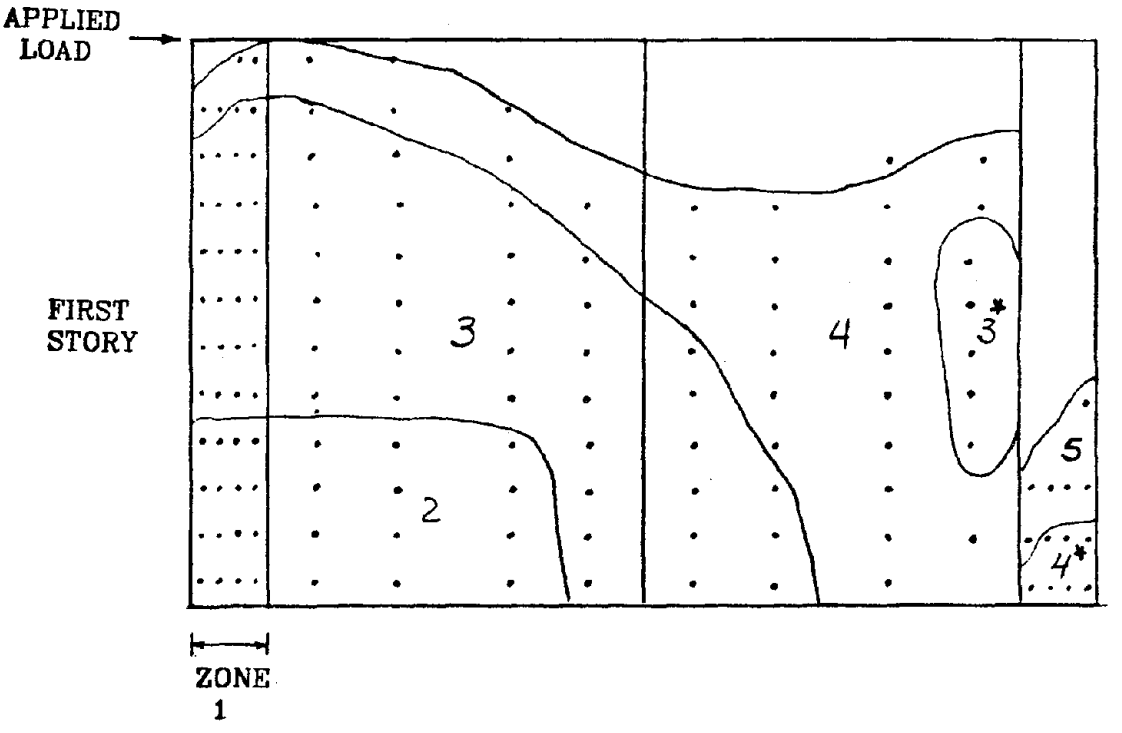

Fig. 6.34 - Failure pattern obtained in the analytical model of the wall

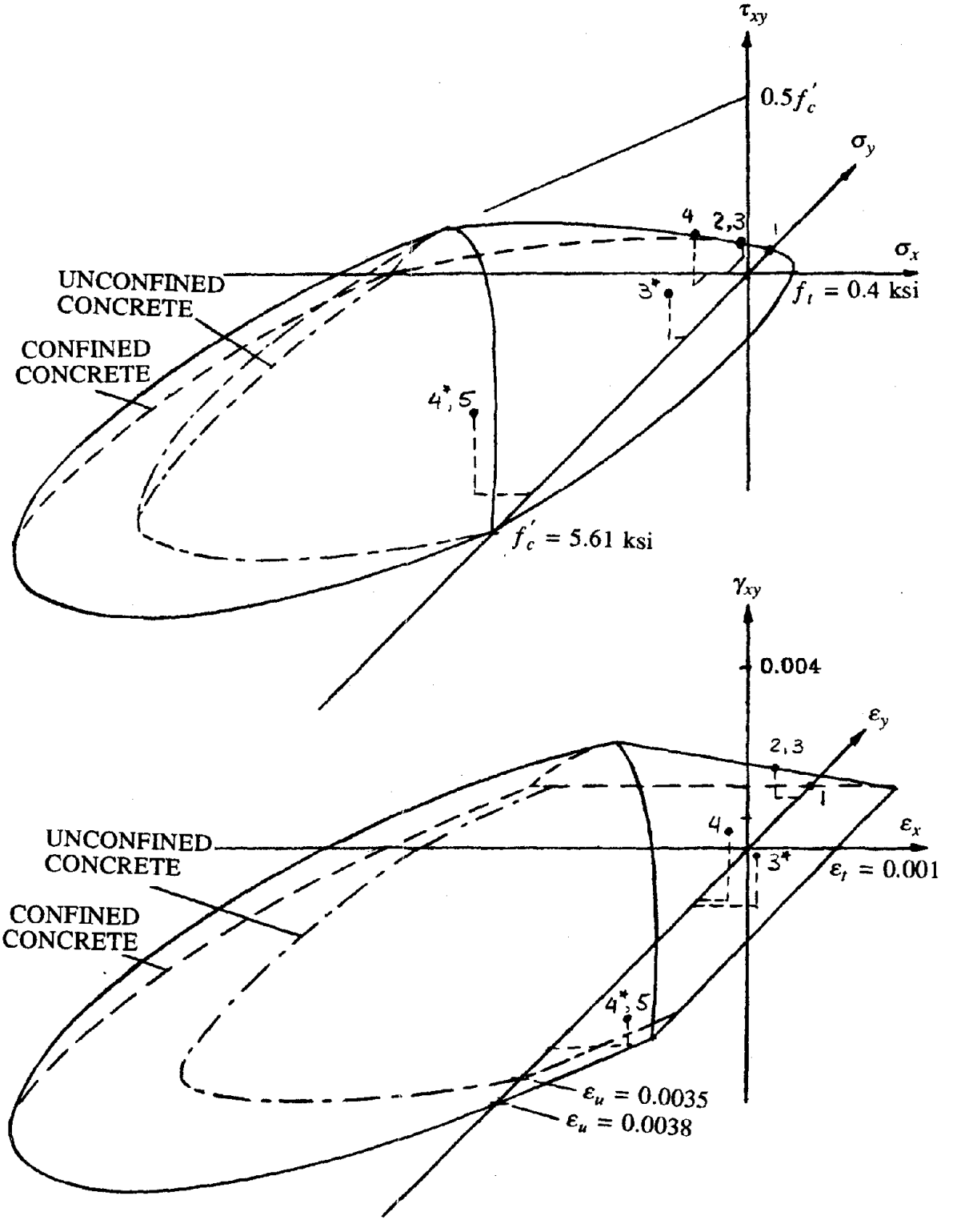

Fig. 6.35 - The stress and strain state in the concrete layer at the time of failure. The numbers 1, 2, 3, 4, and 5 correspond to the failure zone identified in Fig. 6.34.

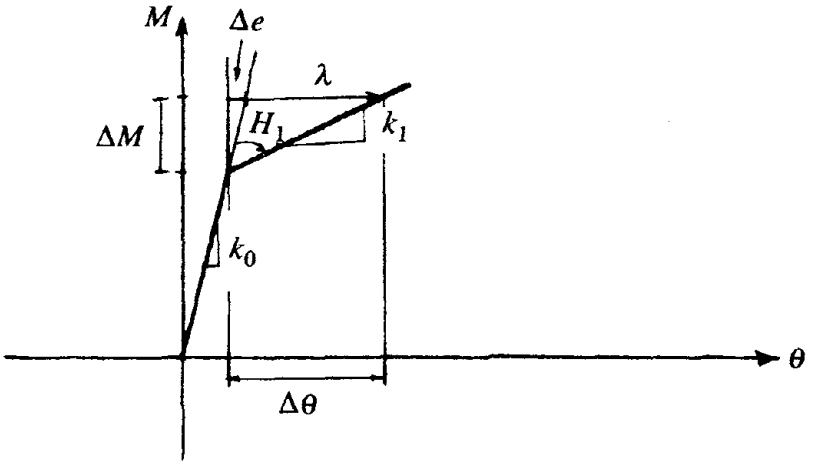

Fig. A.1 - Force deformation relationship

EARTHQUAKE ENGINEERING RESEARCH CENTER REPORT SERIES

EERC reports are available from the National Information Service for Earthquake Engineering(NISEE) and from the National Technical Information Service(NTIS). Numbers in parentheses are Accession Numbers assigned by the National Technical Information Service; these are followed by a price code. Contact NTIS, 5285 Port Royal Road, Springfield Virginia, 22161 for more information. Reports without Accession Numbers were not available from NTIS at the time of printing. For a current complete list of EERC reports (from EERC 67-1) and availablity information, please contact University of California, EERC, NISEE, 1301 South 46th Street, Richmond, California 94804.

UCB/EERC-79/01 "Hysteretic Behavior of Lightweight Reinforced Concrete Beam-Column Subassemblages," by B.Forzani, E.P.Popov and Bertero, V.V., April 1979, (PB 298 267)A06.

UCB/EERC-79/02 "The Development of a Mathematical Model to Predict the Flexural Response of Reinforced Concrete Beams to Cyclic Loads, Using System Identification," by J.Stanton and McNiven, H., January 1979, (PB 295 879) A10.

UCB/EERC-79/03 "Linear and Nonlinear Earthquake Response of Simple Torsionally Coupled Systems, ," by Kan, C.L. and Chopra, A.K., February 1979, (PB 298 266)A06.

UCB/EERC-79/04 "A Mathematical Model of Masonry for Predicting its Linear Seismic Response Characteristics," by Mengi, Y. and McNiven, H.D., February 1979, (PB 298 266)A06

UCB/EERC-79/05 "Mechanical Behavior of Lightweight Concrete Confined by Different Types of Lateral Reinforcement," by Manrique, M.A., Bertero, V.V. and Popov, E.P., May 1979, (PB 301 114) A06.

UCB/EERC-79/06 "Static Tilt Tests of a Tall Cylindrical Liquid Storage Tank," by Clough, R.W. and Niwa, A., February 1979, (PB 301 167)A06.

UCB/EERC-79/07 "The Design of Steel Energy Absorbing Restrainers and Their Incorporation into Nuclear Power Plants for Enhanced Safety: Volume 1 - Summary Report," by Spencer, P.N., Zackay, V.F. and Parker, E.R., February 1979, (UCB/EERC- 79/07)A09.

UCB/EERC-79/08 "The Design of Steel Energy Absorbing Restrainers and their Incorporation into Nuclear Power Plants for Enhanced Safety: Volume 2- The Development of Analyses for Reactor System Piping, -Simple Systems -and Complex Systems," by Lee, M.C., Penzien, J., Chopra, A.K., Suzuki, K., Powell, G.H., Wilson, E.L., Clough, R.W. and Row, D.G., February 1979, (UCB/EERC- 79/08)A10.

UCB/EERC-79/09 "The Design of Steel Energy Absorbing Restrainers and Their Incorporation into Nuclear Power Plants for Enhanced Safety: Volume 3- Evaluation of Commerical Steels," by Owen, W.S., Pelloux, R.M.N., Ritchie, R.O., Faral, M., Ohhashi, T., Toplosky, J., Hartman, S.J., Zackay, V.F. and Parker, E.R., February 1979, (UCB/EERC- 79/09)A04.

UCB/EERC-79/10 "The Design of Steel Energy Absorbing Restrainers and Their Incorporation into Nuclear Power Plants for Enhanced Safety:Volume 4-A Review of Energy-Absorbing Devices," by Kelly, J.M. and Skinner, M.S., February 1979, (UCB/EERC-79/10)A04.

UCB/EERC-79/11 "Conservatism in Summation Rules for Closely Spaced Modes," by Kelly, J.M. and Sackman, J.L., May 1979, (PB 301 328)A03.

UCB/EERC-79/12 "Cyclic Loading Tests of Masonry Single Piers; Volume 3 - Height to width Ratio of 0.5," by Hidalgo, P.A., Mayes, R.L., McNiven, H.D. and Clough, R.W., May 1979 , (PB 301 321)A08.

UCB/EERC-79/13 "Cyclic Behavior of Dense Course-Gained Materials in Relation to the Seismic Stability of Dams," by Banerjee, N.G., Seed, H.B. and Chan, C.K., June 1979, (PB 301 373)A13.

UCB/EERC-79/14 "Seismic Behavior of Reinforced Concrete Interior Beam-Column Subassemblages," by Viwathanatepa, S., Popov, E.P. and Bertero, V.V., June 1979, (PB 301 326)A10.

UCB/EERC-79/15 "Optimal Design of Localized Nonlinear Systems with Dual Performance Criteria under Earthquake Exitations," by Bhatti, M.A., July 1979, (PB 80 167 109)A06.

UCB/EERC-79/16 "OPTDYN - A General Purpose Optimization Program for Problems with or without Dynamic Constraints," by Bhatti, M.A., Polak, E. and Pister, K.S., July 1979, (PB 80 167 091)A05.

UCB/EERC-79/17 "Ansr-II, Analysis of Nonlinear Structural Response, User's Manual," by Mondkar, D.P. and Powell, G.H., July 1979, (PB 80 113 301)A05.

UCB/EERC-79/18 "Soil Structure Interaction in Different Seismic Environments," by Gomez-Masso, A., Lysmer, J., Chen, J. and Seed, H.B., August 1979, (PB 80 101 520)A04.

UCB/EERC-79/19 "ARMA Models for Earthquake Ground Motions," by Chang, M.K., Kwiatkowski, J.W. and Oliver, R.M., July 1979, (PB 301 166)A05.

UCB/EERC-79/20 "Hysteretic Behavior of Reinforced Concrete Structural Walls," by Vallenas, J.M., Bertero, V.V. and Popov, E.P., August 1979, (PB 80 165 905)A12.

UCB/EERC-79/21 "Studies on High-Frequency Vibrations of Buildings-1: The Column Effect," by Lubliner, J., August 1979, (PB 80 158 553)A03.

UCB/EERC-79/22 "Effects of Generalized Loadings on Bond Reinforcing Bars Embedded in Confined Concrete Blocks," by Viwathanatepa, S., Popov, E.P. and Bertero, V.V., August 1979, (PB 81 124 018)A14.

UCB/EERC-79/23 "Shaking Table Study of Single-Story Masonry Houses, Volumn 1: Test Structures 1 and 2," by Gulkan, P., Mayes, R.L. and Clough, R.W., September 1979, (HUD-000 1763)A12.

UCB/EERC-79/24 "Shaking Table Study of Single-Story Masonry Houses, Volume 2: Test Structures 3 and 4," by Gulkan, P., Mayes, R.L. and Clough, R.W., September 1979, (HUD-000 1836)A12.

UCB/EERC-79/25 "Shaking Table Study of Single-Story Masonry Houses, Volumn 3: Summary, Conclusions and Recommendations," by Clough, R.W., Mayes, R.L. and Gulkan, P., September 1979, (HUD-000 1837)A06.

UCB/EERC-79/26 "Recommendations for a U.S.-Japan Cooperative Research Program Utilizing Large-Scale Testing Facilities," by U.S.-Japan, Planning Group, September 1979, (PB 301 407)A06.

UCB/EERC-79/27 "Earthquake-Induced Liquefaction Near Lake Amatitlan, Guatemala," by Seed, H.B., Arango, I., Chan, C.K. and Gomez-Masso, A., September 1979, (NUREG-CR1 341)A03.

UCB/EERC-79/28 "Infill Panels: Their Influence on Seismic Response of Buildings," by Axley, J.W. and Bertero, V.V., September 1979, (PB 80 163 371)A10.

UCB/EERC-79/29 "3D Truss Bar Element (Type 1) for the ANSR-II Program," by Mondkar, D.P. and Powell, G.H., November 1979, (PB 80 169 709)A02.

UCB/EERC-79/30 "2D Beam-Column Element (Type 5 - Parallel Element Theory) for the ANSR-II Program," by Row, D.G., Powell, G.H. and Mondkar, D.P., December 1979, (PB 80 167 224)A03.

UCB/EERC-79/31 "3D Beam-Column Element (Type 2 - Parallel Element Theory) for the ANSR-II Program," by Riahi, A., Powell, G.H. and Mondkar, D.P., December 1979, (PB 80 167 216)A03.

UCB/EERC-79/32 "On Response of Structures to Stationary Excitation," by Der Kiureghian, A., December 1979, (PB 80 166 929)A03.

UCB/EERC-79/33 "Undisturbed Sampling and Cyclic Load Testing of Sands," by Singh, S., Seed, H.B. and Chan, C.K., December 1979, (ADA 087 298)A07.

UCB/EERC-79/34 "Interaction Effects of Simltaneous Torsional and Compressional Cyclic Loading of Sand," by Griffin, P.M. and Houston, W.N., December 1979, (ADA 092 352)A15.

UCB/EERC-80/01 "Earthquake Response of Concrete Gravity Dams Including Hydrodynamic and Foundation Interaction Effects," by Chopra, A.K., Chakrabarti, P. and Gupta, S., January 1980, (AD-A087297)A10.

UCB/EERC-80/02 "Rocking Response of Rigid Blocks to Earthquakes," by Yim, C.S., Chopra, A.K. and Penzien, J., January 1980, (PB80 166 002)A04.

UCB/EERC-80/03 "Optimum Inelastic Design of Seismic-Resistant Reinforced Concrete Frame Structures," by Zagajeski, S.W. and Bertero, V.V., January 1980, (PB80 164 635)A06.

UCB/EERC-80/04 "Effects of Amount and Arrangement of Wall-Panel Reinforcement on Hysteretic Behavior of Reinforced Concrete Walls," by Iliya, R. and Bertero, V.V., February 1980, (PB81 122 525)A09.

UCB/EERC-80/05 "Shaking Table Research on Concrete Dam Models," by Niwa, A. and Clough, R.W., September 1980, (PB81 122 368)A06.

UCB/EERC-80/06 "The Design of Steel Energy-Absorbing Restrainers and their Incorporation into Nuclear Power Plants for Enhanced Safety (Vol 1a): Piping with Energy Absorbing Restrainers: Parameter Study on Small Systems," by Powell, G.H., Oughourlian, C. and Simons, J., June 1980.

UCB/EERC-80/07 "Inelastic Torsional Response of Structures Subjected to Earthquake Ground Motions," by Yamazaki, Y., April 1980, (PB81 122 327)A08.

UCB/EERC-80/08 "Study of X-Braced Steel Frame Structures under Earthquake Simulation," by Ghanaat, Y., April 1980, (PB81 122 335)A11.

UCB/EERC-80/09 "Hybrid Modelling of Soil-Structure Interaction," by Gupta, S., Lin, T.W. and Penzien, J., May 1980, (PB81 122 319)A07.

UCB/EERC-80/10 "General Applicability of a Nonlinear Model of a One Story Steel Frame," by Sveinsson, B.I. and McNiven, H.D., May 1980, (PB81 124 877)A06.

UCB/EERC-80/11 "A Green-Function Method for Wave Interaction with a Submerged Body," by Kioka, W., April 1980, (PB81 122 269)A07.

UCB/EERC-80/12 "Hydrodynamic Pressure and Added Mass for Axisymmetric Bodies," by Nilrat, F., May 1980, (PB81 122 343)A08.

UCB/EERC-80/13 "Treatment of Non-Linear Drag Forces Acting on Offshore Platforms," by Dao, B.V. and Penzien, J., May 1980, (PB81 153 413)A07.

UCB/EERC-80/14 "2D Plane/Axisymmetric Solid Element (Type 3-Elastic or Elastic-Perfectly Plastic)for the ANSR-II Program," by Mondkar, D.P. and Powell, G.H., July 1980, (PB81 122 350)A03.

UCB/EERC-80/15 "A Response Spectrum Method for Random Vibrations," by Der Kiureghian, A., June 1981, (PB81 122 301)A03.

UCB/EERC-80/16 "Cyclic Inelastic Buckling of Tubular Steel Braces," by Zayas, V.A., Popov, E.P. and Martin, S.A., June 1981, (PB81 124 885)A10.

UCB/EERC-80/17 "Dynamic Response of Simple Arch Dams Including Hydrodynamic Interaction," by Porter, C.S. and Chopra, A.K., July 1981, (PB81 124 000)A13.

UCB/EERC-80/18 "Experimental Testing of a Friction Damped Aseismic Base Isolation System with Fail-Safe Characteristics," by Kelly, J.M., Beucke, K.E. and Skinner, M.S., July 1980, (PB81 148 595)A04.

UCB/EERC-80/19 "The Design of Steel Emergy-Absorbing Restrainers and their Incorporation into Nuclear Power Plants for Enhanced Safety (Vol.1B): Stochastic Seismic Analyses of Nuclear Power Plant Structures and Piping Systems Subjected to Multiple Supported Excitations," by Lee, M.C. and Penzien, J., June 1980, (PB82 201 872)A08.

UCB/EERC-80/20 "The Design of Steel Energy-Absorbing Restrainers and their Incorporation into Nuclear Power Plants for Enhanced Safety (Vol 1C): Numerical Method for Dynamic Substructure Analysis," by Dickens, J.M. and Wilson, E.L., June 1980.

UCB/EERC-80/21 "The Design of Steel Energy-Absorbing Restrainers and their Incorporation into Nuclear Power Plants for Enhanced Safety (Vol 2): Development and Testing of Restraints for Nuclear Piping Systems," by Kelly, J.M. and Skinner, M.S., June 1980.

UCB/EERC-80/22 "3D Solid Element (Type 4-Elastic or Elastic-Perfectly-Plastic) for the ANSR-II Program," by Mondkar, D.P. and Powell, G.H., July 1980, (PB81 123 242)A03.

UCB/EERC-80/23 "Gap-Friction Element (Type 5) for the Ansr-II Program," by Mondkar, D.P. and Powell, G.H., July 1980, (PB81 122 285)A03.

UCB/EERC-80/24 "U-Bar Restraint Element (Type 11) for the ANSR-II Program," by Oughourlian, C. and Powell, G.H., July 1980, (PB81 122 293)A03.

UCB/EERC-80/25 "Testing of a Natural Rubber Base Isolation System by an Explosively Simulated Earthquake," by Kelly, J.M., August 1980, (PB81 201 360)A04.

UCB/EERC-80/26 "Input Identification from Structural Vibrational Response," by Hu, Y., August 1980, (PB81 152 308)A05.

UCB/EERC-80/27 "Cyclic Inelastic Behavior of Steel Offshore Structures," by Zayas, V.A., Mahin, S.A. and Popov, E.P., August 1980, (PB81 196 180)A15.

UCB/EERC-80/28 "Shaking Table Testing of a Reinforced Concrete Frame with Biaxial Response," by Oliva, M.G., October 1980, (PB81 154 304)A10.

UCB/EERC-80/29 "Dynamic Properties of a Twelve-Story Prefabricated Panel Building," by Bouwkamp, J.G., Kollegger, J.P. and Stephen, R.M., October 1980, (PB82 138 777)A07.

UCB/EERC-80/30 "Dynamic Properties of an Eight-Story Prefabricated Panel Building," by Bouwkamp, J.G., Kollegger, J.P. and Stephen, R.M., October 1980, (PB81 200 313)A05.

UCB/EERC-80/31 "Predictive Dynamic Response of Panel Type Structures under Earthquakes," by Kollegger, J.P. and Bouwkamp, J.G., October 1980, (PB81 152 316)A04.

UCB/EERC-80/32 "The Design of Steel Energy-Absorbing Restrainers and their Incorporation into Nuclear Power Plants for Enhanced Safety (Vol 3): Testing of Commercial Steels in Low-Cycle Torsional Fatique," by Spanner, P., Parker, E.R., Jongewaard, E. and Dory, M., 1980.

UCB/EERC-80/33 "The Design of Steel Energy-Absorbing Restrainers and their Incorporation into Nuclear Power Plants for Enhanced Safety (Vol 4): Shaking Table Tests of Piping Systems with Energy-Absorbing Restrainers," by Stiemer, S.F. and Godden, W.G., September 1980, (PB82 201 880)A05.

UCB/EERC-80/34 "The Design of Steel Energy-Absorbing Restrainers and their Incorporation into Nuclear Power Plants for Enhanced Safety (Vol 5): Summary Report," by Spencer, P., 1980.

UCB/EERC-80/35 "Experimental Testing of an Energy-Absorbing Base Isolation System," by Kelly, J.M., Skinner, M.S. and Beucke, K.E., October 1980, (PB81 154 072)A04.

UCB/EERC-80/36 "Simulating and Analyzing Artificial Non-Stationary Earth Ground Motions," by Nau, R.F., Oliver, R.M. and Pister, K.S., October 1980, (PB81 153 397)A04.

UCB/EERC-80/37 "Earthquake Engineering at Berkeley - 1980," by , September 1980, (PB81 205 674)A09.

UCB/EERC-80/38 "Inelastic Seismic Analysis of Large Panel Buildings," by Schricker, V. and Powell, G.H., September 1980, (PB81 154 338)A13.

UCB/EERC-80/39 "Dynamic Response of Embankment, Concrete-Gavity and Arch Dams Including Hydrodynamic Interation," by Hall, J.F. and Chopra, A.K., October 1980, (PB81 152 324)A11.

UCB/EERC-80/40 "Inelastic Buckling of Steel Struts under Cyclic Load Reversal.," by Black, R.G. , Wenger, W.A. and Popov, E.P., October 1980, (PB81 154 312)A08.

UCB/EERC-80/41 "Influence of Site Characteristics on Buildings Damage during the October 3,1974 Lima Earthquake," by Repetto, P., Arango, I. and Seed, H.B., September 1980, (PB81 161 739)A05.

UCB/EERC-80/42 "Evaluation of a Shaking Table Test Program on Response Behavior of a Two Story Reinforced Concrete Frame," by Blondet, J.M., Clough, R.W. and Mahin, S.A., December 1980, (PB82 196 544)A11.

UCB/EERC-80/43 "Modelling of Soil-Structure Interaction by Finite and Infinite Elements," by Medina, F., December 1980, (PB81 229 270)A04.

UCB/EERC-81/01 "Control of Seismic Response of Piping Systems and Other Structures by Base Isolation," by Kelly, J.M., January 1981, (PB81 200 735)A05.

UCB/EERC-81/02 "OPTNSR- An Interactive Software System for Optimal Design of Statically and Dynamically Loaded Structures with Nonlinear Response," by Bhatti, M.A., Ciampi, V. and Pister, K.S., January 1981, (PB81 218 851)A09.

UCB/EERC-81/03 "Analysis of Local Variations in Free Field Seismic Ground Motions," by Chen, J.-C., Lysmer, J. and Seed, H.B., January 1981, (AD-A099508)A13.

UCB/EERC-81/04 "Inelastic Structural Modeling of Braced Offshore Platforms for Seismic Loading. ," by Zayas, V.A., Shing, P.-S.B., Mahin, S.A. and Popov, E.P., January 1981, (PB82 138 777)A07.

UCB/EERC-81/05 "Dynamic Response of Light Equipment in Structures," by Der Kiureghian, A., Sackman, J.L. and Nour-Omid, B., April 1981, (PB81 218 497)A04.

UCB/EERC-81/06 "Preliminary Experimental Investigation of a Broad Base Liquid Storage Tank," by Bouwkamp, J.G., Kollegger, J.P. and Stephen, R.M., May 1981, (PB82 140 385)A03.

UCB/EERC-81/07 "The Seismic Resistant Design of Reinforced Concrete Coupled Structural Walls," by Aktan, A.E. and Bertero, V.V., June 1981, (PB82 113 358)A11.

UCB/EERC-81/08 "Unassigned," by Unassigned, 1981.

UCB/EERC-81/09 "Experimental Behavior of a Spatial Piping System with Steel Energy Absorbers Subjected to a Simulated Differential Seismic Input," by Stiemer, S.F., Godden, W.G. and Kelly, J.M., July 1981, (PB82 201 898)A04.

UCB/EERC-81/10 "Evaluation of Seismic Design Provisions for Masonry in the United States," by Sveinsson, B.I., Mayes, R.L. and McNiven, H.D., August 1981, (PB82 166 075)A08.

UCB/EERC-81/11 "Two-Dimensional Hybrid Modelling of Soil-Structure Interaction," by Tzong, T.-J., Gupta, S. and Penzien, J., August 1981, (PB82 142 118)A04.

UCB/EERC-81/12 "Studies on Effects of Infills in Seismic Resistant R/C Construction," by Brokken, S. and Bertero, V.V., October 1981, (PB82 166 190)A09.

UCB/EERC-81/13 "Linear Models to Predict the Nonlinear Seismic Behavior of a One-Story Steel Frame," by Valdimarsson, H., Shah, A.H. and McNiven, H.D., September 1981, (PB82 138 793)A07.

UCB/EERC-81/14 "ILUSH: A Computer Program for the Three-Dimensional Dynamic Analysis of Earth Dams," by Kagawa, T., Mejia, L.H., Seed, H.B. and Lysmer, J., September 1981, (PB82 139 940)A06.

UCB/EERC-81/15 "Three Dimensional Dynamic Response Analysis of Earth Dams," by Mejia, L.H. and Seed, H.B., September 1981, (PB82 137 274)A12.

UCB/EERC-81/16 "Experimental Study of Lead and Elastomeric Dampers for Base Isolation Systems," by Kelly, J.M. and Hodder, S.B., October 1981, (PB82 166 182)A05.

UCB/EERC-81/17 "The Influence of Base Isolation on the Seismic Response of Light Secondary Equipment," by Kelly, J.M., April 1981, (PB82 255 266)A04.

UCB/EERC-81/18 "Studies on Evaluation of Shaking Table Response Analysis Procedures," by Blondet, J. Marcial, November 1981, (PB82 197 278)A10.

UCB/EERC-81/19 "DELIGHT.STRUCT: A Computer-Aided Design Environment for Structural Engineering. ," by Balling, R.J., Pister, K.S. and Polak, E., December 1981, (PB82 218 496)A07.

UCB/EERC-81/20 "Optimal Design of Seismic-Resistant Planar Steel Frames," by Balling, R.J., Ciampi, V. and Pister, K.S., December 1981, (PB82 220 179)A07.

UCB/EERC-82/01 "Dynamic Behavior of Ground for Seismic Analysis of Lifeline Systems," by Sato, T. and Der Kiureghian, A., January 1982, (PB82 218 926)A05.

UCB/EERC-82/02 "Shaking Table Tests of a Tubular Steel Frame Model," by Ghanaat, Y. and Clough, R.W., January 1982, (PB82 220 161)A07.

UCB/EERC-82/03 "Behavior of a Piping System under Seismic Excitation: Experimental Investigations of a Spatial Piping System supported by Mechanical Shock Arrestors," by Schneider, S., Lee, H.-M. and Godden, W. G., May 1982, (PB83 172 544)A09.

UCB/EERC-82/04 "New Approaches for the Dynamic Analysis of Large Structural Systems," by Wilson, E.L., June 1982, (PB83 148 080)A05.

UCB/EERC-82/05 "Model Study of Effects of Damage on the Vibration Properties of Steel Offshore Platforms," by Shahrivar, F. and Bouwkamp, J.G., June 1982, (PB83 148 742)A10.

UCB/EERC-82/06 "States of the Art and Pratice in the Optimum Seismic Design and Analytical Response Prediction of R/C Frame Wall Structures," by Aktan, A.E. and Bertero, V.V., July 1982, (PB83 147 736)A05.

UCB/EERC-82/07 "Further Study of the Earthquake Response of a Broad Cylindrical Liquid-Storage Tank Model," by Manos, G.C. and Clough, R.W., July 1982, (PB83 147 744)A11.

UCB/EERC-82/08 "An Evaluation of the Design and Analytical Seismic Response of a Seven Story Reinforced Concrete Frame," by Charney, F.A. and Bertero, V.V., July 1982, (PB83 157 628)A09.

UCB/EERC-82/09 "Fluid-Structure Interactions: Added Mass Computations for Incompressible Fluid. ," by Kuo, J.S.-H., August 1982, (PB83 156 281)A07.

UCB/EERC-82/10 "Joint-Opening Nonlinear Mechanism: Interface Smeared Crack Model," by Kuo, J.S.-H., August 1982, (PB83 149 195)A05.

UCB/EERC-82/11 "Dynamic Response Analysis of Techi Dam," by Clough, R.W., Stephen, R.M. and Kuo, J.S.-H., August 1982, (PB83 147 496)A06.

UCB/EERC-82/12 "Prediction of the Seismic Response of R/C Frame-Coupled Wall Structures," by Aktan, A.E., Bertero, V.V. and Piazzo, M., August 1982, (PB83 149 203)A09.

UCB/EERC-82/13 "Preliminary Report on the Smart 1 Strong Motion Array in Taiwan," by Bolt, B.A. , Loh, C.H., Penzien, J. and Tsai, Y.B., August 1982, (PB83 159 400)A10.

UCB/EERC-82/14 "Shaking-Table Studies of an Eccentrically X-Braced Steel Structure," by Yang, M.S., September 1982, (PB83 260 778)A12.

UCB/EERC-82/15 "The Performance of Stairways in Earthquakes," by Roha, C., Axley, J.W. and Bertero, V.V., September 1982, (PB83 157 693)A07.

UCB/EERC-82/16 "The Behavior of Submerged Multiple Bodies in Earthquakes," by Liao, W.-G., September 1982, (PB83 158 709)A07.

UCB/EERC-82/17 "Effects of Concrete Types and Loading Conditions on Local Bond-Slip Relationships," by Cowell, A.D., Popov, E.P. and Bertero, V.V., September 1982, (PB83 153 577)A04.

UCB/EERC-82/18 "Mechanical Behavior of Shear Wall Vertical Boundary Members: An Experimental Investigation," by Wagner, M.T. and Bertero, V.V., October 1982, (PB83 159 764)A05.

UCB/EERC-82/19 "Experimental Studies of Multi-support Seismic Loading on Piping Systems," by Kelly, J.M. and Cowell, A.D., November 1982.

UCB/EERC-82/20 "Generalized Plastic Hinge Concepts for 3D Beam-Column Elements," by Chen, P. F.-S. and Powell, G.H., November 1982, (PB83 247 981)A13.

UCB/EERC-82/21 "ANSR-II: General Computer Program for Nonlinear Structural Analysis," by Oughourlian, C.V. and Powell, G.H., November 1982, (PB83 251 330)A12.

UCB/EERC-82/22 "Solution Strategies for Statically Loaded Nonlinear Structures," by Simons, J.W. and Powell, G.H., November 1982, (PB83 197 970)A06.

UCB/EERC-82/23 "Analytical Model of Deformed Bar Anchorages under Generalized Excitations," by Ciampi, V., Eligehausen, R., Bertero, V.V. and Popov, E.P., November 1982, (PB83 169 532)A06.

UCB/EERC-82/24 "A Mathematical Model for the Response of Masonry Walls to Dynamic Excitations," by Sucuoglu, H., Mengi, Y. and McNiven, H.D., November 1982, (PB83 169 011)A07.

UCB/EERC-82/25 "Earthquake Response Considerations of Broad Liquid Storage Tanks," by Cambra, F.J., November 1982, (PB83 251 215)A09.

UCB/EERC-82/26 "Computational Models for Cyclic Plasticity, Rate Dependence and Creep," by Mosaddad, B. and Powell, G.H., November 1982, (PB83 245 829)A08.

UCB/EERC-82/27 "Inelastic Analysis of Piping and Tubular Structures," by Mahasuverachai, M. and Powell, G.H., November 1982, (PB83 249 987)A07.

UCB/EERC-83/01 "The Economic Feasibility of Seismic Rehabilitation of Buildings by Base Isolation," by Kelly, J.M., January 1983, (PB83 197 988)A05.

UCB/EERC-83/02 "Seismic Moment Connections for Moment-Resisting Steel Frames.," by Popov, E.P., January 1983, (PB83 195 412)A04.

UCB/EERC-83/03 "Design of Links and Beam-to-Column Connections for Eccentrically Braced Steel Frames," by Popov, E.P. and Malley, J.O., January 1983, (PB83 194 811)A04.

UCB/EERC-83/04 "Numerical Techniques for the Evaluation of Soil-Structure Interaction Effects in the Time Domain," by Bayo, E. and Wilson, E.L., February 1983, (PB83 245 605)A09.

UCB/EERC-83/05 "A Transducer for Measuring the Internal Forces in the Columns of a Frame-Wall Reinforced Concrete Structure," by Sause, R. and Bertero, V.V., May 1983, (PB84 119 494)A06.

UCB/EERC-83/06 "Dynamic Interactions Between Floating Ice and Offshore Structures," by Croteau, P., May 1983, (PB84 119 486)A16.

UCB/EERC-83/07 "Dynamic Analysis of Multiply Tuned and Arbitrarily Supported Secondary Systems. ," by Igusa, T. and Der Kiureghian, A., July 1983, (PB84 118 272)A11.

UCB/EERC-83/08 "A Laboratory Study of Submerged Multi-body Systems in Earthquakes," by Ansari, G.R., June 1983, (PB83 261 842)A17.

UCB/EERC-83/09 "Effects of Transient Foundation Uplift on Earthquake Response of Structures," by Yim, C.-S. and Chopra, A.K., June 1983, (PB83 261 396)A07.

UCB/EERC-83/10 "Optimal Design of Friction-Braced Frames under Seismic Loading," by Austin, M.A. and Pister, K.S., June 1983, (PB84 119 288)A06.

UCB/EERC-83/11 "Shaking Table Study of Single-Story Masonry Houses: Dynamic Performance under Three Component Seismic Input and Recommendations," by Manos, G.C., Clough, R.W.
and Mayes, R.L., July 1983, (UCB/EERC-83/11)A08.

UCB/EERC-83/12 "Experimental Error Propagation in Pseudodynamic Testing," by Shiing, P.B. and Mahin, S.A., June 1983, (PB84 119 270)A09.

UCB/EERC-83/13 "Experimental and Analytical Predictions of the Mechanical Characteristics of a 1/5-scale Model of a 7-story R/C Frame-Wall Building Structure," by Aktan, A.E., Bertero, V.V., Chowdhury, A.A. and Nagashima, T., June 1983, (PB84 119 213)A07.

UCB/EERC-83/14 "Shaking Table Tests of Large-Panel Precast Concrete Building System Assemblages," by Oliva, M.G. and Clough, R.W., June 1983, (PB86 110 210/AS)A11.

UCB/EERC-83/15 "Seismic Behavior of Active Beam Links in Eccentrically Braced Frames," by Hjelmstad, K.D. and Popov, E.P., July 1983, (PB84 119 676)A09.

UCB/EERC-83/16 "System Identification of Structures with Joint Rotation," by Dimsdale, J.S., July 1983, (PB84 192 210)A06.

UCB/EERC-83/17 "Construction of Inelastic Response Spectra for Single-Degree-of-Freedom Systems," by Mahin, S. and Lin, J., June 1983, (PB84 208 834)A05.

UCB/EERC-83/18 "Interactive Computer Analysis Methods for Predicting the Inelastic Cyclic Behaviour of Structural Sections," by Kaba, S. and Mahin, S., July 1983, (PB84 192 012)A06.

UCB/EERC-83/19 "Effects of Bond Deterioration on Hysteretic Behavior of Reinforced Concrete Joints," by Filippou, F.C., Popov, E.P. and Bertero, V.V., August 1983, (PB84 192 020)A10.

UCB/EERC-83/20 "Analytical and Experimental Correlation of Large-Panel Precast Building System Performance," by Oliva, M.G., Clough, R.W., Velkov, M. and Gavrilovic, P., November 1983.

UCB/EERC-83/21 "Mechanical Characteristics of Materials Used in a 1/5 Scale Model of a 7-Story Reinforced Concrete Test Structure," by Bertero, V.V., Aktan, A.E., Harris, H.G.
and Chowdhury, A.A., October 1983, (PB84 193 697)A05.

UCB/EERC-83/22 "Hybrid Modelling of Soil-Structure Interaction in Layered Media," by Tzong, T.-J. and Penzien, J., October 1983, (PB84 192 178)A08.

UCB/EERC-83/23 "Local Bond Stress-Slip Relationships of Deformed Bars under Generalized Excitations," by Eligehausen, R., Popov, E.P. and Bertero, V.V., October 1983, (PB84 192 848)A09.

UCB/EERC-83/24 "Design Considerations for Shear Links in Eccentrically Braced Frames," by Malley, J.O. and Popov, E.P., November 1983, (PB84 192 186)A07.

UCB/EERC-84/01 "Pseudodynamic Test Method for Seismic Performance Evaluation: Theory and Implementation," by Shing, P.-S. B. and Mahin, S.A., January 1984, (PB84 190 644)A08.

UCB/EERC-84/02 "Dynamic Response Behavior of Kiang Hong Dian Dam," by Clough, R.W., Chang, K.-T., Chen, H.-Q. and Stephen, R.M., April 1984, (PB84 209 402)A08.

UCB/EERC-84/03 "Refined Modelling of Reinforced Concrete Columns for Seismic Analysis," by Kaba, S.A. and Mahin, S.A., April 1984, (PB84 234 384)A06.

UCB/EERC-84/04 "A New Floor Response Spectrum Method for Seismic Analysis of Multiply Supported Secondary Systems," by Asfura, A. and Der Kiureghian, A., June 1984, (PB84 239 417)A06.

UCB/EERC-84/05 "Earthquake Simulation Tests and Associated Studies of a 1/5th-scale Model of a 7-Story R/C Frame-Wall Test Structure," by Bertero, V.V., Aktan, A.E., Charney, F.A. and Sause, R., June 1984, (PB84 239 409)A09.

UCB/EERC-84/06 "R/C Structural Walls: Seismic Design for Shear," by Aktan, A.E. and Bertero, V.V., 1984.

UCB/EERC-84/07 "Behavior of Interior and Exterior Flat-Plate Connections subjected to Inelastic Load Reversals," by Zee, H.L. and Moehle, J.P., August 1984, (PB86 117 629/AS)A07.

UCB/EERC-84/08 "Experimental Study of the Seismic Behavior of a Two-Story Flat-Plate Structure. ," by Moehle, J.P. and Diebold, J.W., August 1984, (PB86 122 553/AS)A12.

UCB/EERC-84/09 "Phenomenological Modeling of Steel Braces under Cyclic Loading," by Ikeda, K., Mahin, S.A. and Dermitzakis, S.N., May 1984, (PB86 132 198/AS)A08.

UCB/EERC-84/10 "Earthquake Analysis and Response of Concrete Gravity Dams," by Fenves, G. and Chopra, A.K., August 1984, (PB85 193 902/AS)A11.

UCB/EERC-84/11 "EAGD-84: A Computer Program for Earthquake Analysis of Concrete Gravity Dams," by Fenves, G. and Chopra, A.K., August 1984, (PB85 193 613/AS)A05.

UCB/EERC-84/12 "A Refined Physical Theory Model for Predicting the Seismic Behavior of Braced Steel Frames," by Ikeda, K. and Mahin, S.A., July 1984, (PB85 191 450/AS)A09.

UCB/EERC-84/13 "Earthquake Engineering Research at Berkeley - 1984," by , August 1984, (PB85 197 341/AS)A10.

UCB/EERC-84/14 "Moduli and Damping Factors for Dynamic Analyses of Cohesionless Soils," by Seed, H.B., Wong, R.T., Idriss, I.M. and Tokimatsu, K., September 1984, (PB85 191 468/AS)A04.

UCB/EERC-84/15 "The Influence of SPT Procedures in Soil Liquefaction Resistance Evaluations," by Seed, H.B., Tokimatsu, K., Harder, L.F. and Chung, R.M., October 1984, (PB85 191 732/AS)A04.

UCB/EERC-84/16 "Simplified Procedures for the Evaluation of Settlements in Sands Due to Earthquake Shaking," by Tokimatsu, K. and Seed, H.B., October 1984, (PB85 197 887/AS)A03.

UCB/EERC-84/17 Evaluation of Energy Absorption Characteristics of Bridges under Seismic Conditions," by Imbsen, R.A. and Penzien, J., November 1984.

UCB/EERC-84/18 "Structure-Foundation Interactions under Dynamic Loads," by Liu, W.D. and Penzien, J., November 1984, (PB87 124 889/AS)A11.

UCB/EERC-84/19 "Seismic Modelling of Deep Foundations," by Chen, C.-H. and Penzien, J., November 1984, (PB87 124 798/AS)A07.

UCB/EERC-84/20 "Dynamic Response Behavior of Quan Shui Dam," by Clough, R.W., Chang, K.-T., Chen, H.-Q., Stephen, R.M., Ghanaat, Y. and Qi, J.-H., November 1984, (PB86 115177/AS)A07.

UCB/EERC-85/01 "Simplified Methods of Analysis for Earthquake Resistant Design of Buildings," by Cruz, E.F. and Chopra, A.K., February 1985, (PB86 112299/AS)A12.

UCB/EERC-85/02 "Estimation of Seismic Wave Coherency and Rupture Velocity using the SMART 1 Strong-Motion Array Recordings," by Abrahamson, N.A., March 1985, (PB86 214 343)A07.

UCB/EERC-85/03 "Dynamic Properties of a Thirty Story Condominium Tower Building," by Stephen, R.M., Wilson, E.L. and Stander, N., April 1985, (PB86 118965/AS)A06.

UCB/EERC-85/04 "Development of Substructuring Techniques for On-Line Computer Controlled Seismic Performance Testing," by Dermitzakis, S. and Mahin, S., February 1985, (PB86 132941/AS)A08.

UCB/EERC-85/05 "A Simple Model for Reinforcing Bar Anchorages under Cyclic Excitations," by Filippou, F.C., March 1985, (PB86 112 919/AS)A05.

UCB/EERC-85/06 "Racking Behavior of Wood-framed Gypsum Panels under Dynamic Load," by Oliva, M.G., June 1985.

UCB/EERC-85/07 "Earthquake Analysis and Response of Concrete Arch Dams," by Fok, K.-L. and Chopra, A.K., June 1985, (PB86 139672/AS)A10.

UCB/EERC-85/08 "Effect of Inelastic Behavior on the Analysis and Design of Earthquake Resistant Structures," by Lin, J.P. and Mahin, S.A., June 1985, (PB86 135340/AS)A08.

UCB/EERC-85/09 "Earthquake Simulator Testing of a Base-Isolated Bridge Deck," by Kelly, J.M., Buckle, I.G. and Tsai, H.-C., January 1986, (PB87 124 152/AS)A06.

UCB/EERC-85/10 "Simplified Analysis for Earthquake Resistant Design of Concrete Gravity Dams," by Fenves, G. and Chopra, A.K., June 1986, (PB87 124 160/AS)A08.

UCB/EERC-85/11 "Dynamic Interaction Effects in Arch Dams," by Clough, R.W., Chang, K.-T., Chen, H.-Q. and Ghanaat, Y., October 1985, (PB86 135027/AS)A05.

UCB/EERC-85/12 "Dynamic Response of Long Valley Dam in the Mammoth Lake Earthquake Series of May 25-27, 1980," by Lai, S. and Seed, H.B., November 1985, (PB86 142304/AS)A05.

UCB/EERC-85/13 "A Methodology for Computer-Aided Design of Earthquake-Resistant Steel Structures," by Austin, M.A., Pister, K.S. and Mahin, S.A., December 1985, (PB86 159480/AS)A10 .

UCB/EERC-85/14 "Response of Tension-Leg Platforms to Vertical Seismic Excitations," by Liou, G.-S., Penzien, J. and Yeung, R.W., December 1985, (PB87 124 871/AS)A08.

UCB/EERC-85/15 "Cyclic Loading Tests of Masonry Single Piers: Volume 4 - Additional Tests with Height to Width Ratio of 1," by Sveinsson, B., McNiven, H.D. and Sucuoglu, H., December 1985.

UCB/EERC-85/16 "An Experimental Program for Studying the Dynamic Response of a Steel Frame with a Variety of Infill Partitions," by Yanev, B. and McNiven, H.D., December 1985.

UCB/EERC-86/01 "A Study of Seismically Resistant Eccentrically Braced Steel Frame Systems," by Kasai, K. and Popov, E.P., January 1986, (PB87 124 178/AS)A14.

UCB/EERC-86/02 "Design Problems in Soil Liquefaction," by Seed, H.B., February 1986, (PB87 124 186/AS)A03.

UCB/EERC-86/03 "Implications of Recent Earthquakes and Research on Earthquake-Resistant Design and Construction of Buildings," by Bertero, V.V., March 1986, (PB87 124 194/AS)A05.

UCB/EERC-86/04 "The Use of Load Dependent Vectors for Dynamic and Earthquake Analyses," by Leger, P., Wilson, E.L. and Clough, R.W., March 1986, (PB87 124 202/AS)A12.

UCB/EERC-86/05 "Two Beam-To-Column Web Connections," by Tsai, K.-C. and Popov, E.P., April 1986 , (PB87 124 301/AS)A04.

UCB/EERC-86/06 "Determination of Penetration Resistance for Coarse-Grained Soils using the Becker Hammer Drill," by Harder, L.F. and Seed, H.B., May 1986, (PB87 124 210/AS)A07.

UCB/EERC-86/07 "A Mathematical Model for Predicting the Nonlinear Response of Unreinforced Masonry Walls to In-Plane Earthquake Excitations," by Mengi, Y. and McNiven, H.D., May 1986, (PB87 124 780/AS)A06.

UCB/EERC-86/08 "The 19 September 1985 Mexico Earthquake: Building Behavior," by Bertero, V.V., July 1986.

UCB/EERC-86/09 "EACD-3D: A Computer Program for Three-Dimensional Earthquake Analysis of Concrete Dams," by Fok, K.-L., Hall, J.F. and Chopra, A.K., July 1986, (PB87 124 228/AS)A08.

UCB/EERC-86/10 "Earthquake Simulation Tests and Associated Studies of a 0.3-Scale Model of a Six-Story Concentrically Braced Steel Structure," by Uang, C.-M. and Bertero, V.V., December 1986.

UCB/EERC-86/11 "Mechanical Characteristics of Base Isolation Bearings for a Bridge Deck Model Test," by Kelly, J.M., Buckle, I.G. and Koh, C.-G., 1987.

UCB/EERC-86/12 "Modelling of Dynamic Response of Elastomeric Isolation Bearings," by Koh, C.-G. and Kelly, J.M., 1987.

UCB/EERC-87/01 "FPS Earthquake Resisting System: Experimental Report," by Zayas, V.A., Low, S.S. and Mahin, S.A., June 1987.

UCB/EERC-87/02 "Earthquake Simulator Tests and Associated Studies of a 0.3-Scale Model of a Six-Story Eccentrically Braced Steel Structure," by Whittaker, A., Uang, C.-M. and Bertero, V.V., July 1987.

UCB/EERC-87/03 "A Displacement Control and Uplift Restraint Device for Base-Isolated Structures," by Kelly, J.M., Griffith, M.C. and Aiken, I.G., April 1987.

UCB/EERC-87/04 "Earthquake Simulator Testing of a Combined Sliding Bearing and Rubber Bearing Isolation System," by Kelly, J.M. and Chalhoub, M.S., 1987.

UCB/EERC-87/05 "Three-Dimensional Inelastic Analysis of Reinforced Concrete Frame-Wall Structures," by Moazzami, S. and Bertero, V.V., May 1987.